INSTITUTO POTOSINO DE INVESTIGACIÓN CIENTÍFICA Y TECNOLÓGICA, A.C.

POSGRADO EN CIENCIAS AMBIENTALES

Novel application of graphene oxide-based nanomaterials as redox mediators to improve the reductive transformation of iopromide

Tesis que presenta

Eduardo Toral Sánchez

Para obtener el grado de

Doctor en Ciencias Ambientales

Codirectores de la Tesis:

Dr. José René Rangel Méndez

Dr. Francisco Javier Cervantes Carrillo

San Luis Potosí, S.L.P., Mayo 2018

IPICYT

Constancia de aprobación de la tesis

La tesis ***"Novel application of graphene oxide-based nanomaterials as redox mediators to improve the reductive transformation of iopromide"*** presentada para obtener el Grado de Doctor en Ciencias Ambientales, fue elaborada por **Eduardo Toral Sánchez** y aprobada el once de junio del dos mil dieciocho por los suscritos, designados por el Colegio de Profesores de la División de Ciencias Ambientales del Instituto Potosino de Investigación Científica y Tecnológica, A.C.

Dr. Francisco Javier Cervantes Carrillo
Codirector de la tesis

Dr. José René Rangel Méndez
Codirector de la tesis

Dr. Emilio Muñoz Sandoval
Miembro del Comité Tutoral

Dr. Luis Felipe Cházaro Ruiz
Miembro del Comité Tutoral

Dr. Germán Buitrón Méndez
Miembro del Comité Tutoral

Créditos Institucionales

Esta tesis fue elaborada en los Laboratorio de Fisicoquímica y Biotecnología Ambiental de la División de Ciencias Ambientales del Instituto Potosino de Investigación Científica y Tecnológica, A.C., bajo la codirección del Dr. José René Rangel Méndez y Dr. Francisco Javier Cervantes Carrillo.

Durante la realización del trabajo el autor recibió una beca académica del Consejo Nacional de Ciencia y Tecnología No. 378326 y del Instituto Potosino de Investigación Científica y Tecnológica, A. C.

IPICYT

Instituto Potosino de Investigación Científica y Tecnológica, A.C.

Acta de Examen de Grado

El Secretario Académico del Instituto Potosino de Investigación Científica y Tecnológica, A.C., certifica que en el Acta 011 del Libro Primero de Actas de Exámenes de Grado del Programa de Doctorado en Ciencias Ambientales está asentado lo siguiente:

En la ciudad de San Luis Potosí a los 11 días del mes de junio del año 2018, se reunió a las 11:00 horas en las instalaciones del Instituto Potosino de Investigación Científica y Tecnológica, A.C., el Jurado integrado por:

Dr. Germán Buitrón Méndez	**Presidente**	**UNAM**
Dr. Emilio Muñoz Sandoval	**Secretario**	**IPICYT**
Dr. Francisco Javier Cervantes Carrillo	**Sinodal**	**IPICYT**
Dr. José René Rangel Méndez	**Sinodal**	**IPICYT**
Dr. Luis Felipe Cházaro Ruiz	**Sinodal**	**IPICYT**

a fin de efectuar el examen, que para obtener el Grado de:

DOCTOR EN CIENCIAS AMBIENTALES

sustentó el C.

Eduardo Toral Sánchez

sobre la Tesis intitulada:

Novel application of graphene oxide-based nanomaterials as redox mediators to improve the reductive transformation of iopromide

que se desarrolló bajo la dirección de

Dr. Francisco Javier Cervantes Carrillo
Dr. José René Rangel Méndez

El Jurado, después de deliberar, determinó

APROBARLO

Dándose por terminado el acto a las 13:32 horas, procediendo a la firma del Acta los integrantes del Jurado. Dando fe el Secretario Académico del Instituto.

A petición del interesado y para los fines que al mismo convengan, se extiende el presente documento en la ciudad de San Luis Potosí, S.L.P., México, a los 11 días del mes de junio de 2018.

Dr. Horacio Flores Zúñiga
Secretario Académico

Mtra. Ivonne Lizette Cuevas Vélez
Jefa del Departamento del Posgrado

INSTITUTO POTOSINO DE INVESTIGACIÓN CIENTÍFICA Y TECNOLÓGICA, A.C.
IPICYT
SECRETARIA ACADEMICA

Promoters:

Dr. José René Rangel Méndez
División de Ciencias Ambientales.
Instituto Potosino de Investigación Científica y Tecnológica A.C.

Dr. Francisco Javier Cervantes Carrillo
División de Ciencias Ambientales.
Instituto Potosino de Investigación Científica y Tecnológica A.C.

Members of the examination committee:

Dr. Luis Felipe Cházaro Ruiz
División de Ciencias Ambientales.
Instituto Potosino de Investigación Científica y Tecnológica A.C.

Dr. Emilio Muñoz Sandoval
División de Materiales Avanzados.
Instituto Potosino de Investigación Científica y Tecnológica A.C.

Dr. Germán Buitrón Méndez
Laboratorio de Procesos Avanzados de Tratamiento de Aguas.
Instituto de Ingeniería de la UNAM

Collaborating Members:

Prof. Robert Hurt
School of Engineering.
Brown University.

Institutional Support

The research described in this thesis was financially supported by grants from the Council of Science and Technology of Mexico (Grants SEP-CB-2014-237118 and 1289 of the Frontiers of Science program), and the Marcos Moshinsky Foundation. Also, the experimental methodology was performed at the Labs of the Environmental Sciences Division of Instituto Potosino de Investigación Científica y Tecnológica (IPICyT), supervised by Prof. José R. Rangel-Méndez and Prof. Francisco J. Cervantes.

The work described in Chapter 4 was carried out at School of Engineering of Brown University, supervised by Prof. Robert Hurt and financially supported by Superfund Research Program of the National Institute of Environmental Health Sciences, grant 2P42 ES013660.

The author of this thesis was financially supported by the Council of Science and Technology of Mexico with the scholarship 378326.

Dedicado a mis padres Eduardo y Julieta quienes han sido la guía de mi vida y mí ejemplo a seguir. Gracias por todo el apoyo, consejos y amor que me han brindado. A mis hermanos Carolina y Jorge por cuidarme, apoyarme y animarme cuando más lo he necesitado. A mis hijos Hugo, Valentina y Jorge quienes son mi razón de seguir adelante.

Este logro es para ustedes.

Agradecimientos

Quiero agradecer infinitamente al **Dr. René Rangel** y **Dr. Francisco Cervantes** por todo el apoyo brindado, críticas, consejos profesionales y por haberme guiado en esta etapa de mi vida. Gracias por haberme aceptado como su estudiante. Sin duda alguna, son ejemplos a seguir para mi futuro como investigador.

Al Dr. Luis F. Cházaro a quién le agradezco sus consejos profesionales y apoyo no solo como asesor, sino como amigo.

Dr. Emilio Muñoz y Dr. Germán Buitrón, gracias por sus consejos y críticas para enriquecer esta tesis doctoral.

Un agradecimiento especial al Prof. Robert Hurt por haberme aceptado en su grupo de investigación y por apoyarme durante mi estancia de investigación doctoral en Brown University.

A mis compañeros del grupo de Adsorción e Intercambio Iónico y Biotecnología Ambiental, con quienes pasé muy buenos momentos. Gracias por todas sus críticas y apoyo durante el trabajo de investigación de esta tesis.

A mis amigos fuera del IPICyT y familia en San Luis Potosí, gracias por todos los buenos momentos, palabras de aliento y valiosa amistad.

Finalmente, quiero agradecer a J.P. Rodas, G. Vidriales y B. Rivera por el apoyo técnico brindado en este trabajo de investigación. Especialmente, quiero agradecer a D. Partida, M. del C. Rocha, A. Colunga, E. Cortés, A. Aguilar y G. Arriaga por todo el apoyo técnico y administrativo, pero sobre todo, por su valiosa amistad.

CONTENTS

Chapter 1: Introduction

Chapter 2: Role of the intrinsic properties of partially reduced graphene oxide on the chemical transformation of iopromide

Chapter 3: Tailoring partially reduced graphene oxide as redox mediator for enhanced biotransformation of iopromide under methanogenic and sulfate-reducing conditions

Chapter 5: Novel application of magnetic nano-carbon composites as redox mediators in the reductive biodegradation of iopromide in anaerobic continuous systems

Chapter 6: General discussion

Chapter 7: Final conclusions, perspectives and scientific products

LIST OF TABLES

LIST OF FIGURES

Abbreviations

AC	Activated carbon
ACF	Activated carbon fibers
AOP	Advanced oxidation processes
AS	Appendix section
CNT	Carbon nanotubes
COD	Chemical oxygen demand
CV	Cyclic voltammetry
EDS	Energy dispersive spectrometer
FT-IR	Fourier transform-infrared
GNS	Graphene nanosacks
GO	Graphene oxide
HPLC	High-performance liquid chromatography
HPLC-MS	High-performance liquid chromatography coupled to mass spectroscopy
HRT	Hydraulic residence time
ICM	Iodinated X-ray contrast media
IOP	Iopromide
MrGO-N	Magnetic reduced graphene oxide nanosacks
NPs	Nanoparticles
ORP	Oxidation-reduction potential
pH_{PZC}	Point of zero charge
rGO	Partially reduced graphene oxide
R-ctrl	Reactor operated without magnetic nanosacks: control reactor
RM	Redox mediator
R-MN	Reactor supplemented with magnetic nanosacks: working reactor
SEM	Scanning electron microscopy
TP	Transformation product
UASB	Upflow anaerobic sludge blancket reactor
XPS	X-ray photoelectron spectroscopy
WWT	Wastewater treatment

Abstract

Iopromide (IOP), a tri-iodinated X-ray contrast medium, is a persistent pollutant, which is poorly removed from conventional wastewater treatment system and frequently released into environmental compartments. Accordingly, several techniques have been employed for the removal of this pollutant from contaminated water. The use of graphene oxide (GO)-based materials as redox mediators (RM) is an attractive option for reductive transformation of IOP. However, the major challenge for the application of GO-based is its recovery and retention in a biological continuous wastewater system. This work reported, for the first time, the successful application of GO, partially reduced GO (rGO) and magnetic rGO nanosacks (MrGO-N) as redox mediator (RM) to facilitate the chemical and biological transformation of IOP in batch incubations and biological continuous system under anaerobic conditions.

The results demonstrated that the redox activity of GO-based materials enhanced the removal and transformation degree of IOP up to 5.0-fold in chemical/biological systems performed in batch assays. Also, results indicated a correlation between the intrinsic properties of GO-based materials and their redox performance. Moreover, the application of MrGO-N in an upflow anaerobic sludge blancket (UASB) reactor under methanogenic conditions was evaluated. Results indicated a high removal efficiency of IOP (~82 %) in the bioreactor supplied with the MrGO-N as RM, indicating their contribution in the redox conversion of this contaminant.

For chemical and biological experiments mentioned above, reductive transformation pathways of IOP were proposed. Transformation byproducts with simpler chemical structures than IOP molecule were identified, involving completely dehalogenation of the

aromatic ring and partial rupture of ramifications of IOP by several reductive reactions, which is the first step toward its mineralization by conventional treatment techniques. In addition, reductive mechanisms that carried out during degradation of IOP were elucidated. The results presented in this doctoral thesis demonstrated the great potential to apply GO, rGO and MrGO-N as electron shuttles in the redox conversion of IOP in water, offering a simple and feasible alternative to tailoring GO-based materials in wastewater treatment systems and industrial effluents to facilitate the reductive transformation of persistent pollutants from contaminated water.

Keywords: Graphene oxide; iopromide; redox mediator; reductive transformation; X-ray contrast medium

Resumen

La iopromida (IOP), un medio de contraste yodado, es un contaminante persistente el cual es difícilmente removido en los sistemas convencionales de tratamiento de aguas residuales y por consiguiente, frecuentemente liberado al medio ambiente. En consecuencia, diferentes técnicas de degradación se han empleado para la remoción de este contaminante presente en el agua. Una atractiva opción para la transformación reductiva de la IOP es el uso de materiales a base de óxido de grafeno (OG), como mediadores redox (MR), debido a su excelente actividad redox. Sin embargo, el mayor reto para la aplicación de estos nanomateriales es su recuperación y retención en un sistema biológico de tratamiento de aguas residuales operado en continuo. Este trabajo reporta, por primera vez, la aplicación exitosa del OG, OG parcialmente reducido (OG-r) y nanosacos magnéticos de OG-r (NMOG-r) como MR en la transformación química y biológica de IOP en ensayos en lote y en un sistema biológico en continuo, bajo condiciones anaerobias.

Los resultados demostraron que la actividad redox de los materiales a base de OG mejoró la remoción y grado de transformación de la IOP hasta en 5 veces en los sistemas químicos/biológicos realizados en ensayos en lote. También, los resultados indicaron una correlación entre las propiedades intrínsecas de los materiales a base de OG y su desempeño catalíticos. Asimismo, se evaluó la aplicación de los NMOG-r en un reactor anaerobio de flujo ascendente (UASB) bajo condiciones metanogénicas. Los resultados indicaron una alta eficiencia de remoción de la IOP (~82 %) en el bioreactor enriquecido con los NMOG-r como MR, indicando su contribución en la conversión redox de este contaminante.

Para los sistemas químicos y biológicos mencionados anteriormente, se propusieron las vías de transformación reductiva de la IOP. En este sentido, se identificaron subproductos de transformación con una estructura química más simple que la molécula de la IOP, involucrando la completa deshalogenación del anillo aromático y la ruptura parcial de las ramificaciones de esta molécula, lo cual es el primer paso hacia su mineralización mediante técnicas de tratamiento convencionales. Además, se elucidaron los mecanismos reductivos que se llevan a cabo durante los procesos de degradación de la IOP.

Los resultados presentados en esta tesis doctoral demuestran el gran potencial del OG, OG-r y los NMOG-r como MR en la conversión redox de la IOP, ofreciendo una alternativa simple y factible para adaptar a los materiales a base de OG en sistemas de tratamiento de aguas residuales y efluentes industriales con la finalidad de facilitar la transformación reductiva de contaminantes persistentes presentes en aguas contaminadas.

Palabras clave: Óxido de grafeno; iopromida; mediador redox, transformación reductiva; medios de contraste de rayos X.

Outline of thesis

Chapter 1 contains the background of this doctoral thesis; an overview of the properties and application of GO-based materials as electron shuttles in the reduction of persistent pollutants from water; the occurrence, fate and ecotoxicological problems of pharmaceuticals in environmental compartments. At the end of the chapter, the presence in aquatic environments and removal of strategies of iopromide (IOP), the model pharmaceutical pollutant considered here, is described.

Chapter 2 reports the role of the intrinsic properties of partially reduced graphene oxide as redox mediator (RM) in the chemical transformation of IOP in batch assays. The deep characterization of these nanomaterials and its correlation between redox properties and reductive transformation mechanisms of IOP is explored.

Similarly, **Chapter 3** reports the importance of chemical surface of partially reduced graphene oxide and its application as RM in the biotransformation of IOP under methanogenic and sulfate-reducing conditions.

Chapter 4 studies the application of magnetic graphene nanosacks as RM to improve the reductive transformation of IOP in batch incubations. The redox-mediating capacity of characterization of graphene nano-composites is evaluated for the first time.

Chapter 5 reports the novel applications of magnetic nano-graphene composites as RM in the biotransformation of IOP in an upflow anaerobic sludge blanket (UASB) reactor under methanogenic conditions. From **Chapter 2 to 5**, transformation pathways and reductive mechanisms involved in the redox conversion of IOP are also elucidated.

Finally, the results obtained in this research are globally discussed in **Chapter 6.**

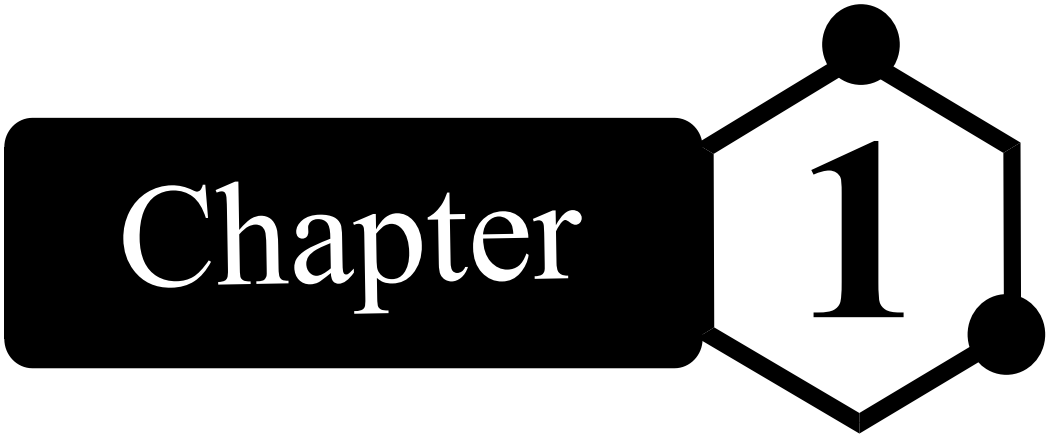

Introduction

1.1. Pollution of water

The increase of anthropogenic activities has created a great demand for natural resources and the pollution of several systems, especially aquatic environments. Water pollution occurs when toxic substances enter receiving water bodies such as lake, rivers, oceans and then, getting dissolved in them. Also, the contaminants can also be seep through of soils and reach the groundwater[1]. Water pollution is often caused by the discharge of inadequately treated wastewater into natural bodies of water, leading to environmental degradation of aquatic ecosystems[2].

Nowadays, the removal of emerging pollutants from water represents one of the greatest scientific and technological challenges of the new century. Among these compounds that stand out due to their difficulty to degrade in aquatic environments and to their uncertain adverse effects on living organisms are pharmaceutical compounds. Accordingly, several research areas have the major interest to develop degradation techniques for these compounds.

1.2. Pharmaceutical compounds: priority pollutants in the environment

Recently, increasing attention has been focused on the presence of pharmaceuticals in aquatic environments and soils around the world[3]. Especially, pharmaceuticals are founded in most aquatic environments (e.g. rivers and lagoons) at trace levels (ng/L to μg/L), and their continuous input could cause a long-term potential risk for aquatic and terrestrial organisms[4,5]. In fact, the main problem of pharmaceuticals in environmental compartments lies on the little knowledge about their toxicity, behavior and adverse effects on humans and ecosystems health due to continuous exposure to these pollutants[6]. Accordingly, pharmaceuticals are catalogued as emerging pollutants[7].

1.2.1. Occurrence, fate and eco-toxicity of pharmaceuticals in aquatic environments

The occurrence and fate of pharmaceuticals in the aquatic environment have been recognized as one of the emerging issues in environmental chemistry[2]. Due to their large consumption and production, pharmaceuticals may enter aqueous environments by anthropogenic activities, resulting in their detection in receiving water bodies, groundwater and drinking water[8,9]. The main sources for the occurrence of pharmaceuticals in the environment are the discharge of waste effluents from manufacturing processes, sewage treatment plants, the inappropriate disposal of expired drugs and landfill leachate[10]. The use of medicines by humans is the main route of these pollutants in aquatic environments. After use, pharmaceuticals and their metabolites are excreted by feces or urine and released into wastewater treatment (WWT) systems. During treatment processes of WWT plants, pharmaceuticals are poorly removed and subsequently discharged to water bodies and soils[2,6]. In addition, another route of pharmaceuticals occurrence is the discharged of medicines from hospital effluents in municipal drainage and finally to WWT facilities[2,10]. Figure 1.1 shows the sources and transport routes of pharmaceuticals in environmental compartments.

Some investigations performed in Austria, Brazil, Canada, Croatia, England, Germany, Greece, Italy, Spain, Switzerland, The Netherlands and the U.S.A have detected more than 80 pharmaceuticals and several drugs in surface waters located near to WWT plants[2,10]. Moreover, the presence of pharmaceuticals in potable water has been lightly studied in recent years due to the lack of monitoring programs in water treatment plants, as well as the improvement of detection techniques[11]. Studies conducted in Germany, Italy, United Kingdom, U. S. A, Canada, Brazil, Spain and China have reported the presence of several

drugs in samples of water for human consumption[11,12]. Among identified pharmaceuticals are analgesics and anti-inflammatories, antibiotics, beta-blockers, hormones and steroids, lipids regulators and serotonin inhibitors[2,10,13]. Iodinated X-ray contrast media (ICM) have also had a special interest because of their high persistence and occurrence in soils and surface waters[14].

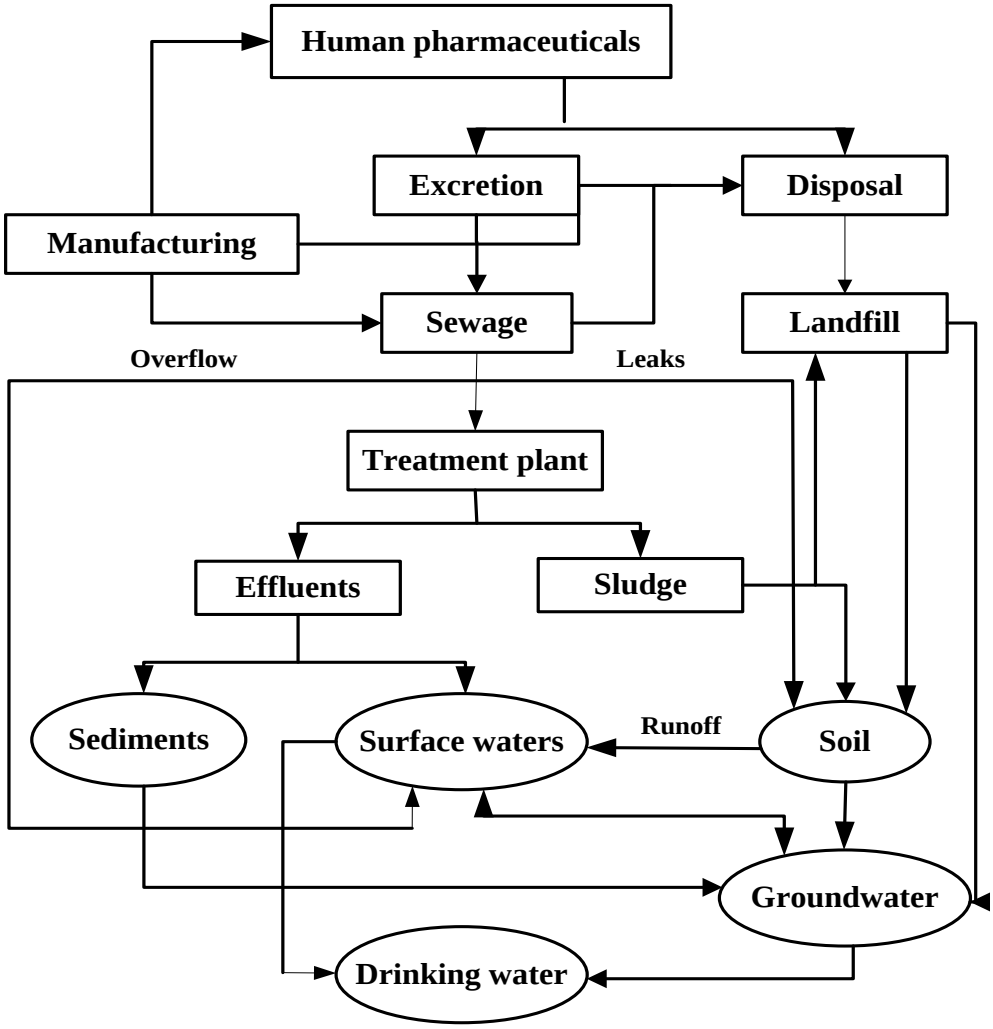

Figure 1.1. Major pathways by which pharmaceuticals reach the environment (modified for reference[10]).

On the other hand, the distribution and fate of pharmaceuticals are dependent on their physicochemical properties, and on the persistence and biological activity of their transformation byproducts in aquatic and terrestrial environments[6,10]. In the environments, the transformation and degradation reactions alter the mobility, persistence and fate of pharmaceuticals[3,15]. The fate of pharmaceuticals in the aquatic environment is determined by sorption to sediments and/or degradation by chemical and/or biological processes[16,17]. In surface waters, microbial degradation is slower that during WWT processes because the diversity and density of bacteria is much lower in surface waters[18]. The abiotic degradation of pharmaceuticals could occur by photodegradation, which is the dominant mechanism for their chemical transformation in aquatic environments[10,16].

Finally, the toxicological effects of pharmaceuticals on the environments have been poorly explored. Some studies have indicated that medicines have the potential to interfere with the metabolism and behavior of aquatic and terrestrial organisms[19,20]. In addition, it has been reported that hormones, analgesics and anticancer drugs are the pharmaceuticals with greatest eco-toxicological effect in aquatic organisms, such as bioaccumulation, bioavailability and biopersistence[21,22].

1.3. X-ray contrast media in aquatic environments

ICM are chemically inert drugs which are supplied intravascularly in very high amounts with very short time period[23]. These pharmaceuticals are among the most widely used around the world with a global consumption of approximately 3.5×10^6 kg per year[24,25]. ICM are diagnostic drugs that are applied to improve the contrast between organs or vessel examined and surrounding tissues during radiological tests[26]. ICM are administered at high daily doses (up to 200 g/d) and mostly excreted nonmetabolized (>95%) by urine or feces

during the first 24 h after its application[27,28]. All intravascular contrast media are tri-iodinated benzene derivatives with iodine atoms in position 2, 4 and 6. The other ring positions are substituted by ramifications that gives to ICM high water solubility and low toxicity[23]. Currently, ICM are classified in ionic monomers, ionic dimers, non-ionic monomers and non-ionic dimers[29]. Due to their physicochemical properties and its poor removal from WWT effluents, ICM are emerging contaminants, which are beginning to be studied due to their presence in environmental compartments. Furthermore, it has been reported that exposure to ICM could cause human health impacts that include allergic reactions, cardiac problems and systemic manifestations like headache, vomiting and arms pain[29]. Within ICM with greater environmental relevance is the diatrizoate, iomeprol and iopromide, the latter being the contaminant of interest in the present thesis.

1.3.1. Iopromide: properties, presence and toxicological effects in the aquatic environment

Iopromide (IOP) is non-ionic ICM widely used in radiography studies, which due to its chemical structure, physicochemical properties and low microbial degradability by aerobic bacteria is considered a recalcitrant pollutant[30,31]. Figure 1.2 shows the chemical structure and physicochemical properties of IOP.

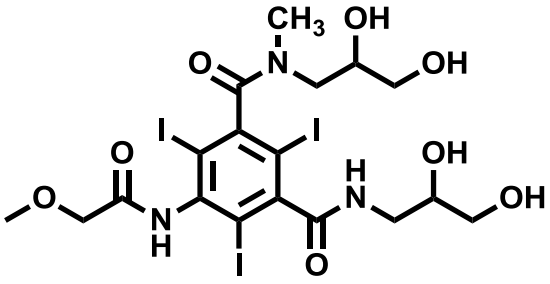

Iopromide	
Chemical formula:	**$C_{18}H_{24}I_3N_3O_8$**
Molecular weight:	**790.87**
Osmolarity (mOsmol/L):	**496**
Viscosity (cP) @ 20°C:	**22**
Density (g/mL) @ 20°C:	**1.4**
Polarity (log Kow):	**-2.33**
Solubility (mol/L-H_2O):	**0.97**

Figure 1.2. Chemical structure and physicochemical properties of IOP.

As mentioned above, IOP is a pharmaceutical, which is hardly removed in conventional WWT systems, and thus it is constantly released into receiving water bodies[31,32]. Since IOP is resistant in WWT processes, the detected concentration in wastewater effluents, surface water (rivers and lakes), groundwater, and even in treated tap water is relative high at μg/L levels[24,25,33]. Few studies have reported the concentration of IOP in effluents of sewage treatment plants, which vary in the range of 10 to 100 μg/L[14,25,31]. In hospital effluents, it has been reported a concentration of this pharmaceutical around to 50 and 300 μg/L[34].

Wastewaters are the primary route of entry of IOP into aquatic environments, and hospitals are considered important source and significant contributors of IOP residues in influents of municipal WWT plants[35,36]. In this sense, it has been documented the presence of IOP in environmental compartments. For example, Putschew et al.,[25] reported the presence of IOP in surface water and raw drinking water at around 10 μg/L. In addition, it has been detected the presence of this pollutant in WWT effluents, as well as its poor elimination during aerobic conventional treatments, which remained in the aqueous phase[31,32]. Also, Wang et al., reported the presence of IOP metabolites in wastewater and receiving surface water of the Pearls River Delta, China[37]. Kreuzinger et al., reported that IOP is present in groundwater trough infiltration of WWT effluents discharged in the soil of a rural arid area of Asia[38]. Finally, Ternes et al., identified this pharmaceutical in the effluents from a German municipal WWT plant at a concentration of 5.7 μg/L[39]. According to these reports, the occurrence and fate of IOP in aquatic environments is a topic that has had interest in recent years.

Moreover, Steger-Hartmann et al., reported that no toxic effects of IOP were observed in both short-term and chronic toxicity tests[26]. However, the environmental safety of IOP

cannot be guaranteed since the side and toxic effects on renal cells by IOP have been documented. In this context, different studies have reported toxic effect at cellular levels conducting to the vacuolization and apoptosis of tubular cells, and endothelial dysfunction leading to kidney damage[40–42]. Consequently, several chemical and biological removal techniques have been studied in order to improve the degradation and/or transformation of this pollutant from contaminated water[43,44].

1.3.2. Degradation strategies of IOP from water

Several studies have explored degradation strategies of IOP, such as advanced oxidation processes (AOP), ozonation, electrochemical oxidation, as well as aerobic degradation by activated sludge and white-rod fungi, etc. Among these strategies, the electrochemical oxidation treatment of reverse osmosis concentrates reported up to 96 % of IOP removal after 7.5 h[45]. Metal-catalyzed (Pd-Ni catalyst) treatment with H_2-5% system achieved complete dehalogenation (deiodination) of aromatic ring of IOP with the generation of a final stable organic product[27]. In addition, anaerobic strategies have been also applied in order to promote reductive biotransformation reactions of IOP. Pat-Espadas et al.,[46] and Cruz-Zavala et al.,[47] reported the microbial transformation of IOP in a biological continuous systems by the use of bio-catalysts. Moreover, other works have focused on proposing the transformation pathways of IOP in WWT effluents, hospital effluents and surface waters[14,27,28,36,45]. Tables 1.1 and 1.2 summarized the studies that involve the biological and chemical degradation/transformation of IOP, respectively.

Table 1.1. Overview of biological strategies for removal and/or biotransformation of IOP

Strategy	Experimental conditions	IOP removal (%)	Reference
Aerobic treatment	Experiments performed under aerobic conditions using activated sludge, river water and sediments in batch incubations. Also, transformation products of IOP were identified.	85 % during 54 h	[48]
Aerobic treatment	Biodegradation of IOP by white-rot fungus *Trametes versicolor* in batch assays and 10 L-bioreactor fluidized by air pulse operated in batch and glucose as substrate. Also, biotransformation byproducts were identified by HPLC-MS.	60 % (batch incubations) and 65.4 % (bioreactor) during 12 days.	36
Aerobic treatment	Biodegradation of IOP by nitrifying activated sludge as inoculums (3300 VSS/L) in bioreactors operated in batch mode and supplemented with NH_4-N.	86 % during 100 h	[49]
Aerobic treatment	Biodegradation of IOP by activated sludge or nitrifying activated sludge in a batch reactor with a volume of 1 L.	90 % during 9 days	[50]
Aerobic treatment	Biodegradation tests of IOP in groundwater/solid systems under environmental conditions and in batch assays were performed. In addition, bio-transformation byproduct were identified	80 % during 20 days	28

Continuation of **Table 1.1**

Aerobic treatment	Pseudomonas sp.I-24 isolated from activated sludge was used to biodegrade IOP in batch assays. Also, different cosubstrates were tested as carbon source.	88.24 % during 100 h	51
Anaerobic treatment	Reductive biotransformation of IOP by immobilization of biogenic Pd(0) in anaerobic granular sludge using an anaerobic continuous reactor (UASB) under methanogenic conditions. Biotransformation pathway of IOP was elucidated.	81 % during 21 days	46
Anaerobic treatment	Metal-humic complex were applied as RM in the biotransformation of IOP in a continuous UASB reactor under methanogenic conditions. Transformation pathway of IOP was reported.	80 % during 40 days	47

Table 1.2. Overview of chemical strategies for removal and/or transformation of IOP

Strategy	Experimental conditions	IOP removal (%)	Reference
Ozonation/ ultrasound	Reduction of IOP by the application of O3 pulses (1.24 mg/L) coupled to ultrasound (0.235 W/mL) in batch assays.	65 % in 30 min	[52]
Electrochemical treatment	Anodic oxidation at boron doped diamond electrode as well as cathodic reduction using a platinum electrode were evaluated for IOP removal under conditions of reverse osmosis in batch assays. Furthermore, Elucidation of the degradation pathway of this pollutant was studied.	96 % in 7.5 h	[45]
Advanced oxidation process	Photocatalityc degradation of IOP assisted by different TiO_2 materials under simulated solar irradiation in a continuous system. Also, intermediates and reaction pathways were determined.	70 % irradiating for 45 min	[53]
Advanced oxidation process	Removal of IOP using electron bean irradiation technology with hydroxyl radical and hydrate electron in presence of hydrogen peroxide, bicarbonate and sulfite ions in batch incubations.	90 % with a dose of 19.6 KGy of irradiation	[50]
Advanced oxidation/ reduction process	Degradation of IOP by pulses of radiolysis and γ-radiolysis. Also, the degradation mechanisms of IOP were reported.	72 % with a dose of 8.0 KGy	4

Continuation of **Table 1.2**

Ozonation/ O_3/H_2O_2 and O_3/UV systems	Degradation of IOP in a pilot plant assisted by ozone (15 mg/L), UV irradiation (90 %) and H_2O_2 (10 mg/L) in a continuous systems.	Higher than 80 % in all systems	39
Ozonation	Oxidation of IOP in a pilot-scale plant operated with activated sludge and supplemented with O_3 (15 mg/L) in a continuous system.	95 %	[54]
Metal-catalyzed hydro-dehalogenation	Reductive treatment of IOP with hydrogen gas in combination with supported Pd-Ni porous catalysts in batch assays. Also, chemical transformation pathway was elucidated.	95 % in70 min	27

On the other hand, it has been documented the use of redox-mediating substances as a good option to accelerate the redox conversion of recalcitrant pollutants in contaminated waters[55–59], which is the degradation strategy proposed in this doctoral thesis for the reductive transformation of IOP.

1.4. Redox mediator: generalities

Several studies have reported the use of chemical substances with quinone groups (two resonance carbonyl groups[60]) in their chemical structure, which can facilitate the reductive transformation of persistent pollutants by oxidation-reduction processes[56,57,59,61]. Such chemical substances with the ability to receive and yield electrons are known as redox mediators (RM)[60] and the catalysis in the redox conversion is within their potential applications[57]. Quinone groups can serve as electron acceptor in the oxidation of

chemical/biological electron donors, and can be reused as electron acceptor multiple times when there are reoxidation mechanisms[62]. The general oxidation-reduction mechanism that involves RM substances is shown in Figure 1.3. In general, the biological process that involves RM substances (Figure 1.3) consists of three stages: i) anaerobic oxidation of the electron donor by microorganisms (biological reactions), ii) the RM substances can accept electrons from the biological oxidation of the substrate, and iii) the electrons are transferred from RM substances to the final electron acceptor, which is reduced by chemical reactions[61,63].

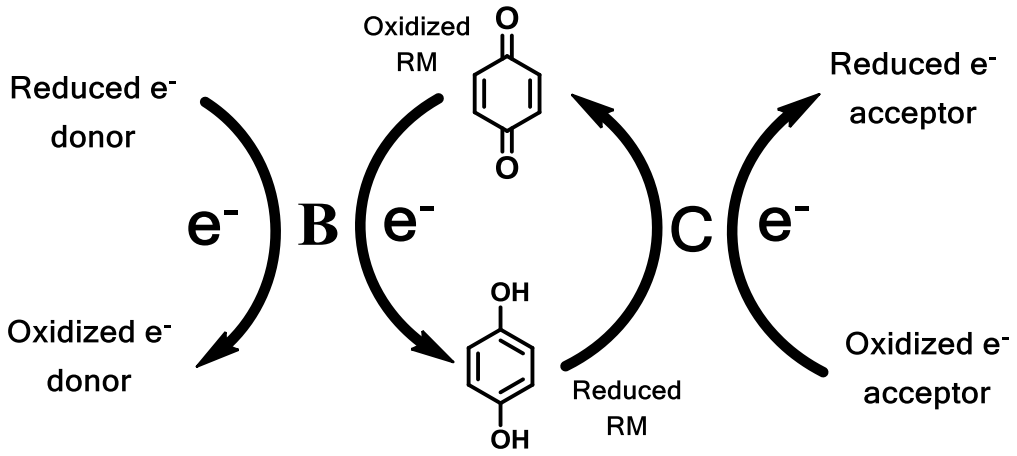

Figure 1.3. Oxidation –reduction processes of RM substances. B and C indicate biological or chemical reactions, respectively[63].

Quinone-hydroquinone couples are the perfect example of electron shuttle systems that enhance the electron transfer process in the reductive transformation of environmental contaminants[64,65]. The great redox activity of these functionalities lies in the capacity to accept and donate electrons by resonance phenomenon[60,65]. The electron transfer activity of quinone groups has been previously proposed[60]. In this sense, two carbonyl groups (quinone groups) located at edges of a common graphene layer can act in concert to stabilize radicals via resonance. The radicals can accept electrons and become anions.

Subsequently, the anions can transfer electrons back and become radicals, or they can interact with protons in solution. Finally, reversible proton transfer leads to phenolic (hydroquinone) sites[60].

Moreover, the electrochemical reduction of quinone groups in aqueous solution has been studied and the mechanism of such reduction is represented in Figure 1.4. This scheme shows the two-electron, two protonation reduction of quinone moieties in solution (final reaction of Figure 1.4)[65].

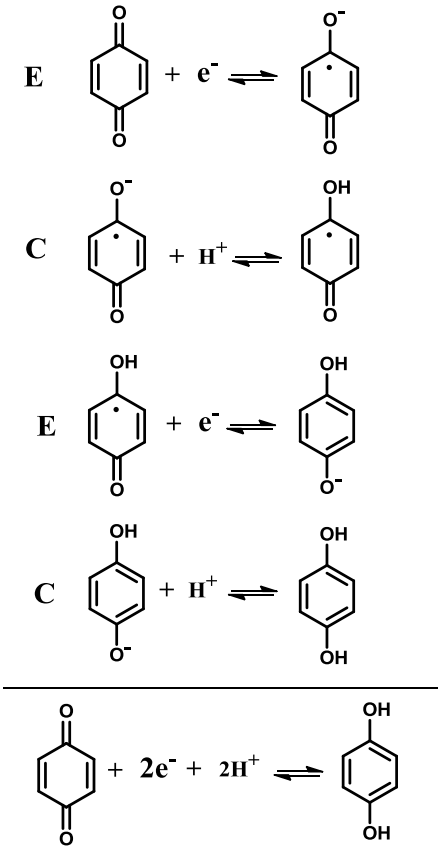

Figure 1.4. Electrochemical reduction mechanism of quinone complex in solution.

The sequence of the reactions is described as two rounds of electron-transfer coupled (electrochemical reactions, **E**) to proton acceptance (chemical reactions, **C**) that is a

bielectronic mechanism of ECEC type[65]. In the absence of protons, the quinone complex is reduced to its dianion[65] as can be seen in Figure 1.5.

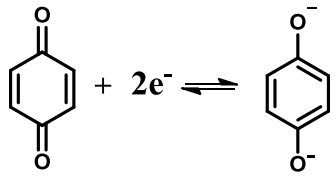

Figure 1.5. Two-electron reduction of quinone in aqueous solution (taken from reference[65])

Accordingly, the presence of quinone groups in redox conversion processes is a key factor for improving the electron transfer mechanisms toward electron acceptor pollutants.

On the other hand, the suggestion that other oxygenated functional groups, besides quinone moieties could be involved in electron transfer processes has only been indirectly substantiated by electrochemical methods[60]. However, it can be presumed that the only requirement for a heteroatom (e.g. oxygen, nitrogen and sulfur) bearing an unshared pair of electrons to act as electron shuttle would be its association with a substrate containing free radicals estabilized by resonance[60,66]. Since the redox-mediating ability of these functional groups has not been addressed in detail, most reports of surface oxygenated groups that are involved in electron transferring are generally attributed to quinone-type groups only[60].

1.4.1. Carbon-based materials as redox mediators

Several studies have explored the catalytic activity of carbon-based materials in the reductive transformation of contaminants by redox processes due do the presence of quinone groups in their chemical surface[60,64]. Especially, activated carbon has been widely applied in the anaerobic transformation of persistent compounds such as azo dyes[56,59,67–70] and trace organic pollutants[71] because the presence of a diversity of surface functional groups, including quinone groups, promotes enhanced transformation rate. Activated

carbon fibers have been also applied as RM in the reduction of azo dyes[63] and nitrocompounds[57,72]. In addition, the redox activity of carbon nanotubes has been explored to facilitate reductive dehalogenation reactions of organic pollutants[73,74].

Nowadays, graphene-based nanomaterials have attracted great interest in many research areas (e.g. as redox catalysts) due to their chemical and physical properties, making them versatile materials for multiple applications[75]. The unique properties of graphene and its applications will be reviewed in the next section.

1.5. Graphene: properties, characteristics and synthesis

Graphene is an allotrope of carbon consisting of a single atomic plane of carbon atoms arranged in a hexagonal lattice[75,76]. This carbon material is a two dimensional (2D) crystal that is stable under ambient conditions, which confers excellent electronic properties due to its anomalous quantum Hall effects[77,78]. Since it was first synthesized by Geim y Novoselov in 2004[79], graphene has attracted great interest in several research areas due to its exceptional properties, such as high electrical and thermal conductivity, elasticity, mechanical strength, resistance (higher than steel), flexibility, transparency, high theoretical surface area (~2600 m^2/g [80]) and unique catalytic activity[75,81].

Graphene properties make it an ideal material for multiple applications in technology, especially in electronic areas. Among potential applications of this material is the electronic devices manufacture, sensors, nanoelectronics, biomedicine, transistors, environmental remediation, solar cells, energy storage and antibacterial applications[82,83]. The main current problem in the application of graphene is its massive production. Investigations in graphene production are focused in its synthesis by chemical and physical from graphite materials nowadays[84].

In this sense, graphene can be produced by micro-mechanical exfoliation of highly ordered pyrolitic graphite, epitaxial growth, liquid phase exfoliation, and the reduction of graphene oxide (GO)[77,85–88]. Figure 1.5 shows a schematic representation of the ways of reduced GO synthesis. The first three methods can produce graphene with high crystallinity and excellent properties[75,77]. However, the production of graphene by reduction of GO has been of great interest because the costs of production and raw materials are relatively low with a high yield, and the material can form stable aqueous colloids that facilitate its assembly in macroscopic carbon structures by simple and cheap processes[77]. Accordingly, reduction of GO is promising for large-scale production of graphene.

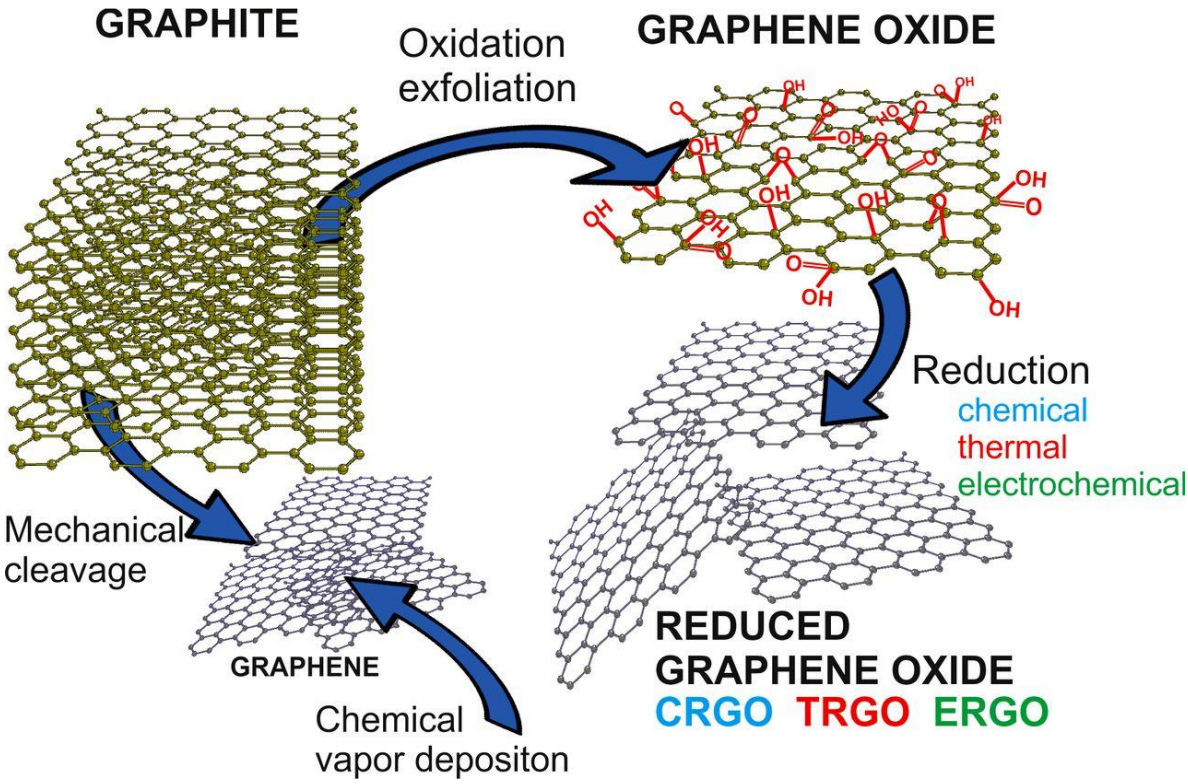

Figure 1.6. Schematic ways of graphene and graphene-based materials synthesis: CRGO (chemically reduced GO), TRGO (thermally reduced GO) and ERGO (electrochemically reduced GO) (taken from reference[89]).

1.5.1. Graphene oxide: characteristics and reduction strategies

Graphene oxide can be defined as a graphene sheet functionalized with different oxygenated groups[90]. The chemical structure of this carbon material has been widely studied in previous works[90,91]. GO can be synthesized by a simple methodology of oxidation of graphite usually named Hummers method[92]. By this method, graphite is reacted with a mixture of potassium permanganate, sodium nitrate and sulfuric acid[77,92].

Currently, different chemical structure models have been proposed for GO. Several early studies have proposed that the structure of GO has regular lattice composed of discrete repeat units[93], and the chemical structure of GO widely accepted is the proposed by Lerf-Klinowski[94] shown in Figure. 1.6. This model proposed that the oxygenated functional groups on the basal plane in GO consist of epoxy and hydroxyl groups[93,95]. Carbonyl and carboxyl groups are also present[77,90,94]. Currently, investigations have reported the presence of lactones, phenols, lactols, pyrones, ketones and anhydrates on the edge of GO sheets[93,95–97]. However, the presence of epoxy and hydroxyl groups on the graphitic sheets are still dominant[90].

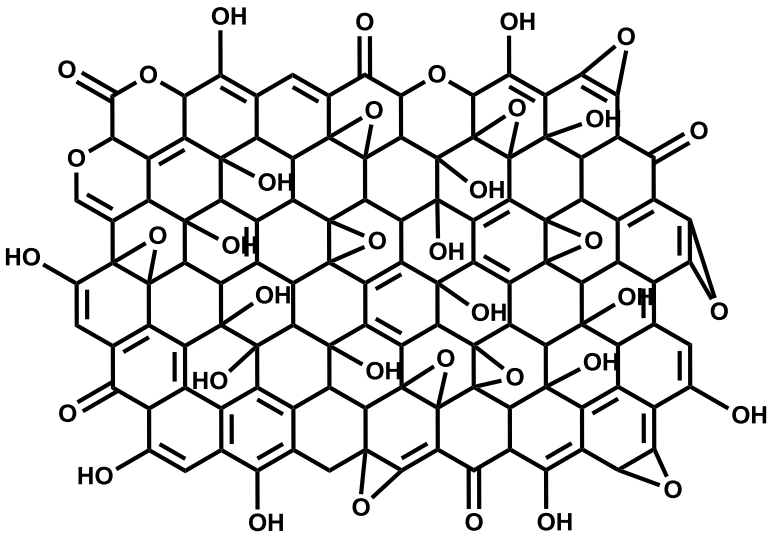

Figure 1.7. Theoretical chemical structure of GO based on Lerf-Klinowski model[77,94].

As mentioned above, the interest of GO is that it can be used as a precursor to produce graphene by reduction processes. The most attractive property of GO is that it can be partly reduced to graphene-like sheets by removing the oxygenated groups with the recovery of a conjugated structure, which is the most important goal in the reduction methodologies[77]. In this context, several strategies have been employed in order to remove oxygenated groups from GO sheets.

The deoxygenation strategies are focused in thermal annealing, chemical, photocatalyst, solvothermal, electrochemical and multi-steps reduction techniques[77]. Especially, thermal and chemical reduction strategies have been widely studied in several works. For the case of thermal reduction, GO can be reduced solely by heat treatment at mild and high temperatures in order to exfoliate graphite oxide to achieve graphene[98–101]. The temperature increase makes the oxygenated groups attached on graphene sheets decompose into gases[77]. Also, this strategy removes carbon atoms from carbon plane, producing defects in the graphitic sheets[84,102,103]. In addition, it has been reported the mechanism that carried out during thermal reduction of GO, which identified the oxygenated groups firstly removed as temperature increase[99].

On the other hand, the chemical reduction of GO implies the use of chemical reagents and their chemical reactions with this nanomaterial. Usually, this strategy is performed at room temperature or moderate heating[104]. Accordingly, chemical reduction strategy is a good option in comparison with thermal methodology since the equipment and environment is not critical for production of graphene[77]. The reducing agent mostly used in chemical reduction process is hydrazine[84], obtaining a good performance in the production of graphene. As a result, hydrazine has been accepted as a good chemical reagent to reduced GO[105–107]. However, this reducing agent (and its chemical derivatives) is highly toxic for

the environment. As a consequence, several reducing agents have been employed to reduce GO sheets. Few researches about environment-friendly strategies to produce graphene have been documented[108,109]. It has been reported that L-ascorbic acid (vitamin C) can serve as reducing agent to reduce GO reaching the same results as those obtained in the reduction with hydrazine[102,109–111]. The importance of the use of vitamin C lies in that it is a natural antioxidant in cells, is stable and unreactive in the environment, and it does not cause cellular damage[109].

The final product after the reduction strategies is partially reduced GO (rGO) sheets, which are usually considered a chemical derivative from graphene[77]. Figure 1.7 shows a scheme of rGO sheet. Residual oxygenated groups and defects alter the chemical structure of GO sheets, which involves that the properties of rGO sheets are substantially different. According to that, the final application of rGO materials depends on their reduction degree[77,90]. Moreover, the versatility of GO-based materials is related to the facility with which it can be functionalized for specific applications, such as optical devices, biomedical sensors, energy generators/storages, corrosion resistant coatings, medicine transportation and solar cells[112,113]. On the other hand, several works have explored the catalytic activity of GO-based materials and its application in the removal of pollutants from water by redox processes, serving as RM as mentioned below.

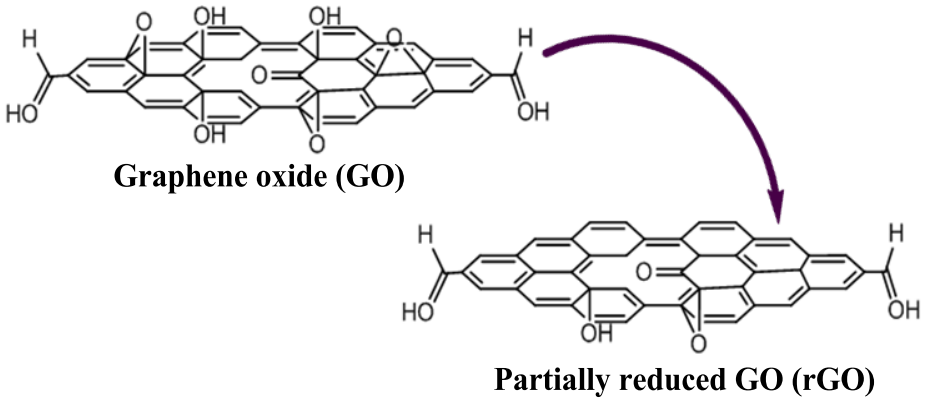

Figure 1.8. Schematic representation of oxygenated groups removal.

1.5.2. GO-based materials as redox mediators

Lately, it has been documented that GO, rGO and graphene composites can promote the redox conversion of some persistent contaminants in chemical or biological systems by enhancing electron transfer processes[43,61,114]. This environmental application can be explained by the superior redox catalytic activity of quinone groups presents in the chemical structure of GO-bases materials, and by its high electrical conductivity in graphene basal plane, which improves the electron transfer mechanism toward electron acceptor compounds[43,84,90]. Also, it has been reported that graphene materials exhibit better performance to transfer electrons through quinone groups or delocalized π-electrons from graphitic sheets[68]. In addition, it has been stated that the edges of graphene sheets have high chemical reactivity due to the non-bonding π-electrons localized at the zigzag site[81], which can interact with the chemical structure of organic compounds promoting reductive reactions [43]. According to that, the application of GO-based materials is a new approach for the treatment of contaminated water. Table 1.3 summarizes the studies that have employed these carbon nanomaterials as RM in the removal of environmental contaminants from

water. Otherwise, other graphene-based materials have emerged as a new approach to multifunctional hybrid composites as mentioned below.

1.5.3. Hybrid graphene-based composites

The chemical synthesis of hybrid nanoparticles (NPs) is of interest in several research areas, especially in biomedicine, radiology, nanochemistry and electronic technologies. The functions may involve a combination of magnetic, photonic, radiological, electrical, fluorescent and delivery behaviours[115–117].

Multifunctional nanostructures combine different solid-phase chemistries in a single structure through a series of chemical synthesis steps[115]. Recently, it has been demonstrated the encapsulation of NPs or macromolecules in crumpled graphene structures[124,125]. In this sense, a continuous and simple aerosol manufacturing process has been described for the co-assembly of NPs and rGO sheet in the form of particles-filled graphene nanosacks by fast microdroplet drying[115,126,127]. Figure 1.8 shows a scheme of synthesis of graphene nanosacks.

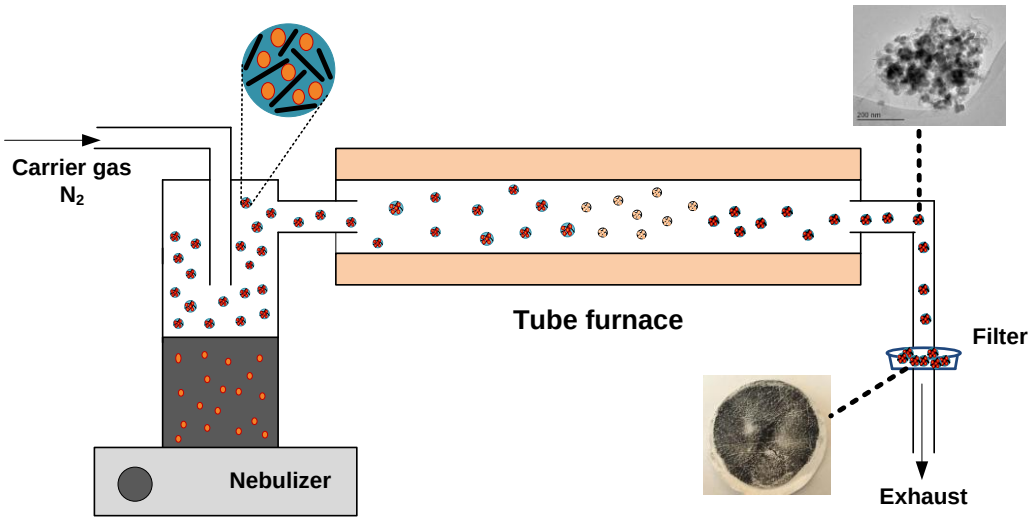

Figure 1.9. Simplified scheme of aerosol-phase synthesis of magnetic rGO nanosacks. Modified from references[115,126].

Table 1.3. Overview of reductive transformation of pollutant by GO-based materials as RM

Pollutant	Description of strategy	Reference
Azo dye (reactive red 2) and 3-chloronitrobenzene	GO was applied as electron shuttle in the removal of persistent pollutants under methanogenic and sulfate-reducing conditions in batch incubations.	118
Acid yellow 36	Application of quinone-rGO composite in abiotic and biotic systems in batch assays.	119
Nitrobenzene	Redox mediator capacity of GO GO was evaluated for enhance reduction of nitrobenzene in sulfide-containing aqueous solution in chemical batch systems.	64
Nitrobenzene	Reduced GO was used as catalyst for hydrogenation of nitrocompounds at room temperature in batch experiments.	120
Nitrobenzene	Biological transformation of nitrocompounds was performed by redox activity of novel graphene-anaerobic sludge composite in batch assays under anaerobic conditions.	121
Nitrobenzene	Reduced GO was explored as catalyst for reductive transformation of nitroaromatic pollutants by anaerobic mixed cultures in batch systems. Also, the role of their chemical properties was studied.	122
Hexachloroethane	GO was applied as RM to improve the reductive dechlorination of polyhalogenated compound by sulfide in aqueous solution and humic acids in batch experiments.	73
2,4-dinitrotoluene, pendimethalin and triflurarin	Redox properties of rGO was explored for the abiotic reduction of nitroaromatic pollutants by hydrogen sulfide through batch incubations	123

The most attractive feature of this co-assembly process is the potential to use different NPs in order to fabricate multifunctional hybrid composites with specific properties for magnetic, electrical, biomedical, sensory and energy storage applications[126,128–130]. Especially, magnetic rGO nanosacks (MrGO-N) have been applied in magnetic resonance and removal of Cr (VI) from water. However, its redox catalytic activity in reductive transformation of pollutants, like pharmaceuticals, has not been reported yet.

1.6. Motivation for this research

Nowadays, the presence of priority pollutants, which are difficult to degrade in aquatic systems, is a subject of great interest due to the toxicological problems associated with their presence both in the environmental compartments and in living organisms.

In the WWT train, secondary treatments, which involve biological processes, are very important in the degradation of persistent pollutant in water. However, due to the physicochemical properties of these pollutants, their complete degradation is difficult or in some cases nil. This is the case of IOP, which is a pollutant hardly removed due to its resistant to conventional WWT processes and thus, constantly released in receiving water bodies and soils. Accordingly, it is demanded to contribute to the development of novel treatment techniques that enhance the degradation of recalcitrant pollutants, like IOP, during the secondary treatments of WWT systems.

A new approach has emerged in the application of GO-based materials as RM for the reduction of persistent water pollutants. This application lies on the redox properties and great catalytic activity of GO-based materials, which could lead in the tailoring of these carbon materials as promising catalysts. The use of GO-based materials as RM in the degradation of organics is a promising alternative to solve the eco-toxicological problems caused by the presence of pollutants in environmental compartments. However, the main technological challenge of these redox catalysts is their application in a continuous biological system due to the facility with which can be lost during the process. Therefore, the main motivation of this doctoral thesis was to propose a novel strategy that allows GO-based materials to be retained and implemented, in a future, in the secondary treatments of WWT plants as a complementary pollutant degradation technique. According to what was

reviewed in the literature, this is the first study that proposed the use of GO-based materials in a continuous biological system, with the purpose of being used in a WWT system.

As mentioned above, several degradation techniques, especially the AOP, have shown a high removal efficiency and reduction rate of IOP. However, these processes are focused on the tertiary treatments of WWT systems. Accordingly, the novelty of this research lies in designing a hybrid treatment system, which involves physicochemical (reductive reactions) and biological (metabolic activity) processes, to be potentially tailored in the secondary treatments of WWT systems. In this sense, the redox conversion of a persistent model pollutant (IOP) by the use of GO-based materials as redox catalysts was proposed to evaluate the performance of this complementary treatment strategy.

For practical applications, it is quite important to understand the redox conversion processes of pollutants by the use of GO-based materials as RM, which involves the deep study of intrinsic properties of these nanomaterials, the importance of biological activity by microorganisms, and the reductive transformation mechanisms that take place in the reductive transformation of IOP. In this sense, this dissertation explores in detail these three key factors, contributing to scientific knowledge in the area of degradation of pollutants by the use of redox catalysts. In addition, the good understanding of the redox-mediating activity of GO-based materials is fundamental for their future application in the degradation of any pollutant in anaerobic biological treatments of WWT plants.

According to the aforementioned, this thesis evaluated, for the first time, the application of GO-based materials (GO, rGO and MrGO-N) as RM for reductive transformation of IOP from water in batch assays. In addition, the redox-mediating ability of MrGO-N was

studied in a continuous biological system at lab-scale to improve the biodegradation of IOP.

1.7. Hypothesis

The redox-mediating capacity of GO-based materials, will promote high removal efficiency and chemical/biological transformation degree of IOP in batch and biological continuous systems due to their excellent redox catalytic activity. Also, the chemical and physical properties of GO-based materials will be related to the ability to mediate reductive reactions of IOP because of their redox properties.

1.8. Objectives

1.8.1. General objectives

To evaluate the catalytic capacity of different materials based on GO as RM, in the reduction and transformation of IOP in a chemical and biological systems under reductive environments.

1.8.2. Specific objectives

- To assess the effect of the physical, morphological and surface chemical properties of GO-based materials on their redox-mediating capacity, through their detailed characterization.
- To evaluate the redox catalytic activity of GO, rGO and MrGO-N in the reduction and chemical transformation of IOP in batch assays using Na_2S as the primary electron donor.

- To study the reductive biodegradation of IOP using these nanomaterials as RM under methanogenic and sulfate-reducing conditions in batch incubations and with ethanol/lactate as electron donor and carbon source.
- To determine the catalytic effect of MrGO-N as RM in the removal and microbial transformation of IOP in a continuous biological system, using a UASB reactor under methanogenic conditions and glucose as electron donor and carbon source.
- To elucidate the reductive transformation pathway of IOP in chemical and biological systems by the identification of transformation byproducts based on high performance liquid chromatography coupled to mass spectroscopy analysis.
- To explain the possible mechanisms taking place in the reductive transformation of IOP by studying the intrinsic properties of GO-based materials as RM.

Chapter 2

Role of the intrinsic properties of partially reduced graphene oxides on the chemical transformation of iopromide*

*This chapter was adapted from: E. Toral-Sánchez, Juan A. Ascacio Valdés, Cristóbal N. Aguilar, F.J. Cervantes and J.R. Rangel-Mendez. (2016) *Carbon* **99**: 456-465.

2.1. Abstract

The role of the intrinsic properties of graphene oxide (GO) and partially reduced graphene oxide (rGO), and their use as redox mediator (RM) is reported, for the first time, on the chemical transformation of iopromide (IOP), an iodinated X-ray contrast medium, under anaerobic conditions. The structural and physicochemical properties of GO containing different types of oxygenated groups, were analyzed by Boehm titrations, point of zero charge (pH_{PZC}), pKa's distribution, scanning electron microscopy (SEM), electrochemical analysis, as well as by Raman, Fourier transform infrared and UV-Vis spectroscopy. Complete characterization of GO-based materials revealed the removal of different oxygenated groups, such as epoxy and hydroxyl groups, and a transition from an amorphous to a more crystalline structure on partially reduced GO. Moreover, when rGO materials were tested as RM, they promoted a faster and greater extent of IOP transformation up to 5.2-fold with sulfide as electron donor. Results showed a correlation between the reduction degree of GO and its ability to act as RM, which was reflected in the dehalogenation and transformation degree of IOP. Additionally, the chemical transformation pathway of IOP is proposed based on HPLC-MS analysis.

2.2. Introduction

Graphene is a two-dimensional crystal structure with a thickness of one atom, and is composed of sp^2-bonded carbon atoms densely packed in two crystal sub-networks[76]. Such two-dimensional carbon sheet possesses unique properties such as, mechanical strength, high surface area (2600 m^2/g[80]) and rapid electron transfer capacity[75], which promote its broad application in sensors, nanoelectronics, biomedicine, capacitors, among other industrial uses[76]. Also, graphene-based nanomaterials possess distinct open edges around

their periphery, allowing to have high reactivity due to their nonbonding π-electrons[131] and therefore, extraordinary catalytic activities are observed[120,132]. In addition, graphene-based materials, such as graphene oxide (GO), present a wide array of oxygenated groups in their chemical structure like hydroxyl, epoxy, carboxyl and carbonyl groups[133]. In this sense, it has been reported that the use of chemical substances with quinone groups (two carbonyl groups[60]) in their structure can mediate the transformation of organics by enhancing electron transfer processes[56,58,59]. Such chemical substances with the capacity to receive and yield electrons are known as redox mediators (RM) and they have been applied to accelerate the transformation of pollutants[55]. On the other hand, it was reported that the graphene basal planes of GO-based materials have very high electric conductivity[84,90], which has been reported as another mechanism to mediate the reductive transformation of contaminants by enhancing electron transfer, due to the electric conductivity properties of the graphitic carbon surface[132].

Carbon materials like activated carbon, activated carbon fibers, carbon xerogel, graphite and carbon nanotubes (CNT), have been used as RM in the reductive transformation of recalcitrant pollutants such as azo dyes[56,59,63], nitroaromatic compounds[57,123,134–137], nitramine compounds[134,138–140], nitroglycerin[141], nitro herbicides[142], dibromophenol[143], and tetrachloroethane[74], since they have a diversity of surface oxygenated groups like quinone groups, which can mediate the reduction of these pollutants. Recently, it was shown that graphene-based materials, such as GO and partially reduced graphene oxide (rGO), can facilitate the reduction of some recalcitrant pollutants by enhancing electron transfer[56,114]. For example, Colunga et al.,[118] reported the use of GO as RM for the biotic and abiotic reduction of an azo dye (reactive red 2) and 3-chloronitrobenzene, showing that the presence of GO increased up to 10-fold and 3.6-fold the abiotic and biotic reduction,

respectively. Similarly, Lu et al.,[119] reported a removal up to 90% for biotic and abiotic reduction of acid yellow 36 using a quinone-rGO composite as RM. Fu and Zhu[132] and Gao et al.,[120] evaluated the abiotic reduction of nitrobenzene using GO and rGO as RM, respectively, concluding that the properties of these carbon materials facilitated the reduction of this pollutant. Also, Wang et al.,[121] reported an increase up to 2-fold in the biotic transformation of nitrobenzene when a rGO-anaerobic sludge composite was used as novel biocatalyst. Fu et al.,[73] tested the capability of GO and CNT on the reductive dechlorination of hexachloroethane, concluding that the mediation efficiency of these materials is 10 times higher than humic acid material. Finally, Oh et al.,[123] investigated the abiotic reduction of nitroaromatic compounds, such as dinitrotoluene, pendimethalin and trifluralin using rGO and CNT as RM, achieving a removal for the tree pollutants of around 50% and 88% for CNT and rGO, respectively. Therefore, it can be inferred that graphene-based materials could mediate redox reactions involved in the transformation of organic compounds. However, the use of these nanomaterials on the abiotic transformation of pharmaceutical compounds has not been reported yet.

Iodinated X-ray contrast media (ICM), such as iopromide (IOP), are pharmaceuticals widely used in intravascular administration with a global consumption of approximately 3.5 x 10^6 Kg per year[144]. IOP is a priority pollutant, which is beginning to be studied because of its high recalcitrance through conventional wastewater treatment, as well as in environment compartments. Moreover, IOP has been detected in effluents from sewage treatment plants, surface water systems, groundwater, and even in drinking water at μg/L levels[24,25]. In addition, it has been reported that 15 % of people who have been exposed to this pharmaceutical have suffered some adverse reactions such as nauseas, vomiting, headache, hives, etc.[29]. Recent reports indicate that IOP is poorly removed in conventional wastewater

treatment facilities and thus it is released into receiving water bodies[30–32]. Its recalcitrance is attributed to low biodegradability by aerobic bacteria[145] and to the high hydrophilicity of the benzene ring substituents (hydroxyl and carboxyl groups)[25]. As a consequence, it is necessary to propose strategies for the reductive transformation of this pollutant.

The aim of the present work was to evaluate the intrinsic properties of both GO and partially reduced GO and their effect on the abiotic transformation of IOP in basal medium, conducted in batch systems, and to explain the reduction mechanisms taking place under non-oxidizing conditions. Additionally, the chemical surface and morphological characterization was carried out by Fourier transform infrared spectroscopy, Boehm titrations, point of zero charge (pH_{PZC}), pKa's distribution, scanning electron microscopy (SEM), electrochemical analysis, Raman and UV-Vis spectroscopy, in order to elucidate the importance of these properties in the ability to act as electron shuttle.

2.3. Experimental

2.3.1. Chemicals

All chemicals with 99% purity were used as received. IOP (CAS No. 73334-07-3) was obtained from Bayer Schering Pharma (Mexico City, Mexico) with commercial name Ultravist® 370; L-ascorbic acid (L-AA, ACS grade) from GOLDEN BELL (Mexico City, Mexico) and sodium sulfide ($Na_2S{\cdot}9H_2O$) from Fisher-Scientific (New Jersey, USA). The basal medium (pH = 7.6) used in abiotic reduction assays was composed of (g/L): K_2HPO_4 (0.25), $NaHCO_3$ (5.0), $MgSO_4{\cdot}7H_2O$ (0.1), NH_4Cl (0.28), $CaCl_2{\cdot}2H_2O$ (0.01), and trace elements (1 mL/L), with a composition described elsewhere[58]. A phosphate buffer (pH= 7.0) was used during electrochemical analysis with a composition of (g/L): K_2HPO_4 (3.32) and KH_2PO_4 (4.21). All chemicals used for basal medium and phosphate buffer elaboration

were obtained from either Sigma-Aldrich or Merck. All solutions were prepared with deionized water (18.1 MΩ·cm).

Commercial graphene oxide used in the present study was purchased from Graphene Supermarket® (New York, USA), which has the following characteristics: high density and viscosity, concentration of 6.2 g/L in aqueous solution, single-layer > 60 %, flake size between 0.5 and 5 µm, C/O ratio 3.95.

2.3.2. Chemical reduction of GO

GO was reduced with L-AA as follows: 10 mL of GO solutions (0.1 mg/mL) and 100 mg of L-AA were placed in a 30 mL beaker. Immediately, samples were vigorously stirred at room temperature. In order to obtain materials with different reduction degrees, reduction kinetics of GO were carried out for 0.5, 1, 1.5, 2, 3 and 4 hours. After the reduction time, samples were centrifuged at 13,300 rpm for 10 min in order to remove all L-AA remaining by decantation. Recovered rGO was rinsed with deionized water three times and then dispersed in the same medium (deionized water).

2.3.3. Physical and chemical characterization of GO-based materials

2.3.3.1. Zeta potential and oxidation reduction potential (ORP)

Zeta potential measurements of samples were performed in aqueous solution at pH 7.0 in a MICROTRAC Zetatrac NPA152-31A equipment. On the other hand, ORP of GO samples and of IOP were assessed under experimental conditions of chemical reduction using a Thermo Scientific electrode with a reference solution of Ag/AgCl Orion 900011 (+415 mV at 30°C). All ORP measurements were performed inside an anaerobic chamber with a N_2:H_2 (95:5% v/v) atmosphere.

2.3.3.2. Chemical characterization of GO samples

Fourier transform-infrared (FT-IR) spectra were recorded on a Thermo-Scientific FTIR (Nicolet 6700 model) spectrophotometer in transmission mode with a resolution of 4 cm^{-1} and 128 scans. For sample preparation, GO-based materials were mixed with KBr at a ratio of 1:99% (w/w) for subsequent drying at 60 °C for 48 h, and then compressed into a transparent pellet for measurement.

Carbonyl, phenolic, lactonic and carboxylic groups were quantified by potentiometric titrations as described by Boehm[146] with an automatic titrator (Mettler-Toledo T70) as follow: 0.05 g/L of GO-based materials were contacted with 25 mL of neutralizing solutions. The solutions were continuously stirred at 125 rpm for 5 days. After that, samples were titrated with 0.1 N HCl. The point of zero charge (pH_{PZC}) of GO-based materials was determined according to Bandosz [147] with the automatic titrator mentioned above. For this procedure, 0.005 mg/mL of GO-based materials were contacted with 25 mL of 0.01 N NaCl. The solutions were stirred at 125 rpm for 24 h. Finally, the samples were titrated with 0.1 N NaOH. The surface charge and pKa distributions were determined by the SAEIU-pK-Dist© (1994) program[148].

2.3.3.3. Morphological and optical properties

Microscopic observations were carried out on a FEI Helios Nanolab 600 Dual Beam Scanning Electron Microscope (SEM) operated at 5.00 kV and 86 pA. Samples were suspended in isopropanol and then sonicated for 30 min. Elemental analyses were carried out by energy dispersive spectrometer (EDS) on the same equipment. Raman spectra were recorded at room temperature with a RENISHAW Micro-Raman Invia spectrometer with laser frequency of 514 nm as excitation source trough a 50 X objective. UV-Vis

transmittance spectra of GO-based materials in aqueous dispersion were collected by a Thermo Spectronic Aqua Mate UV-Vis spectrophotometer at a wavelength of 550 nm. The wavelength scan was performed from 400 to 600 nm using deionized water as blank.

2.3.3.4. Electrochemical characterization

Electrochemical analysis of GO-based materials was assessed by cyclic voltammetry (CV) technique using a VSP SAS Biologic system controlled by the EC-Lab software V 10.23 with a three-electrode cell configuration containing a Ag/AgCl/KCl (sat) as the reference electrode, and a graphite rod and glassy carbon electrode (GCE) as the counter and working electrode, respectively. The electrolytic solution was a phosphate buffer at pH 7.0 (See section 2.3.1) saturated with argon for 5 min. All experiments were carried out at room temperature. The working electrode was prepared as follows, GO or rGO was dispersed in ethanol (spectrophotometric grade) and then 8 µL were suspended in the GCE surface. Ethanol was volatilized and the material remained deposited on the GCE surface. Before deposition, the GCE was polished in a nylon cloth with alumina suspension.

2.3.4. Adsorption isotherms

These experiments were conducted to evaluate the IOP adsorption capacity of the GO-based materials at pH of basal medium (pH= 7.6, see Section 2.3.1). Into plastic tubes of 15 mL of capacity, 5 mg/L of materials and IOP (from 200 to 800 µg/L) were added. Afterwards, the tubes were filled with basal medium to give a total volume of 10 mL. Samples were kept under stirring and constant temperature (125 rpm and 25 °C) for 5 days. The remaining concentration of IOP in solution was measured by high-performance liquid chromatography (HPLC) as described in Section 2.3.6.

2.3.5. Chemical transformation of iopromide

The capacity of GO-based materials to serve as RM in the chemical transformation of IOP was evaluated providing Na_2S as primary electron donor. Sulfide is an important reducing compound commonly found in several industrial effluents, and their use as electron donor for redox conversion of different pollutants has been reported[55]. To assess this abiotic reduction, batch incubations were prepared in 60 mL serum flasks as follow: 5 mg/L of GO or rGO were contacted with basal medium and then bubbled for 5 min with a gas mixture of N_2:CO_2 (80:20 %). The flasks were sealed and the gas headspace was flushed for 3 min with the gas mixture mentioned above. Inside an anaerobic chamber (N_2:H_2 (95:5%) atmosphere), sulfide was added from a Na_2S stock solution to obtain a final concentration of 2.6 mM. Bottles were incubated for 24 h with constant stirring and temperature (125 rpm and 25 °C). After pre-incubation, IOP was added from an anaerobic stock solution in order to obtain an initial concentration of 400 µg/L. The total working volume was 50 mL in all incubations. The experiments were carried out for 13 days in the dark. Samples of 1 mL were taken at selected times and the concentration of IOP was measured as described in Section 2.3.6. Control experiments without GO-based materials and/or Na_2S were performed to evaluate the stability of IOP, the direct reduction by sulfide and the adsorption onto the materials.

2.3.6. Analytical procedures

The concentration of IOP was measured by HPLC using a Agilent Technology 1260 series chromatograph, equipped with a column synergi 4U Hydro-RP 80R (250 x 4.60 mm, 4 micron) from Phenomenex. Forty microliters of sample were injected with an autosampler. The mobile phase, composed of HPLC grade water and acetonitrile (85:15 %), was pumped

at a flow rate of 0.5 mL/min. IOP was detected at 30 °C and wavelengths of 238 nm with an Agilent Technologies diode array detector. For the quantification of IOP concentration in solution during adsorption and chemical reduction experiments, a calibration line with different concentrations of IOP (from 100 to 1000 µg/L) in basal medium was performed. The peak area according to each concentration was measured in a retention time of 11.6 min. The detection limit was 100 µg/L.

The transformation products of IOP were identified by HPLC coupled to mass spectroscopy (HPLC-MS) in a Varian ® 500-MS ion trap mass spectrometer, with electrospray ionization of 90 V and mass-to-charge (m/z) range of 100 to 2000 m/z. The transformation pathways of IOP were elucidated according to molecular weight of IOP byproducts identified by HPLC-MS. The structure and chemical formula of transformation byproducts of IOP were proposed using the software ChemBrioDraw Ultra 12.0, based on previous reports in literature. Similarly, the transformation pathways of IOP proposed in **Chapter 3, 4** and **5** were elucidated according to this methodology.

2.4. Results and discussion

2.4.1. Characterization of GO and rGO materials

Seven samples of GO-based materials with different reduction degrees were analyzed by zeta potential and ORP. As known, zeta potential is a physical property exhibited by any material in dispersion and measures the potential difference between the dispersion medium and the stationary layer of fluid attached to dispersed particles[149,150]. Figure 2.1 shows that zeta potential values increased from -23.41 to 25.26 mV as GO was farther reduced for up to 4 h (rGO-4). Negative zeta potential values are due to the presence of negatively charged functional groups, like oxygenated groups, present at the graphitic layers[151]. When the

reduction degree of GO increased, a greater concentration of negatively charged functional groups are eliminated in GO sheets, resulting in an increase on zeta potential values[150]. For this reason, rGO-4 has the most positive zeta potential value (25.26 mV).

ORP is an important parameter to assess the ability of a chemical compound to accept or donate electrons under particular conditions[152]; therefore, it is a fundamental parameter related to the redox mediating activity. In this sense, carbon materials, like GO, exhibit redox activity, which is related to the oxygenated functional groups in the material[153]. The results reported also in Figure 2.1 show that ORP noticeably increased from 60.8 mV for GO to 501.9 mV for rGO-4 as GO was less oxidized, which may be because aromatic ring substituents, such as carbonyl groups, tend to accept electrons when oxygenated groups are eliminated from the basal plane[60,154,155]. Also, it has been reported that quinone groups (a couple of carbonyl groups) can act as electron acceptors[60]. In this sense, the electron activity of quinone groups consist in that carbonyl groups can act in concert to stabilize radicals via resonance. Resonance considerations permit the stabilization of radicals in equilibrium with quinonoid structures. After that, these radicals can accept electrons and become anions. Next, the anions can transfer electrons back and become radicals, or they can interact with protons in solution. Finally, the reversible proton transfer leads to form of phenolic (hydroquinone) sites[60]. As will be discussed below, the carbonyl groups remain after reduction of GO, which might satisfactorily explain the increase in ORP values due to their ability to accept electrons as explained above.

According to these results, three samples were selected for further analysis: GO, rGO for 2 h (rGO-2) and rGO-4 since they contain a low, intermediate and high ORP, which should be a key factor on the electrons transfer during the chemical reduction of IOP.

Photographic images of GO, rGO-2 and rGO-4 are shown in appendix section (AS, Figure A1). A color change from brownish yellow (Figure A1-a) to black (Figure A1-c) was observed as the reduction degree of GO was greater, which is probably a result of an increase in the hydrophobicity of rGO materials, caused by the removal of oxygenated groups, that subsequently causes the agglomeration of graphene-based nanosheets[84] as can be seen in the micrographs reported in AS (Figure A2).

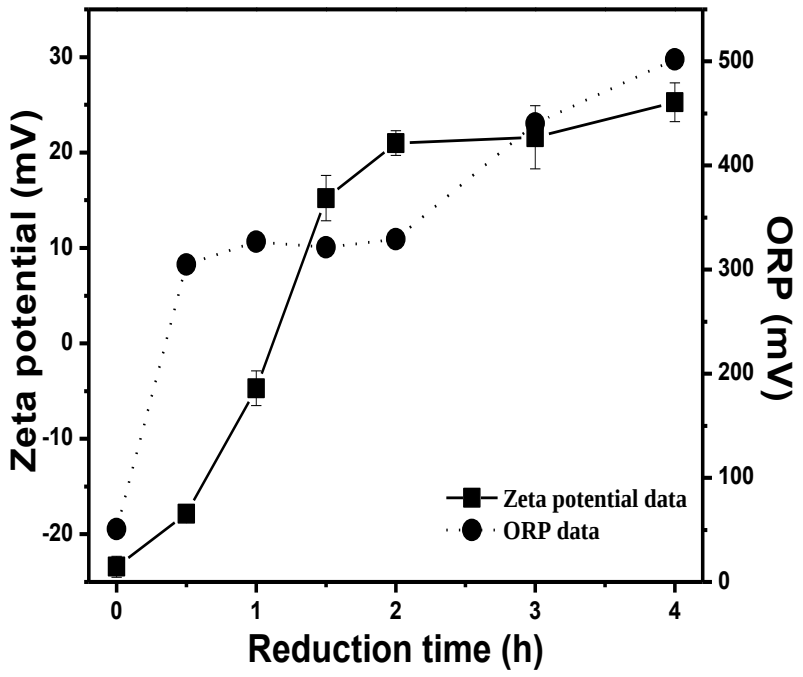

Figure 2.1. Zeta potential (square symbols) and oxidation reduction potential (ORP, circle symbols) of GO-based materials with different reduction degrees at pH 7.

Several studies have reported that transmittance spectra can be used to determine the transparency of GO, which is intrinsically linked to its morphology[156,157]. Nair et al.,[158] estimated that each graphene sheet reduces 2.3 % the transmittance at 550 nm. Therefore, the number of sheets in GO samples was measured under these experimental conditions. Transmittance percent at 550 nm was obtained from the corresponding spectra and it is

shown in AS (Figure A3). Insert of Figure A3, depicts the estimated number of sheets in each sample in aqueous suspension according to Nair et al.[158]. It can be observed that the sheets number integrating the GO-based materials is approximately 6, 22 and 27 for GO, rGO-2 and rGO-4, respectively. This can be attributed to the removal of oxygenated groups as a result of the chemical reduction, which consequently produces hydrophobic graphene sheets that tend to restack due to strong π-π interactions[159]. Hence, graphitic layers are attached to each other, forming materials consisting of a greater number of sheets.

Raman spectroscopy was employed to distinguish the ordered and disordered crystal structures of GO-based materials. Figure 2.2 shows Raman spectra of GO and rGO samples. The presence of G and D bands for GO spectrum at 1599 cm^{-1} and 1354 cm^{-1}, respectively, is evident. The D band corresponds to defects in the graphite network, which are related to the presence of edges of graphitic planes, atomic vacancies, bond-angle disorders, bond-length disorders or oxygenated groups [160,161]. On the other hand, the G band is related to defect-free graphite networks[162], corresponding to the first-order scattering of E2g mode[163]. The reduction of GO should result in structural changes, therefore, it is expected that GO undergoes morphological changes after it has been chemically reduced due to the removal of different oxygenated groups at the basal plane and also at the edges. Raman spectra for rGO-2 and rGO-4 confirm this observation (see Figure 2.2). The G band is moved to a lower wavelength (1595 cm^{-1}), which is closer to the reported value for pristine graphite (1570 cm^{-1}), indicating that the chemical reduction of GO was conducted[98]. Moreover, the relative intensity of the D band around 1350 cm^{-1} increases as the reduction degree is higher, which apparently contradicts the idea that the reduction process should restore the graphitic order as expected by theory. This behavior can be explained due to the holes formed by CO and CO_2 evolution from oxygenated

groups removal forming internal edge sites, which might increase the D band upon deoxygenation. On the other hand, Stankovich et al.,[84] suggested that this behavior is due to that reduction increases the number of aromatic domains of smaller overall size in graphene, which would lead to an increase of the I_D/I_G ratio as will be discussed later. However, Paredes et al.,[103] are at odds with this assumption based on the decrease of the 2D band at 2920 cm^{-1} of GO spectrum. They suggest that this contradiction can be explained by assuming that the carbon lattice in GO has certain degree of amorphous character due to the oxidation process itself[103]. Because the GO sheets contain many oxygenated groups in their chemical structure, a significant distortion of the aromatic rings occurs, and hence, a certain amorphous character is expected after the reduction process due to the remaining oxygenated groups in this material[102]. Therefore, an increase in the intensity of the D band after the GO chemical reduction can be possible [84] as reported by several studies[84,98,102,103,109].

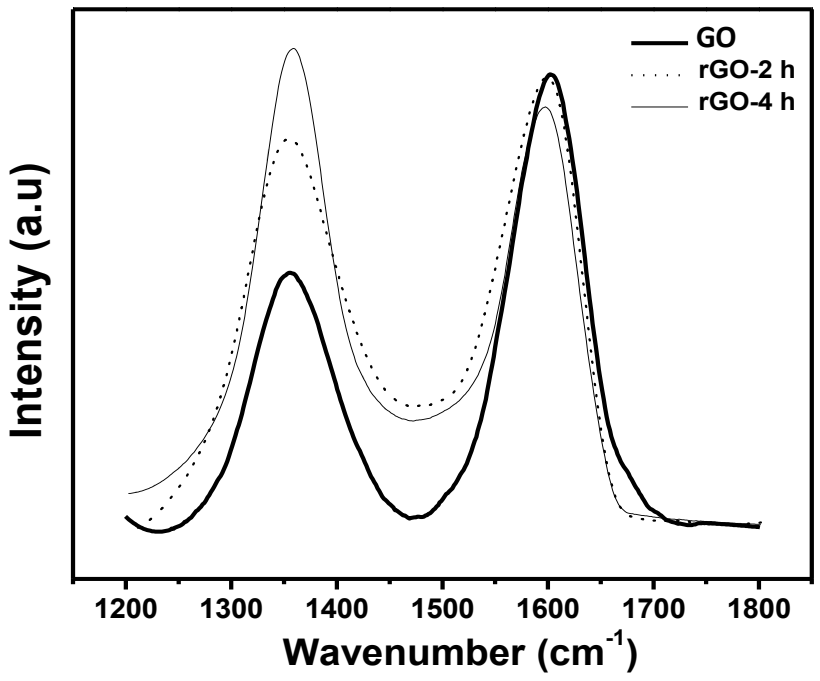

Figure 2.2. Raman spectra of GO-based materials.

On the other hand, it can be seen that the intensity ratio I_D/I_G increased with the reduction degree as follows: 0.56, 0.88 and 1.16 for GO, rGO-2 and rGO-4, respectively. This change suggests a decrease in the average size of the sp^2 domains after chemical reduction of GO[163], due to the partially ordered graphite crystal structure of graphene sheets[84]. Many equations have been employed to estimate the average crystallite size of the sp^2 domains (La) in GO samples using the I_D/I_G ratio[163,164]. Hence, the La values (in nm) of the GO-based materials under study were calculated based on the Cancodo et al., modified equation[165]. The calculated La values are 29.99, 19.48 and 14.69 nm for GO, rGO-2 and rGO-4, respectively. These results indicate that the average crystallite size decreased as the reduction degree of the samples is higher, which can be due to the breakdown of crystallites with initial oxidation[150]. Also, this decrease can be explained by the creation of new graphitic sp^2 domains, which are smaller in size than those present in GO[84]. The La values showed the transition from amorphous GO to a more crystalline form as the reduction grade advanced.

It is clear that the surface chemical properties of GO changed as it was reduced, as shown in Table 2.1. The total concentration of acidic groups decreased from 4.39 to 1.65 milli-equivalents (meq)/g when GO was chemically reduced for 4 h, mainly due to the removal of carboxylic, lactonic and phenolic groups. Moreover, we can observe a reduction percentage (based on total concentration of oxygenated groups) of 19.1 and 64.4 for rGO-2 and rGO-4, respectively. Also, a slight decrease on carbonyl groups was observed, from 1.23 to 1.1 meq/g. Chemical deoxygenation of GO is complex and may be selective to certain groups, depending on the reducing reagent[77]. In this sense, the binding energy between graphene sheets and different oxygenated groups can be an important index to evaluate the reduction of each group attached to the carbon plane[77]. Kim et al.,[166] reported

that epoxy groups are more stable than hydroxyl groups in GO. However, Gao et al.,[101] reported that oxygenated groups attached to the inner aromatic domain are not stable at room temperature and hence, they are removed more easily than those attached at the edges of an aromatic domains. In addition, the authors suggested, based on theoretical calculations, that carboxylic groups are slowly reduced, while carbonyl groups are much more stable. As can be seen in Table 2.1, carbonyl groups were less removed, which may be due to their greater stability in comparison with the other oxygenated groups. Moreover, Gao et al.,[109] proposed that the reduction of GO using L-AA is carried out by two-step SN_2 nucleophilic reactions, where epoxy and hydroxyl groups could be opened by the oxygen anion of L-AA with a SN_2 nucleophilic attack. On the other hand, according to the literature, quinone and chromene groups, which are of particular interest in the present study, have been proposed to act as redox mediators[60,153].

As known, the surface charge distribution and pH_{PZC} of carbon-based materials depend on the type and concentration of oxygen-containing groups. These results are included in Table 2.1 and AS (Figure A4). The pH_{PZC} of GO samples increased as their reduction degree was higher, from 2.3 for GO to 6.55 and 7.25 for rGO-2 and rGO-4, respectively. The acidic surface and low pH_{PZC} of GO is due to high concentration of carboxylic, lactonic and phenolic groups[167]. Accordingly, Boehm titrations (see Table 2.1) revealed that the concentration of carboxylic and phenolic groups decreased about 85% in rGO-4 sample, which was reflected in higher pH_{PZC}[168]. This is in agreement with FT-IR spectra analyses that provided additional evidence of a decrease in acidic oxygenated groups, which will be discussed later.

Table 2.1. Surface chemical properties of GO-based materials with different reduction degrees

Samples	Acid-base functional groups, (meq/L)					Point of Zero Charge (pH_{PZC})
	Carboxylic	Lactonic	Phenolic	Carbonyl	Total	
GO	1.30	1.26	0.59	1.23	4.39	2.30
rGO-2	0.34	0.84	0.21	1.29	3.55	6.55
rGO-4	0.20	0.21	0.14	1.10	1.65	7.25

The surface of carbon materials may contain several functional groups whose acid-basic characteristics may or may not resemble those of individual compounds. Therefore, the presence of ionizable functional groups in the material can be given by their pKa (or pH) values[60]. Distribution of pKa values of GO samples is shown in AS (Figure A5). It can be observed that the most prevalent pKa value of oxygenated groups present in GO is 2.31, which corresponds to carboxylic groups giving acidic character to the material[60]. Also, when the reduction degree of GO is higher, the most marked values are 8.25 and 10.28, suggesting the increase in basicity. It is to be noted that GO is known to be unstable at high pH OH^- can catalyze the conversion of epoxides groups to hydroxyls groups[169]. Hence, the interpretation of pKa values at high pH must be taken with care. On the other hand, the observed distributions of pKa values of ionizable oxygenated groups explain the increases of the pH_{PZC} of samples when these are further reduced (see Table 2.1). Similar results have been reported by Konkena and Vasudevan[170]. They concluded that GO sheets have more acidic groups, such as carboxylic groups (pKa 4.3), in comparison with rGO sheets (pKa 8.0), which was reflected in the increase of zeta potential values.

In order to evidence the removal of different functional groups through the reduction process of GO, FT-IR spectra were recorded as shown in Figure 2.3 It can be observed the stretching vibration of O-H groups from 3000 to 3700 cm^{-1}. The GO spectrum

(Figure 2.3A) shows bands at 1720 and 1570 cm^{-1}, corresponding to C=O stretching vibrations from carboxyl and carbonyl groups, respectively. Furthermore, stretching vibrations of C-OH (1390 cm^{-1}), C-O from epoxy groups (1100 cm^{-1}) and ketone groups (600-630 cm^{-1}) can be observed[3,8,21,22]. As shown in rGO-2 and rGO-4 spectra (Figure 2.3B and 2.3C), intensities of FT-IR bands associated to oxygenated groups, such as C-OH (1390 cm^{-1}) and C=O (1720 from carboxylic groups) slightly decreased, which agrees with data obtained by Boehm titrations (see Table 2.1). Also, the bands intensity of C-O stretching vibration (1100 cm^{-1}) dramatically decreased and the spectral signal related to ketone groups (600-630 cm^{-1}) disappeared. Furthermore, the appearance of aromatic C=C stretching vibration at 1620 cm^{-1} was also observed[100,108,110]. These results show that the bands intensities associated to oxygenated groups strongly decreased with respect to GO, indicating the efficiency of L-AA as reducing agent. Some studies have reported that L-AA mainly remove epoxy and hydroxyl groups[110,111,171].

In addition, FT-IR spectra of GO, rGO-2 and rGO-4 exposed to Na_2S for 1 day (GO-based materials were in contact with 2.6 mol/L of Na_2S at 25 °C and 125 rpm, and dried before analysis) showed that only rGO-based materials exhibit a band at 668 cm^{-1} associated to C-S stretching vibration (see Figure A6). This link can be formed due to the high nucleophilicity of reactive HS^- species and to the charge deficiency on the carbon of the carbonyl groups on rGO materials under study[57]. On the other hand, the reduction of GO by sulfur-containing compounds, such as Na_2S and Na_2SO_3, has been previously reported[172]. However, FT-IR spectra of rGO materials did not show a significant decrease of oxygenated groups, which suggest that sulfide, did not promote reduction of these functional groups in GO materials.

Besides, oxygenated groups present in GO-based materials play a fundamental role in their electrochemical properties[173]. Accordingly, the electrochemical evaluation of GO-based materials deposited on a GCE was carried out by the CV technique as shown in Figure 2.4 It can be observed the reduction peak of GO at -0.82 V (*vs* Ag/AgCl/KCl (saturated)) with a peak current of -0.072 mA. Ramesha and Sampath[174] reported that the reduction of GO is an irreversible electrochemically process, which began at -0.6 V (*vs* saturated calomel electrode (SCE)) and reaches a maximum at -0.87 V (*vs* SCE). Moreover, an inherent reduction peak of GO in the cathodic region around -0.7 and -0.8 V (*vs* Ag/AgCl) has been reported, due to possible reduction of epoxy, peroxy and aldehyde groups[175]. As it was observed in the FT-IR spectrum of GO, one of the identified oxygenated groups is of epoxy type at 1100 cm^{-1}. Therefore, this peak (at -0.82 V) may be related to the reduction process of these oxygenated groups present in GO.

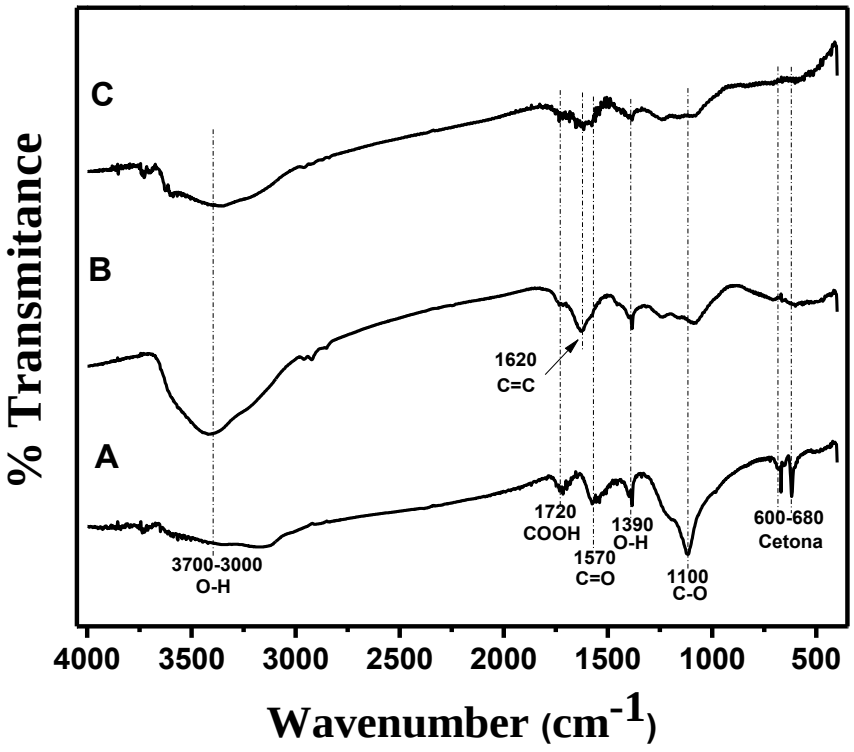

Figure 2.3. FT-IR spectra of GO-based materials: (A) GO, (B) rGO-2 h and (C) rGO-4 h.

Furthermore, it can be seen (Figure 2.4) that the intensity of the cathodic peak current (I_{PC}) varies according to the reduction degree of samples, with values of -0.031 and -0.025 mA for rGO-2 and rGO-4, respectively. It has been reported that a greater C/O atomic ratio in rGO materials is correlated with an improved electron transferring capacity, which is reflected in the current intensity[176]. In order to determine the amount of carbon and oxygen on GO-based materials, an EDS analysis was performed. Results indicated that the carbon content in GO, rGO-2 and rGO-4 was 22.8, 37.9 and 68.9 %, respectively. Similarly, the content of oxygen in GO, rGO-2 and rGO-4 was 77.2, 62.1 and 31.1 %, respectively. As evidenced, rGO materials contain a minor amount of oxygenated groups in their chemical structure as observed also in both FT-IR spectra and Boehm titrations, which increases the C/O ratio as the reduction degree advances. As a consequence, the removal of these oxygenated groups favors the electrons transfer along the graphitic sheets, which is reflected on the GO conductivity.

2.4.2. IOP Adsorption isotherms

Capacities of GO-based materials to adsorb IOP are reported in Figure 2.5. The maximum adsorption capacities for IOP at an equilibrium concentration of 600 µg/L follow this order: GO> rGO-2 > rGO-4 with values of 436.37, 343.92 and 204.31 µg/g, respectively. This decrease in the IOP adsorption capacity onto rGO-based materials can be due to that the active sites in rGO are less accessible since graphene sheets tend to stack due to π-π interactions, which significantly decrease the adsorbent surface area available to IOP molecules. As mentioned in section 2.4.1, the removal of oxygenated groups of GO sheets increase the hydrophobicity of rGO materials forming graphene-based materials agglomerates by π-π interactions[84], which decrease the active area of materials.

Furthermore, it is possible that the IOP adsorption mechanism involves hydrogen bonding interactions between ionized functional groups of GO-based materials and the hydroxyl groups present in IOP molecules[177], as shown in Figure A7 of AS.

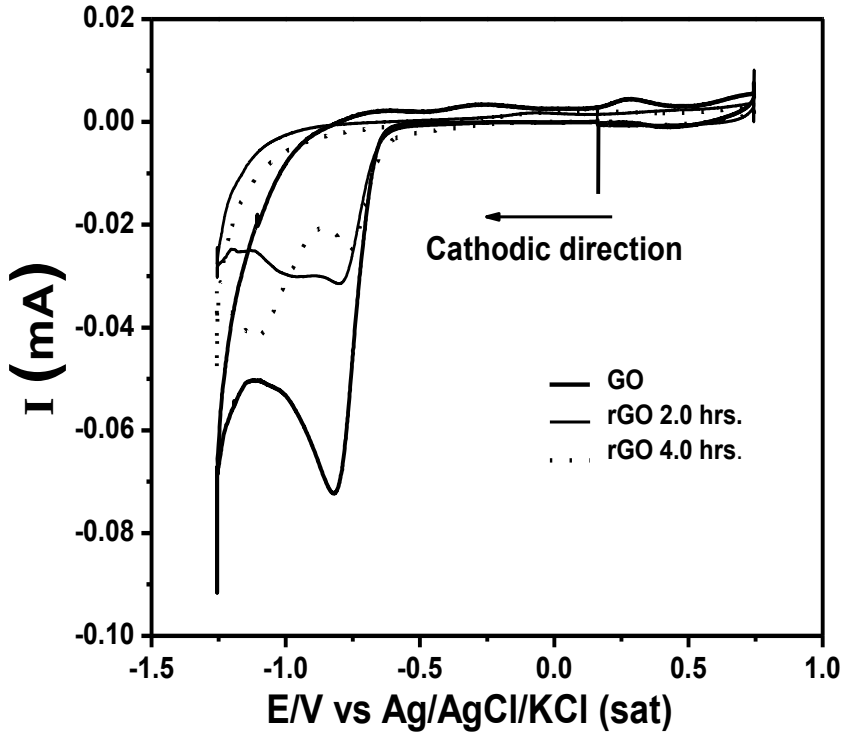

Figure 2.4. Cyclic voltammetry of GO-based materials deposited on GCE electrode and immersed in a phosphate buffer (pH 7.6). The potential scan started at 0.16 V (*vs* Ag/AgCl/KCl (sat)) in cathodic direction to a scan rate of 20 mV/s.

2.4.3. Chemical transformation of IOP

Chemical transformation of IOP by sulfide and the corresponding control experiments are shown in Figure 2.6. The chemical reduction experiments (Na_2S + GO-based materials + IOP) exhibited a decrease in IOP concentration with removal efficiencies of 54, 58 and 66 % for incubations amended with GO, rGO-2 and rGO-4 as RM, respectively. In contrast, control incubated in the absence of RM (Na_2S + IOP) achieved only 25% of IOP removal after 13 days. Adsorption controls (GO-based materials + IOP) showed a diminishment on

the concentration of IOP < 10% in all cases. Also, a negligible removal (< 4%) occurred in stability control during the same incubation period. Moreover, the difference in IOP removal between these experiments and the adsorption controls can be attributed to the conversion of IOP to transformation byproducts.

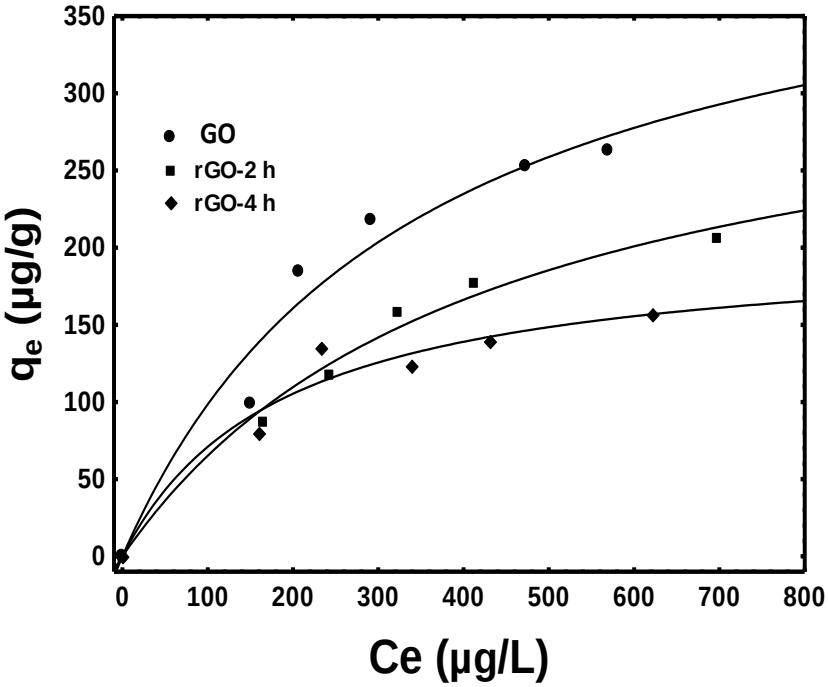

Figure 2.5. Adsorption isotherms of IOP on GO-based materials with different reduction degrees at pH 7.6 and 25 °C.

In addition, the maximum removal rates achieved in assays amended with GO, rGO-2 and rGO-4 were 35.84, 59.79 and 64.74 µg/L-d, respectively. Moreover, the maximum removal rate achieved in the control incubated in the absence of GO-based materials was 12.48 µg/L-d. These results indicated a 1.6 and 1.8-fold increase in the maximum removal rate of IOP in the presence of rGO-2 and rGO-4, respectively, with respect to GO. Moreover, the maximum removal rate of IOP increased 2.8, 4.8 and 5.2-fold in the presence of GO, rGO-2 and rGO-4, respectively, with respect to the control lacking GO-based materials. These results demonstrate that GO-based materials promoted a faster removal of IOP. In the

following section, it will be confirmed that GO-based materials serve as effective redox mediators achieving a greater extent of IOP transformation.

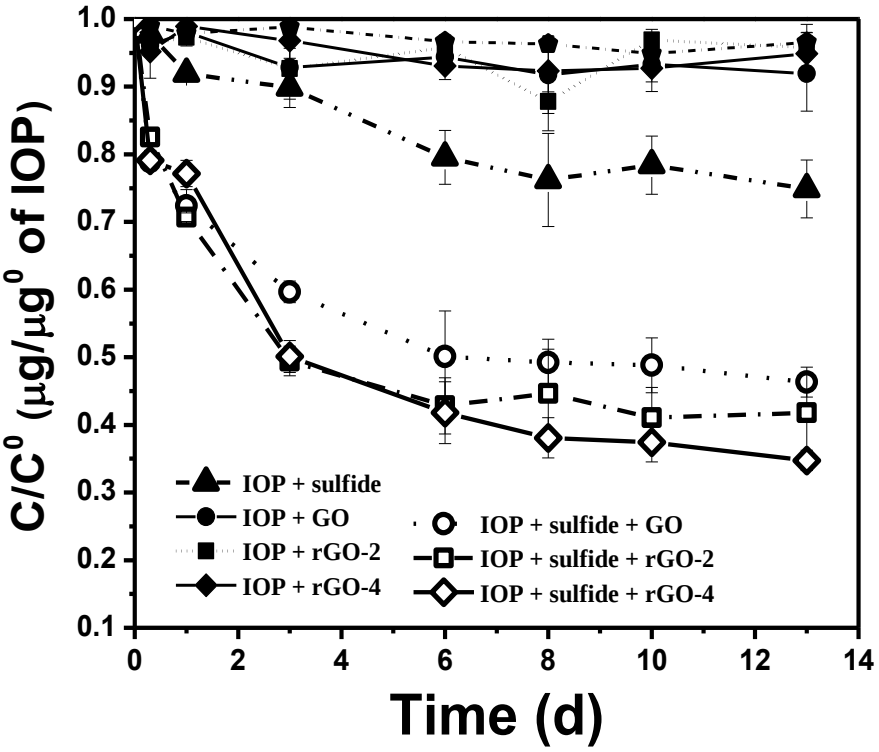

Figure 2.6. GO-based materials catalysis of IOP reduction by sulfide. IOP stability control (pentagon symbol), direct chemical reduction control (triangle symbol, IOP + Na_2S), adsorption controls (full symbols, IOP + GO-based materials) and reduction experiments (open symbols, IOP + Na_2S + GO-based materials) of GO (circles), rGO-2 h (squares) and rGO-4 h (Diamonds).

2.4.4. Transformation pathway of IOP

Samples derived from reduction experiments of IOP in the presence of rGO-4 as redox mediator were analyzed by HPLC-MS in order to propose the transformation pathway of IOP. Based on HPLC-MS analysis, six transformation products (TPs, see Figure A8 in AS) were identified and the suggested chemical transformation pathway of IOP is shown in Figure 2.7.

The structure of TP 788.70 (elemental composition $C_{18}H_{22}I_3N_3O_8$) was proposed by Eversloh et al.,[45], which indicates that this intermediate could be obtained by a loss of two hydrogen atoms at either side chain A or B. The structure of this TP is exemplified in Figure 2.7 as the loss of hydrogen atoms taking place in side chain A. The structure of TP 774 (elemental composition $C_{18}H_{24}I_3N_3O_7$) implies the loss of a molecule of H_2O at side chain B as reported by Pérez et al.,[50] and Gros et al.,[36]. Also, the structure of TP 722.5 (elemental composition $C_{15}H_{20}I_3N_3O_6$) suggests the loss of a molecule of H_2O, demethylation and decarboxylation in side chain B and N-demethylation in side chain A. Similar mechanisms and structure have also been proposed by Gros et al.[36].

The cleavage of the amide bond in side chain B and removal of one iodine atom (HI) of TP 788.7 results in the formation of TP 574 (elemental composition $C_{15}H_{15}I_2N_2O_6$) as shown in Figure 2.7. This structure is similar to that reported by Gros et al.[36]. Moreover, the structure of TP 634.60 (elemental composition $C_{17}H_{23}I_2N_3O_7$) was proposed according to previous studies[36], which indicate that this intermediate is formed by the loss of one iodine atom (HI) and N-demethylation in side chain A of TP 774. Finally, the structure of TP 314.8 (elemental composition $C_{10}H_4INO_3^+$) suggests the removal of side chain A and one iodine atom (HI) of TP 574. The removal of HI yielded a five membered ring structure in side chain C. Similar transformation pathways were reported by Schulz et al.,[28] under aerobic conditions.

The results obtained from batch experiments performed without RM (IOP + Na_2S control) revealed that the main TPs produced were 646.9, 768.7 and 788.8 (See AS, Figure A7). According to these results, it can be concluded that the presence of GO-based materials as RM promoted a higher extent of IOP transformation (involving dehalogenation,

dehydration, demethylation and decarboxylation reactions), as compared to control incubations performed in the absence of GO-based materials, which was evidenced by the formation of TPs with low m/z, such as TP 634.6, TP 574 and TP 314.8. The reductive transformation of IOP and distinct capacities of GO-based materials to act as redox mediator can be explained by their surface chemistry as discussed in the next section.

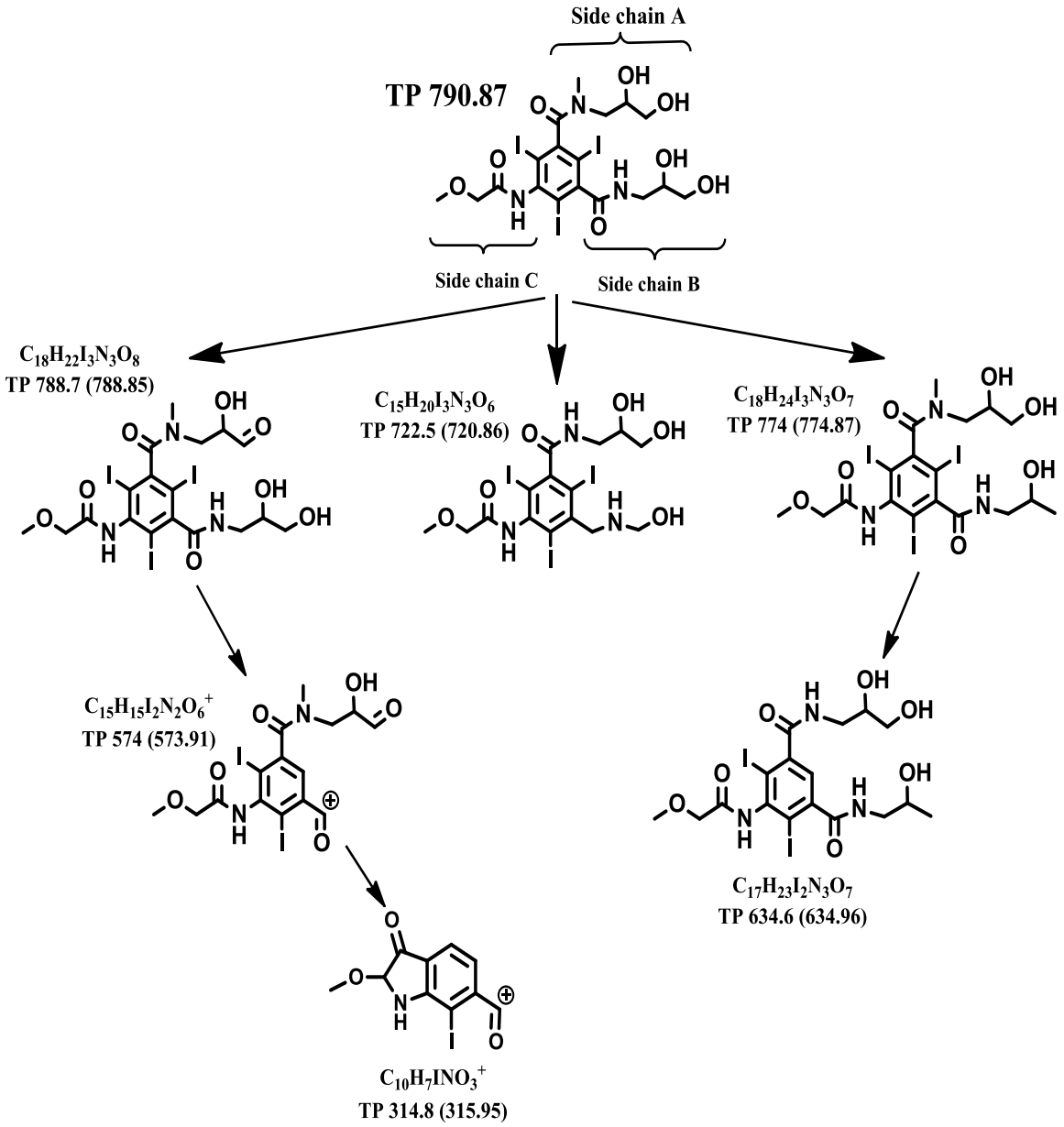

Figure 2.7. Proposed chemical transformation pathway of IOP and final products by rGO-4 h as redox mediator.

2.4.5. Mechanisms of IOP transformation mediated by GO-based materials

The proposed transformation mechanism implies that GO-based materials promoted dehalogenation, dehydration, demethylation and decarboxylation reactions in IOP molecule. Previous studies have reported that carbonaceous materials can mediate reductive reactions of organic compounds by enhancing the electron transfer involved in the reactions[56,114]. In this sense, the reduction of pollutants, such as nitroaromatics, azo dyes and polyhalogenated compounds, promoted by GO as redox mediator has been reported[73,118,119,132]. In addition, it has been reported that the zigzag edges of reduced GO can accelerate the reduction reaction of reactants[120]. In consequence, the increased IOP transformation observed in the presence of rGO-materials can be explained by enhanced electron transfer and possibly by activation of IOP molecules. As mentioned above, the basal plane of GO sheets has very high electric conductivity that depends on the presence of epoxy and hydroxyl groups and is generally proportional to the C/O ratio. As mentioned in section 2.4.1, as the C/O ratio increased in rGO materials the electron transfer on basal plane improved, which was reflected in an increased reduction of IOP. Additionally, as revealed by Boehm titration results (see Table 2.1) rGO materials have a higher percentage of quinone groups (referring to two carbonyl groups), which could contribute to the reduction of IOP since these functional groups serve as redox mediating moieties [60,153] and improved the electric conductivity, i.e. electron transfer of the materials, making best mediators for electron transfer[132].

On the other hand, it has been reported that carbonaceous materials with basic properties exhibit a better performance to transfer electrons through quinone groups or delocalized π-electrons[68]. As discussed in section 2.4.1, the basic properties of GO-based materials increased with the reduction degree, which was reflected in a higher pH_{PZC} (see Table 2.1).

This also explains why the reductive transformation of IOP increased when the materials used as redox mediator had a greater reduction degree.

Additionally, it has also been stated that the carbon atoms at the zigzag edges of graphene sheets have high chemical reactivity due to the non-bonding π-electrons localized at the zigzag site, and hence, are able to interact strongly with H, OH or halogen groups[89]. The IOP molecule has hydroxyl and halogenated (iodated) groups in its chemical structure, which might well interact with the carbon atoms at zigzag edges, favoring the reduction of this pollutant and improving the mediation effect of rGO-based materials as observed in Figure 2.6.

2.5. Summary

The results demonstrated the importance of the chemical and physical properties of GO-based materials to serve as electron shuttle in the chemical transformation of IOP. Moreover, the characterization of rGO-based materials indicated a decrease on oxygen content of 19.1 % and 64.4 % for rGO-2 and rGO-4, respectively, which was related to the reduction and transformation degree of IOP. Chemical reduction experiments demonstrated, for the first time, that GO-based materials can act as redox mediators for the abiotic transformation of IOP with sulfide as electron donor, involving dehalogenation, dehydration, demethylation and decarboxylation reactions. The catalytic activity of materials decreases as follows: rGO-4> rGO-2> GO, due to the partially removal of oxygenated groups, which enhanced the electronic conductivity of the basal plane of the GO sheets towards the model pollutant. Moreover, the presence of oxygenated functional groups at the edge of GO-based materials sheets, such as quinone groups, can also act as electron shuttles that are capable of electron transfer, which was reflected in a better catalytic input in IOP transformation. This is supported by the stability and high

concentration of quinone groups after chemical reduction of GO. Moreover, the reduction of IOP could be enhanced by strong interaction between its hydroxyl and halogenated (iodides) and the carbon atoms on zigzag edges of graphene sheets. Chemical transformation products with a simpler structure than IOP were identified by HPLC-MS, which is the first step towards their mineralization possibly by aerobic processes in a second stage. Also, the chemical transformation pathway of IOP was proposed. Finally, the properties of GO-based materials, such as zeta potential, ORP, pH_{PZC} and conductivity, played an important role in the electron transfer for reductive transformation of IOP.

Chapter 3

Tailoring partially reduced graphene oxide as redox mediator for enhanced biotransformation of iopromide under methanogenic and sulfate-reducing conditions*

* This chapter was adapted from: E. Toral-Sánchez, J.R. Rangel-Mendez, Juan A. Ascacio Valdés, Cristóbal N. Aguilar and F.J. Cervantes. (2017) *Bioresour. Technol.* **223**: 269-276.

3.1. Abstract

This work reports the first successful application of graphene oxide (GO) and partially reduced GO (rGO) as redox mediator (RM) to increase the biotransformation of the iodinated contrast medium, iopromide (IOP). Results showed that GO-based materials promoted up to 5.5 and 2.8-fold faster biotransformation of IOP by anaerobic sludge under methanogenic and sulfate-reducing conditions, respectively. Correlation between the extended of reduction of GO and its redox-mediating capacity was demonstrated, which was reflected in faster removal and greater extent of biotransformation of IOP. Further analysis indicated that the biotransformation pathway of IOP involved multiple reactions including deiodination, decarboxylation, demethylation, dehydration and N-dealkylation. GO-based materials could be strategically tailored and integrated in biological treatment systems to effectively enhance the redox conversion of recalcitrant pollutants commonly found in wastewater treatment systems and industrial effluents.

3.2. Introduction

In recent years, a substantial number of emerging pollutants are released into the environment around the world. Iodinated X-ray contrast media (ICM), such as iopromide (IOP), are pharmaceuticals widely used in intravascular administration with global consumption of approximately 3.5 x 10^6 kg/yr[144], which are used for brain and body imaging, and mostly excreted in urine or feces due to remarkable stability to human metabolism[27]. Because of its chemical properties and low biodegradability, IOP is a recalcitrant pollutant, which is poorly removed in conventional wastewater treatment facilities, and thus it is usually released unaltered into receiving water bodies[30,31]. Accordingly, IOP has been detected in effluents from sewage treatment plants, surface

water systems, groundwater, and even in drinking water[24,25]. Moreover, it has been reported that exposure to this pollutant could cause human health impacts, such as vomiting, nauseas, hives, headache, etc.[29]. In consequence, it is necessary to develop novel treatment techniques to efficiently remove it from contaminated waters.

In this context, biological treatment systems have been explored as feasible options to remove ICM, such as IOP, from water. Recently, few studies have reported the biotransformation of IOP under anaerobic conditions, which includes the use of biogenic palladium(0)[46] and metal-humic acid complexes[47] immobilized in granular sludge as bio-catalyst. Also, the IOP reduction in an abiotic system has been studied by the application of hydrogen gas in combination with supported palladium and porous nickel catalysts[27]. On the other hand, it has also been reported the use of redox mediators (RM) as good option to accelerate the reductive biotransformation of electron-accepting pollutants in contaminated waters[55]. In this sense, carbon based materials like granular activated carbon (GAC)[68], activated carbon fibers (ACF)[57,63], carbon nanotubes[74], black carbon[135] and carbon xerogeles[59], have been applied as RM to increase the reductive transformation of different pollutants, since they have a diversity of surface oxygenated groups like quinone groups, which can mediate the reduction of these contaminants[59,61].

Nowadays, the application of graphene-based nanomaterials has a great interest in many research areas because it possesses unique properties such as mechanical strength, high surface area, rapid electron transfer capacity[76] and extraordinary catalytic activity[131]. Also, graphene-based materials, such as graphene oxide (GO), present a wide array of oxygenated groups in their chemical structure, like carbonyl groups, which can mediate the transformation of pollutants by enhancing electron transfer processes[59,61]. In addition, it was reported that the graphene basal planes of GO-based materials have very high electrical

conductivity[90], which is another mechanism to mediate the redox conversion of contaminants by electron transfer on the graphitic carbon surface[132].

Lately, it has been reported that GO and partially reduced graphene oxide (rGO), can facilitate the biotic and abiotic reduction of recalcitrant pollutants, such as azo dyes[118,132], nitroaromatic compounds[120,121,123,132] and halogenated pollutants[73]. Moreover, the chemical transformation of IOP using GO and rGO as RM and the importance of the physical and chemical properties of GO-based materials on the reductive process have been reported recently[43]. Accordingly, it can be inferred that these graphene-based materials could mediate the redox conversion of contaminants in biological treatment systems. However, the use of these carbon nanomaterials on the biological transformation of pharmaceuticals, like IOP, has not been studied yet.

The aim of the present study was to evaluate, for the first time, the use of GO and rGO materials as RM to achieve the biological transformation of IOP under two relevant environmental conditions: methanogenic and sulfate-reducing. Furthermore, the importance of intrinsic properties of GO-based materials in the ability to act as electron shuttle is studied. Mechanisms taking place in the biotransformation of IOP are also elucidated.

3.3. Materials and methods

3.3.1. Materials and chemicals

IOP (CAS No. 73334-07-3) was obtained from Bayer Schering Pharma with commercial name Ultravist® 370. The basal medium (pH = 7.6) used in sludge incubations and to feed bioreactors was composed of the following (g/L): K_2HPO_4 (0.25), $NaHCO_3$ (5.0), $MgSO_4 \cdot 7H_2O$ (0.1), NH_4Cl (0.28), $CaCl_2 \cdot 2H_2O$ (0.01), and trace elements (1 mL/L), with a composition described elsewhere,[61]. All chemicals used during the experiments were

obtained from either Sigma-Aldrich or Merck. All solutions were prepared with distilled water.

Graphene oxide used in the present study was purchased from Graphene Supermarket®, with the following characteristics: high density and viscosity, concentration of 6.2 g/L in aqueous solution, single-layer > 60%, flake size between 0.5 and 5 µm, C/O ratio 3.95. Commercial bituminous activated carbon (AC) filtrasorb F-400 was obtained from Calgon Inc. Before use, AC was washed with deionized water and then dried at 110 °C for 48 h. Polyacrilonitrile based activated carbon fibers (ACF), with commercial name AW1105, was purchased from KoTHmex and directly used as received from the supplier.

3.3.2. Source of inocula and activation

Anaerobic granular sludge originated from a full-scale upflow anaerobic sludge blanket (UASB) reactor treating effluents from a candy factory (San Luis Potosí, Mexico) was used as inoculum to assess the biotransformation of IOP. The content of volatile suspended solids (VSS) was 12.52 % based on wet weight. The sludge was acclimated for 30 days in lab-scale UASB reactors (1.5 L working volume) operated under methanogenic and sulfate-reducing conditions at a hydraulic residence time of 1 day and with an organic loading rate of 1 g chemical oxygen demand (COD)/L-d at room temperature (25 °C ± 2). A mixture of ethanol/lactate (0.5/0.5 in terms of COD) was used as energy and carbon source for the UASB reactors. The reactors achieved COD removal greater than 95% under steady state conditions. For the sulfate-reducing bioreactor, a concentration of 1 g SO_4^{-2}/L was supplemented to the basal medium (added as Na_2SO_4). The sulfate-reducing UASB reactor achieved a constant SO_4^{-2} removal (> 90%) under steady state conditions.

3.3.3. Chemical reduction of GO

Synthesis of partially reduced GO (rGO) materials was carried out according to Toral-Sánchez et al.[43] In order to obtain materials with different reduction degrees, reduction kinetics of GO were carried out for 0.5, 1, 1.5, 2, 3 and 4 h. Three samples were selected for use as RM in biological incubations: GO, GO reduced for 2 and 4 h (rGO-2 and rGO-4, respectively) since they contain a low (60.8 mV), intermediate (329.2 mV) and high (501.9 mV) oxidation reduction potential (ORP) according to previously reported results[43], which should be a key factor on the transfer of electrons during the biotransformation of IOP.

3.3.4. Physical and chemical characterization of GO-based materials

In order to elucidate the importance of intrinsic properties of synthesized GO-based materials (GO, rGO-2 and rGO-4) on the biotransformation of IOP, physicochemical characterization of these carbon materials was performed. Details on the procedure and conditions are described in previous work[43]. On the other hand, Ionic conductivity measurements of samples were performed in aqueous solution at pH 7.0 in a MICROTRAC Zetatrac NPA 152-31A equipment. In addition, chemical composition of GO-based materials was investigated by X-ray photoelectron spectroscopy (XPS) using a PHI 5000 VersaProbe II equipment with a monochromatic X-ray beam source at 1486.6 eV and 15 kV to scan the surface of the materials.

3.3.5. Batch experiments for the biotransformation of iopromide

The capacity of GO-based materials to serve as RM on the microbial reduction of IOP was evaluated under methanogenic and sulfate-reducing conditions in 60-mL serum flasks as follows: 5 mg/L of GO and rGO were contacted with basal medium and inoculated with 1 g VSS/L of previously stabilized sludge obtained from both UASB reactors. Subsequently,

liquid and headspace were flushed for 3 min with a gas mixture of N_2/CO_2 (80:20, v/v) to ensure anaerobic conditions. An appropriate volume of a mixture of ethanol/lactate was added to the bottles to give a final concentration of 1 g COD/L. Sulfate was provided from a stock solution to obtain a final concentration of 1 g SO_4^{-2}/L for experiments performed under sulfate-reducing conditions. Bottles were incubated for 48 h with constant stirring and temperature (125 rpm and 30 °C). After pre-incubation, an extra pulse of ethanol/lactate (1 g COD/L) and sulfate (1 g/L, for the sulfate-reducing incubations) were supplied, and the IOP was added from an anaerobic stock solution in order to obtain an initial concentration of 400 µg/L. The total working volume was 50 mL in all incubations. The experiments were incubated in the dark to prevent photodegradation of IOP and metabolites derived from its biotransformation. Control experiments with autoclaved sludge (sterile control) and sludge-free were performed to evaluate the adsorption of IOP to the sludge and abiotic reduction due to intrinsic reducing compounds, and to assess the stability of the pollutant. All experimental treatments were conducted in triplicate. Samples were analyzed at specific time intervals to monitor the removal of IOP, methane production and sulfate reduction, as described in section 3.3.6. The same procedures were used to evaluate the biological reduction of IOP using commercial carbon materials as RM (ACF and AC).

3.3.6. Analytical procedures

The concentration of IOP was measured by high-performance liquid chromatography (HPLC) using a Agilent Technology 1260 series chromatograph as indicated by Toral-Sánchez et al.[43] Sulfate concentration was determined in previously centrifuged and filtered (0.22 µm) samples by capillary electrophoresis (Agilent 1600A) as previously described[178]. Methane production was monitored by analyzing 100 µL of biogas samples in an Agilent

Technologies 6890N gas chromatograph under previously reported conditions[179]. COD and VSS concentration were determined according to standard methods. Identification of transformation products of IOP was performed by HPLC coupled to mass spectroscopy (HPLC-MS) in a Varian® 500-MS ion trap mass spectrometer, with electrospray ionization of 90 V and mass-to-charge (m/z) range of 100-2000 m/z.

3.4. Results and discussion

3.4.1. Biotransformation of IOP under methanogenic and sulfate-reducing conditions

The role of intrinsic properties of GO-based materials and their use as electron shuttle was explored for the microbial transformation of IOP under methanogenic and sulfate-reducing conditions. Methanogenic conditions mainly prevail in the degradation of priority pollutants in anaerobic wastewater treatment processes[180]. Moreover, industrial wastewaters from different sectors, like pharmaceuticals, contain high sulfate concentrations[181], therefore sulfate-reducing conditions are also relevant for the reduction of this contaminant. The catalytic input of GO-based materials on the biotransformation of IOP under methanogenic conditions and the corresponding control experiments are shown in Figure 3.1A. It can be seen that biological incubations exhibited a decrease in IOP concentration with removal efficiencies of 64, 75 and 77 % after 11 days, for sludge incubations amended with GO, rGO-2 and rGO-4 as RM, respectively. In contrast, only 20 % of IOP removal occurred in control experiments without RM and methanogenic active biomass during the same incubation period. In addition, the maximum removal rate calculated in assays amended with GO, rGO-2 and rGO-4 were 34.02, 59.12 and 68.76 µg IOP/L-d, respectively. Meanwhile, the maximum removal rate achieved in the control experiment incubated in the absence of GO-based materials was only 12.48 µg IOP/L-d, which

represents a 2.7, 4.7 and 5.5-fold increase in the maximum removal rate of IOP in the presence of GO, rGO-2 and rGO-4, respectively. Also, the same parameter showed an increase of 1.7 and 2.0-fold in the presence of rGO-2 and rGO-4, respectively, with respect to the maximum removal rate calculated for the biological reduction experiment using GO as RM.

Figure 3.1B shows the biological reduction of IOP under sulfate-reducing conditions. It can be observed that GO-based materials also promoted a higher reduction of IOP with removal efficiencies of 61, 81 and 86 % in the presence of GO, rGO-2 and rGO-4, respectively. In contrast, the sulfate-reducing control incubated without RM showed an IOP removal of only 38 % in an incubation period of 8 days (Figure 3.1B). The maximum removal rate achieved in sulfate-reducing incubations amended with GO, rGO-2 and rGO-4 were 61.38, 73.34 and 90.31 µg IOP/L-d, respectively. Biological incubations with sulfate-reducing sludge in absence of GO-based materials showed a maximum removal of 31.2 µg IOP/L-d, which indicates an increase of maximum removal rate of up to 2.89-fold in the presence of RM.

Sterilized controls in the absence and in the presence of GO-based materials as RM showed <10% of IOP removal under both relevant conditions. This slight reduction in a sterile environment could be due to the presence of thermally stable intracellular coenzymes such as flavins, which have the ability to act as RM[182], and/or due to the presence of intrinsic reducing compounds in the biomass[55]. In the case of sulfate-reducing incubations, the slight removal observed in sterilized controls could also be due to remaining sulfide accumulated during the activation of sulfate-reducing biomass in the UASB reactor, which could have promoted the chemical reduction of IOP[43].

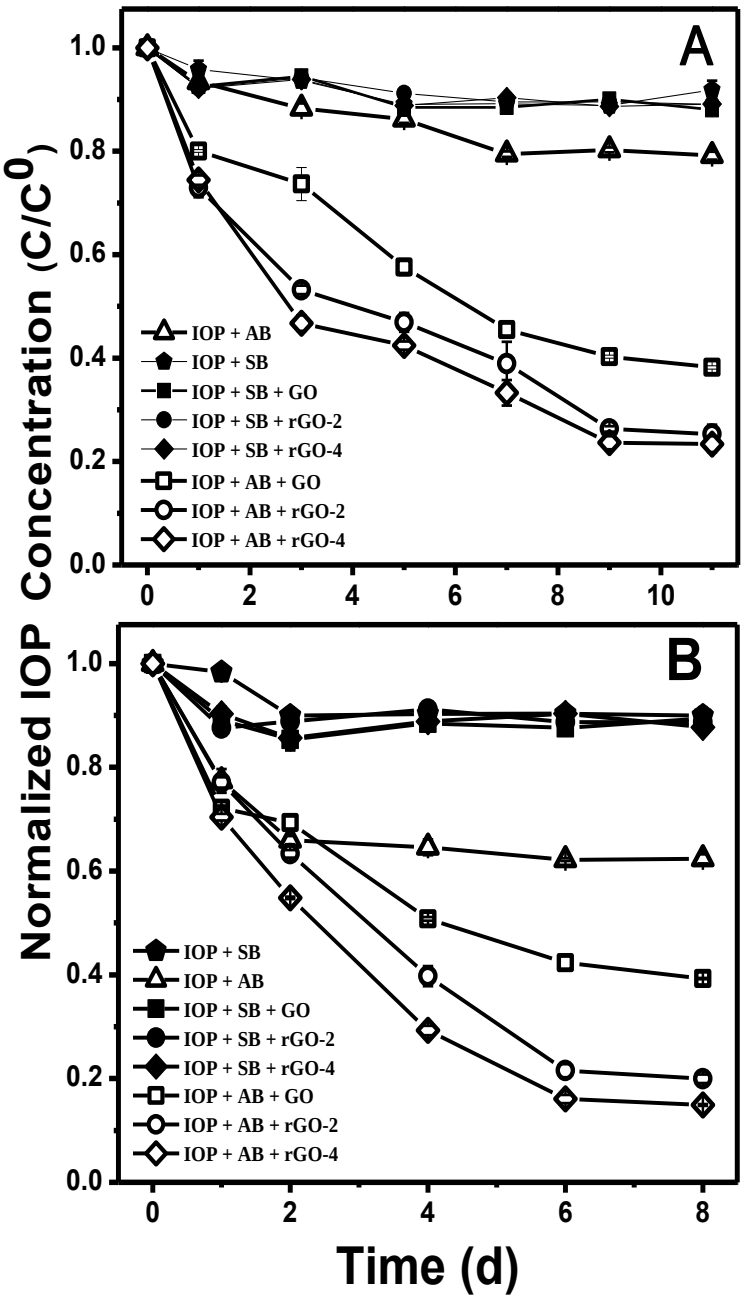

Figure 3.1. GO-based materials catalysis of biological reduction of IOP by anaerobic sludge under methanogenic (A) and sulfate-reducing conditions (B). Sterilized controls with and without GO-based materials (full symbol, Figure A and B). Incubations in the absence of GO-based materials and activated biomass (open triangles, Figure A and B). Biological reduction with GO-based materials as RM (Figure A and B): GO (open squares), rGO-2 (open circles) and rGO-4 (open diamonds).

Furthermore, methane production was measured during the course of biological transformation of IOP under methanogenic and sulfate-reducing conditions. The results showed poor methanogenic activity in the experiments incubated with active methanogenic biomass (See Figure A9 of appendix section AS), which can be explained due to possible inhibitory effects of GO-based materials on the methanogenic consortium[183,184]. However, the concentration of GO-based materials used in the sludge incubation was very small (5 mg/L) in comparison with the minimum inhibitory concentration of GO (50 mg/L) reported by [185]). Certainly, there have been reports showing that methanogenic microorganisms are able to achieve the redox biotransformation of contaminants (azo dyes) in pure culture, but not coupled to methane production[186]. Accordingly, this would suggest that a competition between IOP reduction and methanogenesis for the reducing equivalents available from ethanol/lactate fermentation could have happened in sludge incubations[118]. In the case of sulfate-reducing incubations, the methanogenic activity was negligible, suggesting that the methanogenic consortium was probably inhibited either by sulfate or by sulfide (data not shown). On the other hand, sulfate and sulfide concentrations were measured under sulfate-reducing incubations as shown in Figure A10 of AS. It can be seen that the sulfate-reducing consortium consumed 68% of sulfate over a period of 8 days. Similarly, sulfide production in the same period increased from 1.5 to 6.0 mM, suggesting that the biogenic sulfide generated from sulfate reduction was the main reducing agent promoting the biological reduction of IOP as previously reported for azo dyes and nitrobenzene reduction under sulfate-reducing conditions[118].

The microbial reduction of IOP under methanogenic and sulfate-reducing conditions using commercial carbon materials (ACF and AC) as RM was carried out in order to compare the catalytic activity of these materials with respect to GO-based materials used in this study.

ACF and AC were selected because these carbon materials have been widely used as adsorbents and RM in the adsorption and degradation processes of contaminants, in batch and continuous systems. Figure 3.2A shows the comparative microbial reduction of IOP under methanogenic conditions using the different carbon materials tested as RM with respect to control experiments lacking RM. Also, Table 3.1 shows the summary results of the biological reduction kinetics in both conditions. It can be observed a decrease of IOP concentration in methanogenic incubations of 44 and 59 % for AC and ACF, respectively, in an incubation period of 11 days. In contrast, a higher reduction of IOP is achieved using GO-based materials as RM with removal efficiencies of 64, 75 and 77 % for GO, rGO-2 and rGO-4, respectively (see Table 3.1). On the other hand, similar behavior was observed under sulfate-reducing conditions (see Figure 3.2B and Table 3.1). IOP removal efficiencies reached 44 and 58 % of IOP using AC and ACF, respectively, which is lower than the efficiencies reported for GO-based materials with values of 61, 81 and 86 % for GO, rGO-2 and rGO-4, respectively. Also, the maximum removal rate achieved under methanogenic incubations using AC and ACF was 26.02 and 35.23 µg IOP/L-d, respectively. Under sulfate-reducing conditions, the maximum removal rate reached 31.98 and 39.25 µg IOP/L-d for AC and ACF, respectively, which was lower than those observed for sludge incubation under both conditions in the presence of GO-based materials. These results show that the GO-based materials, especially partially reduced GO materials, promoted a faster and greater catalytic effect on IOP removal than commercial materials, confirming its potential for application as RM in wastewater treatment systems.

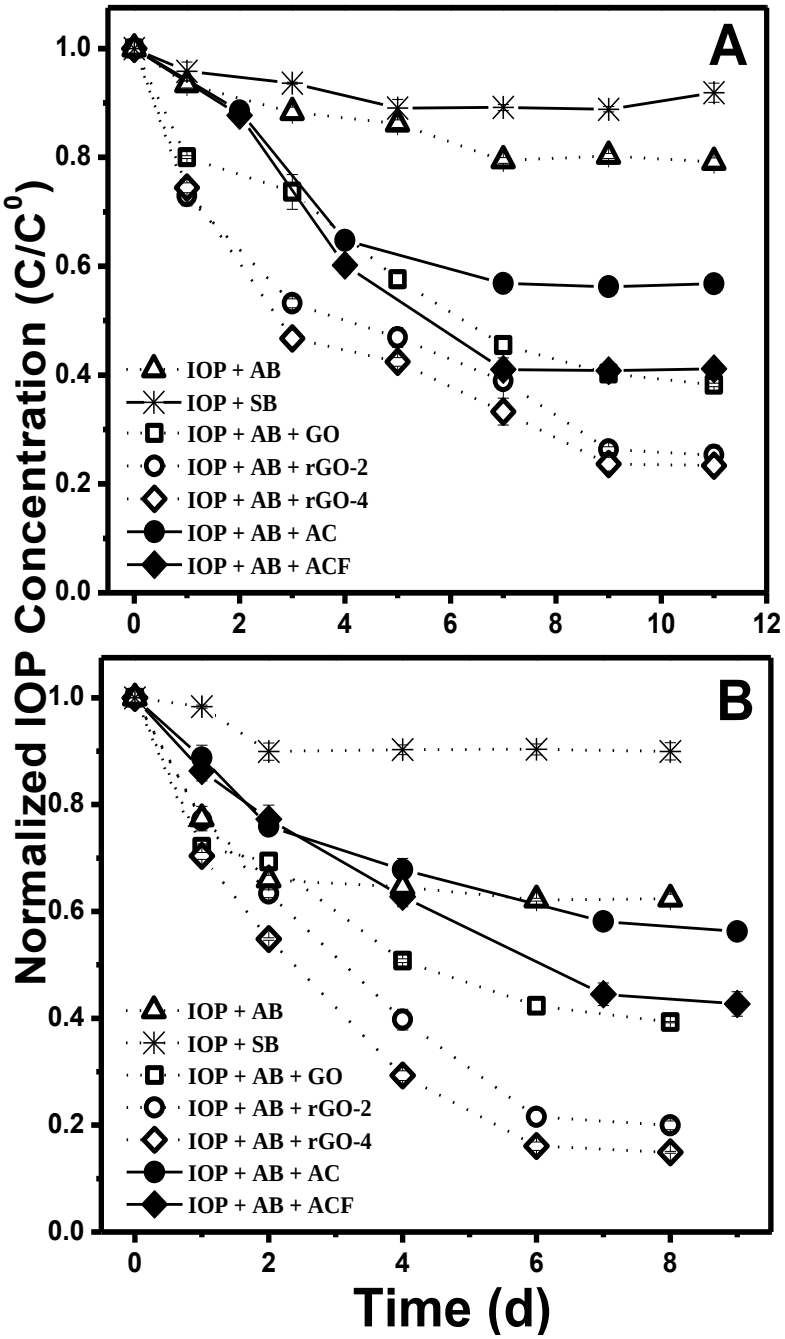

Figure 3.2. Comparative biological reduction of IOP using different carbon materials as RM by anaerobic sludge under methanogenic (A) and sulfate-reducing conditions (B). Sterilized control (asterisks, Figure A and B). Incubations in the absence of GO-based materials and activated biomass (open triangles, Figure A and B). Biological reduction with commercial materials and GO-based materials as RM (Figure A and B): AC (full circles), ACF (full diamonds), GO (open squares), rGO-2 (open circles) and rGO-4 (open diamonds).

Table 3.1. Summary results of biological reduction of IOP using different carbon materials as RM under methanogenic and sulfate-reducing conditions and concentration of carbonyl groups in these materials.

Treatments	Carbonyl groups (meq/g)	IOP reduction (%) Methanogenic	IOP reduction (%) Sulfate-reducing
SB + IOP*		< 10.0	< 10.0
AB + IOP*		20.0	38.0
AB + IOP + AC	< 0.23	44.0	44.0
AB + IOP + ACF	0.775	59.0	58.0
AB + IOP + GO	1.23	64.0	61.0
AB + IOP + rGO-2	1.29	75.0	81.0
AB + IOP + rGO-4	1.10	77.0	86.0

SB: sterile biomass, AB: active biomass. *Control experiments

The redox-mediating capacity can be explained due to the concentration of quinone groups in the carbon materials, which can mediate the transformation of pollutants by enhancing electron transfer[59,61]. Previous studies have reported that the concentration of carbonyl groups in the ACF and AC is 0.775 and < 0.23 milli-equivalents (meq)/g, respectively[57,187]. Also, it was reported by Boehm's acid-base titrations that the concentration of carbonyl groups in the GO, rGO-2 and rGO-4 was 1.23, 1.29 and 1.10 meq/g, respectively[43]. Therefore, it can be suggested that the GO-based materials had a greater catalytic effect in comparison with AC and ACF due to the higher concentration of quinone groups and to their availability since these are readily exposed, which contributes to a better electron transferring process towards IOP. Additionally, the results showed that the rGO-4 material improved the biotransformation of IOP. However, it can be seen a slight decrease in the carbonyl concentration of this material. This behavior can be explained due to the increase

of electrical conductivity, which resulted in the enhancement of electron transfer through basal plane as will be mentioned later.

Table 3.1 shows that the microbial reduction of IOP was higher under sulfate-reducing conditions than under methanogenic conditions (86 % *vs* 77 % with respect to rGO-4), which could be explained due to more prevailing reductive conditions[118]. Also, biogenic sulfide generated under sulfate-reducing conditions may increase the IOP removal, since the conditions involve chemical and biological mechanisms that favor the reduction of IOP.

3.4.2. Biotransformation pathway of IOP

Previous studies have reported the biotransformation pathway of IOP under methanogenic conditions using different removal strategies[46,47]. However, the biotransformation pathway of this pollutant using GO-based materials as RM has not previously been elucidated. Furthermore, the biotransformation pathway of IOP under sulfate-reducing conditions by any removal strategy has not been reported yet. Accordingly, it is important to elucidate the mechanisms that take place during the microbial reduction of IOP under these two relevant conditions. In order to propose the biotransformation pathway of IOP, samples derived from biological reduction of IOP in the presence of rGO-4 as RM were analyzed by HPLC-MS. The molecular weights (*m/z*) of 13 principal transformation products (TP) were identified in sludge incubations under methanogenic conditions. Proposed structures for these TP and their elemental composition, and the suggested biological transformation pathway are shown in Figure 3.3. The chemical structure modification of IOP includes several chemical reactions, which will be briefly described in the following lines.

The proposed structure of TP with *m/z* of 788.85 indicates the loss of two hydrogen atoms at either side chain A or B. The structure of TP 724 suggests the loss of a molecule of H_2O,

demethylation and decarboxylation in side chain B and N-demethylation in side chain A of IOP molecule. The structure of TP 775 implies the loss of a molecule of H_2O at side chain B of IOP molecule. The structures of TP 711 and 647 come from TP 788.80, involving demethylation and decarboxylation reactions in side chain A and dehalogenation of TP 647 (removal of one iodine atom, HI). The structure of TP 599 suggests the loss of a molecule of H_2O and demethylation in side chain A of TP 647. The cleavage of the C-N and amide bonds at the side chain A and B, respectively, and the removal of one iodine atom (HI) of TP 711 results in the formation of TP 375. Moreover, N-demethylation in side chain A of TP 599 results in the formation of TP with *m/z* of 578. The cleavage of amide bond in side chain B, deiodination of the aromatic ring (HI), demethylation and subsequent decarboxylation of side chain C from TP 578, yields TP 317 and 306.8. Finally, the proposed structure of TP with *m/z* of 772.86, 753 and 733, represents a slight modification in side chain A and B of TP 775, which include demethylation, N-demethylation and dehydration reactions.

The biotransformation pathway of IOP under sulfate-reducing conditions was also elucidated and the proposed structure of TPs can be observed in Figure 3.4. Ten TPs were identified and biotransformation of IOP includes several chemical reactions similar to those observed under methanogenic incubations. Structure of TP 778.70 suggests that decarboxylation in side chain B was carried out. TP with m/z of 746.7 indicates removal of two molecules of water and demethylation of side chain B. The structures of the TPs identified as TP 736 and 720.70 result from N-demethylation in side chain A, and demethylation and elimination of one molecule of water of TP 778.70. Furthermore, structures of TP 328.28, 322.90 and 316.9 suggest the cleavage of amide bond in side chain A, dehalogenation (elimination of two iodine molecule of the aromatic ring) and

elimination of the side chain B ramification, with sequential removal of molecules of H_2O and demethylation in side chain C. Moreover, TPs identified with *m/z* of 532 and 390.8 indicate the amide bond rupture in side chain A and B, and sequential deiodination (HI) of aromatic ring from TP 746.7. Finally, TP with m/z of 254.70 was identified as a result of deiodination of aromatic ring and C-N bond rupture in side chain B from TP 390.8. The mechanisms of the biotransformation pathway and m/z of TPs proposed in this work under both conditions are consistent with previous studies[28,36,43,45–47,50]

On the other hand, results obtained from microbial incubations performed without RM and active methanogenic biomass revealed that the main TPs produced were 646.6, 714.8 and 782.7. For sulfate-reducing incubations in the absence of RM, the main TPs with *m/z* identified were 578.9, 662.6, 720.8 and 782.7. According to these results, it can be concluded that the presence of GO-based materials as RM promoted a higher extent of IOP biological transformation (involving dehalogenation, dehydration, demethylation and decarboxylation reactions) in both conditions, which was evidenced by the formation of TPs with low m/z as compared to control incubations performed in the absence of these materials. The biological transformation of IOP under methanogenic and sulfate-reducing conditions and distinct capacities of GO-based materials to act as RM can be explained by their surface chemistry and physical properties as discussed in the next section.

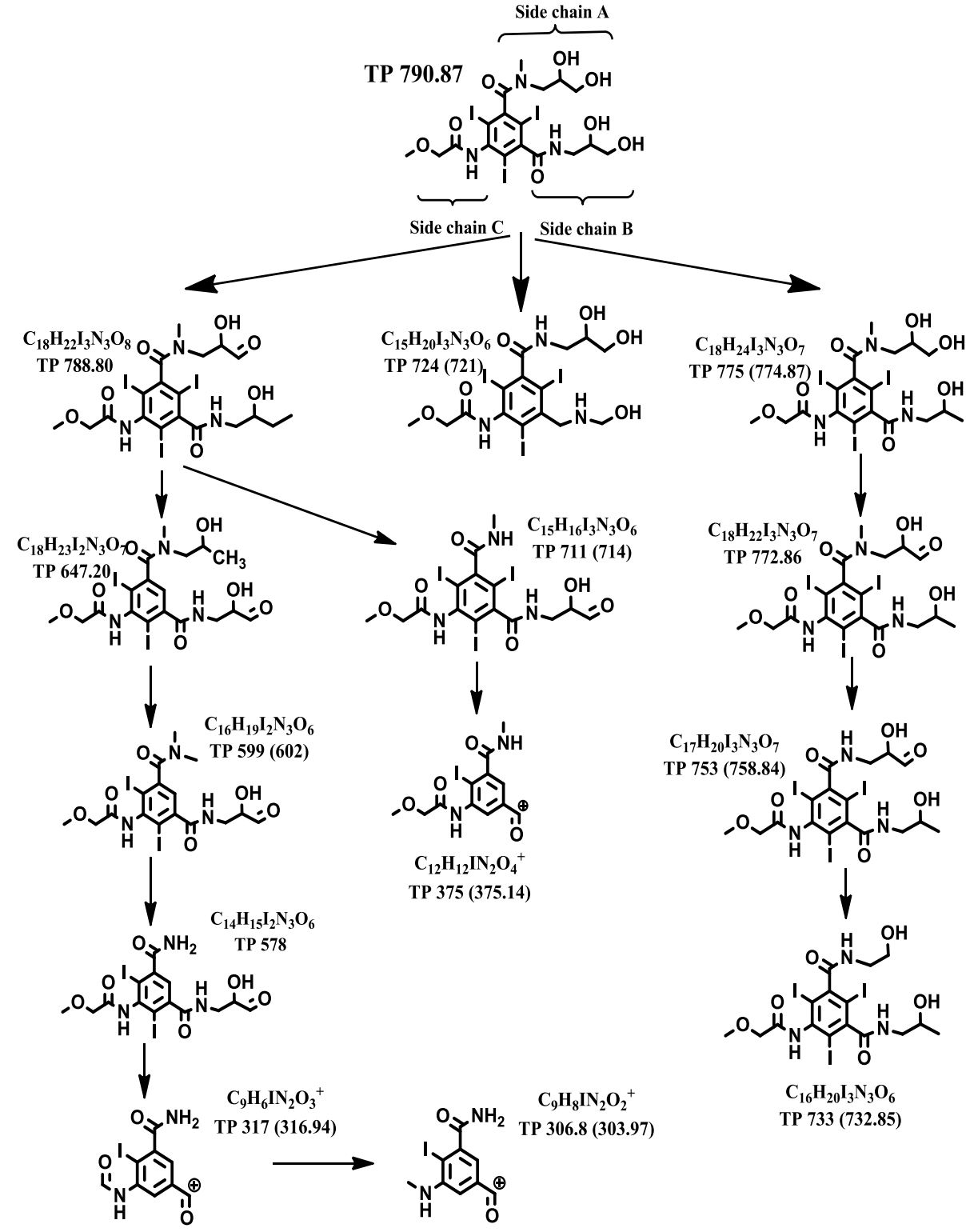

Figure 3.3. Biotransformation pathway of IOP under methanogenic conditions

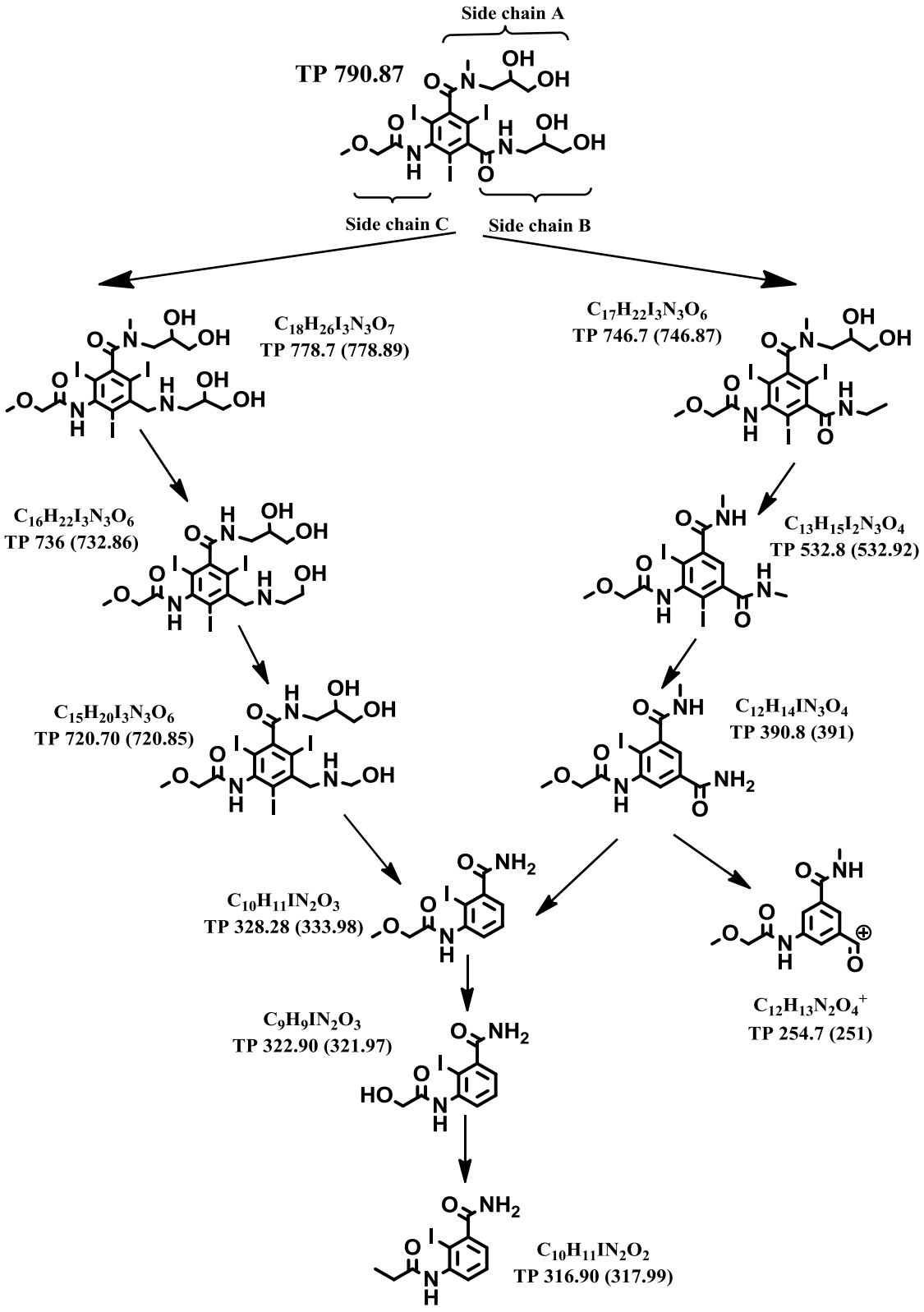

Figure 3.4. Biotransformation pathway of IOP under sulfate-reducing conditions

3.4.3. Mechanisms involved in the biotransformation of IOP mediated by GO-based materials

Several studies have reported that carbonaceous materials can enhance electron transfer in reductive reactions of organic compounds by serving as RM[56,114]. It has been reported that the zigzag edges of rGO materials can accelerate the reduction reactions of contaminants due to the reactivity of their nonbonding π-electrons[120,131]. Moreover, the presence of GO-based materials can enhance extracellular electron transfer process in microorganism[188,189], which is a promising pathway for biological reduction of pollutants[121,190]. In addition, the high electrical conductivity of basal plane of rGO materials provides an excellent opportunity to improve the biotransformation performance of organic pollutants[119,121]. Accordingly, it is expected that different mechanisms are involved in the electron transfer towards IOP mediated by GO-based materials.

As mentioned above, the basal plane of GO sheets has very high electrical conductivity that depends on the presence of epoxy and hydroxyl groups and it is generally proportional to the C/O ratio[43]. In order to determine the amount of carbon and oxygen on GO-based materials, XPS analysis was performed as can be seen on Figure 3.5. The spectra show a peak corresponding to C-C stretching at 284.5 eV. Also, it can be observed that the intensity of the C-O and O-C=O peaks gradually decreases as the reduction degree of the samples is higher. In contrast, the intensity of C=O peak and its content (≈ 5.36 %) remain constant due to their greater stability in comparison with the other oxygenated groups as reported previously[43]. Furthermore, XPS analysis indicated that the carbon content in GO, rGO-2 and rGO-4 was 41.6, 48.8 and 52.2 %, respectively, which indicated an increase in the C/O as the reduction degree advanced.

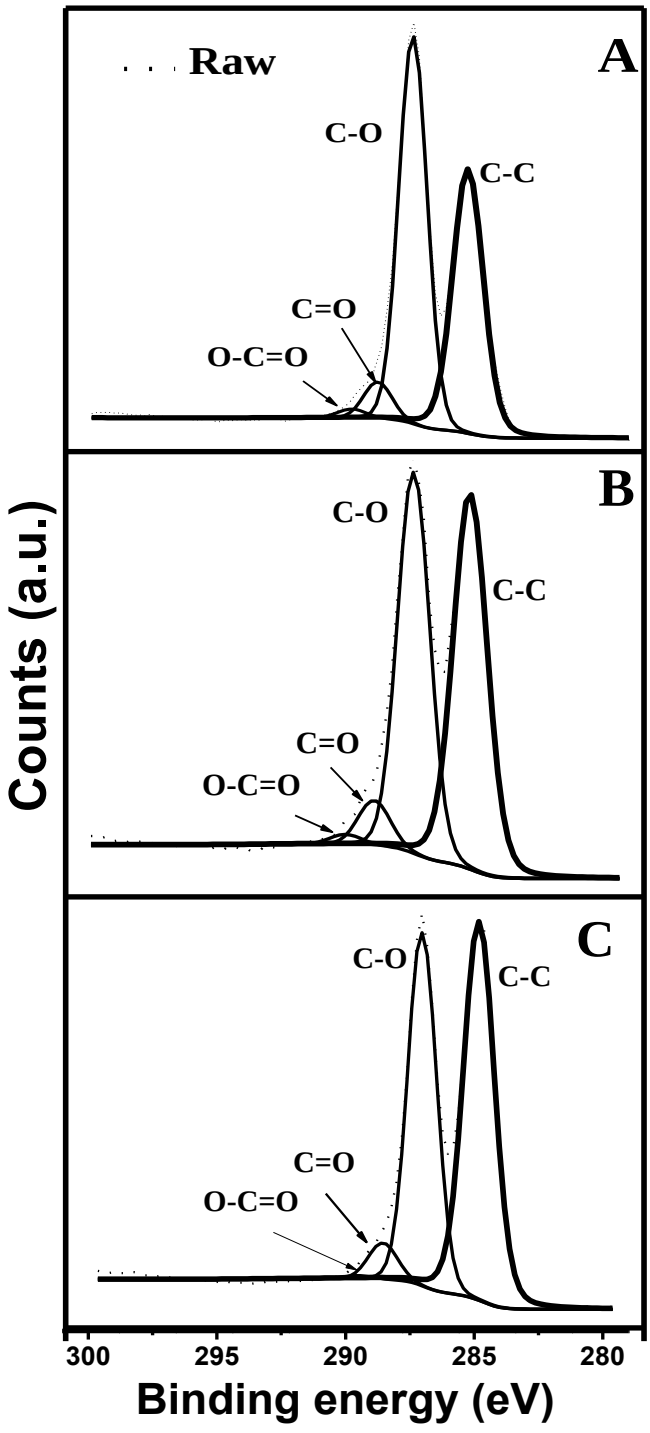

Figure 3.5. X-ray photoelectron spectra of GO-based materials with different reduction degrees: (A) GO, (B) rGO-2 and (C) rGO-4.

On the other hand, Fourier transform-infrared spectra performed in our previous work showed a removal of mainly epoxy and hydroxyl groups when GO was chemically reduced by L-ascorbic acid[43]. Hence, it was observed that the electrical conductivity of GO-materials increased as the reduction degree was higher, which was reflected in an increased biotransformation of IOP (see Figure 3.1A and B).

In order to demonstrate this hypothesis, the ionic conductivity of GO-materials was measured as can be seen in Table 3.2. The results showed that this parameter increased as the reduction degree of GO-based materials was higher with values of 43.33 ± 1.2, 72.3 ± 3.2 and 116.6 ± 0.54 µS/cm for GO, rGO-2 and rGO-4, respectively (see Table 3.2). Furthermore, oxygenated functional groups in carbon materials, like quinone groups, have great redox activity[153] serving as acceptors and electron donors[60], which improve the electrical conductivity of carbon materials, making best mediator for electron transfer[132].

Table 3.2. Content of carbon and oxygen, as well as ionic conductivity of GO-based materials.

Samples	% C	% O	σ (µS/cm)
GO	41.6	58.4	43.33 ± 1.2
rGO-2 hrs	48.8	51.1	72.30 ± 3.2
rGO-4 hrs	52.2	47.8	116.60 ± 0.54

Finally, it has also been reported that the non-bonding π-electrons localized at the zigzag sites of graphene sheets are able to interact strongly with H, OH or halogenated groups[81]. IOP molecule has hydroxyl and halogenated (iodinated) groups in its chemical structure, which might well interact with the non-bonding π-electrons of graphitic sheets[43], favoring

the partial rupture of this molecule during biological incubations as it can be seen in the biotransformation pathway (see Figure 3.3 and 3.4).

3.4.4. Environmental relevance

Major efforts have been made to develop wastewater treatment systems integrating materials with redox mediator capacity and specific properties in order to improve efficient redox transformation of pollutants. Carbon-based materials, such as activated carbon and activated carbon fibers have been widely applied in chemical and biological reduction of a variety of contaminants, including azo dyes[55,59,63], nitroaromatic compounds[57] and poli-halogenated contaminants[73]. Recently, the use of graphene materials, like GO, has been studied as a promising material in the reduction of pollutants due to their physical and chemical properties. However, the use of these carbon nanomaterials in the removal of pharmaceutical compounds has been poorly studied. Also, the applications of graphene-based nanomaterials have a great interest in many research areas, which gives to this material an excellent opportunity to be used in the biological and chemical treatment of different pollutants.

The removal strategy proposed in the present study represents the first step toward a simple and viable alternative to apply GO-based materials in wastewater treatment systems to enhance the reductive transformation of contaminants. Also, the results suggest that the redox catalyst could be applied in the treatment of industrial effluents of pharmaceutical sector. This work has demonstrated that the combination of catalytic activity of GO-based materials and the biological activity of two relevant processes (methanogenic and sulfate-reducing conditions) involved in anaerobic bioreactors, promote the biotransformation of IOP more efficiently than the capacity observed separately. To our knowledge, this is the

first study that demonstrates the effectiveness and successful application of GO-based materials as electron shuttle in the biotransformation of IOP. Derived from this work, new technological challenges are the synthesis of novel GO-based materials for immobilization and application as RM in wastewater treatment systems, in order to improve the biotransformation of persistent pollutants.

3.5. Conclusion

GO-based materials were demonstrated, for the first time, as effective RM stimulating a higher biotransformation of IOP under methanogenic and sulfate-reducing conditions. The results showed the importance of the intrinsic properties of GO-based materials in the biotransformation of IOP. The presence of quinone groups, electrical conductivity and extracellular electron transfer processes appeared as key drivers in the biotransformation of IOP. Engineered GO-based materials combined with biological activity of relevant processes prevailing in anaerobic treatment systems could be applied to enhance the redox conversion of emerging pollutants in industrial effluents.

Chapter 4

Improved reductive transformation of iopromide by hybrid magnetic graphene nanosacks as electron shuttles*

*E. Toral-Sánchez, Robert H. Hurt, Juan A. Ascacio Valdés, Cristóbal N. Aguilar F.J. Cervantes and J.R. Rangel-Mendez. *Submitted.*

4.1. Abstract

Iopromide (IOP) is an emerging pharmaceutical water pollutant, which is hardly removed from wastewater treatment systems and frequently released into environmental compartments. The aim of this work was to evaluate the novel application of magnetic reduced graphene oxide nanosacks (MrGO-N) as electron shuttles to enhance the reductive degradation of IOP. Physicochemical characterization of MrGO-N by Boehm titration, point of zero charge (pH_{PZC}), high resolution transmission electron microscopy (HR-TEM), X-ray diffraction, as well as by Raman and Fourier transform infrared spectroscopies, demonstrated the thermal reduction of precursor graphene oxide sheets, removal of different oxygenate groups and the successful assembly of magnetite nanoparticles in the graphene sacks. Also, results revealed 72 % of IOP removal efficiency and up to 2.5-fold faster reduction of this pollutant performed with MrGO-N as electron shuttle in batch systems and with sulfide as electron donor. Chemical transformation pathway of IOP provides evidence of complete dehalogenation and further transformation of aromatic ring substituents. Superior redox-mediator capacity of MrGO-N was observed, which was reflected in a higher removal rate and further transformation degree of IOP. Transformation byproducts of IOP with simpler chemical structure were identified, which could lead to complete degradation by conventional methodologies in a second treatment stage. Finally, redox activity of MrGO-N could be applied in biological treatments operated in continuous way in order to facilitate the reduction of priority contaminants.

4.2. Introduction

Recently, many emerging pollutants like pharmaceuticals have been identified in wastewater and aquatic environments around the world. Iopromide (IOP) is a tri-iodinated X-ray contrast medium (ICM) commonly used in radiographic tests, which is eliminated by

urine in the first 24 h[27,28]. Because of its low microbial degradation and physicochemical properties, IOP is considered as a persistent pollutant that is resistant to conventional wastewater treatments and consequently discharged into environmental compartments like water bodies and soils[27,30,31]. IOP has been detected in effluents from wastewater treatment plants, receiving water bodies, and even treated tap water at μg/L levels[24,25]. Although no adverse effects have been documented on the chronic exposure of this pollutant[26], different studies have reported toxic effects at cellular level conducting to apoptosis and endothelial dysfunction[33,40,41]. In addition, it has been reported that exposure to ICM could cause human health impacts that include allergic reactions, cardiac problems and systemic manifestations[29]. Therefore, it is essential to develop new degradation strategies as an alternative to remove of this halogenated organic compound from wastewater treatment effluents.

Several studies have documented the use of chemical substances with the ability to act as electron shuttle in order to promote reductive transformation reactions of pollutants, mainly attributed to the presence of quinone groups (two resonant carbonyl groups[60]), which form a well-known redox couple with hydroquinones that facilitate system electron transfer[55]. Quinone-hydroquinone couples are the perfect case of electron shuttle systems, and their redox-mediator nature consist in the capacity to accept and donate electrons by resonance phenomenon[60,65]. Some graphene based-materials including graphene oxide (GO), partially reduced graphene oxide (rGO) and graphene composites have also been applied as electron shuttle with rapid electron transfer capacity and redox catalytic activity[76,90,131], possibly due to the presence of carbonyl groups in the population of diverse oxygen-containing groups on these complex materials[59,61,64].

Recently, it has been explored the catalytic activity of GO-based materials in the redox conversion of environmental contaminants because of their ability to improve the electron transfer process by complex physicochemical mechanisms[64]. For instance, Colunga et al.,[118] and Lu et al.,[119] reported the reduction of azo dyes using GO-based materials as catalysts. Also, Fu et al.,[73] studied the reductive transformation of polyhalogenated organics. Meanwhile, several authors have documented the redox conversion of nitrocompounds[64,120–123]. In addition, our previous work has proved that GO and rGO can act as electron shuttle, facilitating the chemical/biological transformation of IOP in batch incubations[43,44]. There is significant evidence that GO-based materials can promote reductive reactions of pollutants like halogenated organics, but their application in continuous treatment systems is hindered by challenges in capturing and recovering the mediator after use. An important goal is to design graphene-based composite mediators with specific properties that allow them to be retained or captured, and recycled back into treatment processes.

Recently, the immobilization of particles in folded graphene structures has emerged as a new approach to produce versatile hybrid carbon nanomaterials with specific properties and functions[191]. In this context, an aerosol-phase process has been reported for the assembly of nanoparticles (NPs) and rGO sheets in the form of filled graphene nanosacks (GNS) by fast microdroplet drying[126,127]. Nowadays, several studies have reported the use of magnetic NPs, especially magnetite (Fe_3O_4), in environmental and medical biotechnology, removal of water pollutants and catalysis research area, due to their particular properties, such as high surface area, superparamagnetism and reducing catalytic power[192,193]. Recently, the integration of magnetic NPs in hybrid GNS has been demonstrated, and their application in biomedical and chemical technologies has also been studied[126,191]. However, their redox

catalytic properties to facilitate the reductive degradation of organic compounds in water have not been explored yet.

The aim of the present work was to evaluate the novel use of magnetic reduced graphene oxide nanosacks (MrGO-N) as electron shuttle to promote reductive transformation reactions of IOP in chemical systems. The experimental work is conducted in batch incubations, but the goal is to develop and demonstrate the magnetic function that would allow application in biological continuous systems with magnetic recovery. Moreover, the influence of the physical and chemical properties of the magnetic GNS in the capacity to serve as electron shuttles is studied as are the transformation pathways for abiotic reduction of IOP in these systems.

4.3. Materials and methods

4.3.1. Materials and chemicals

IOP was purchased from Bayer Schering Pharma with commercial name Ultravist® 370. Sodium sulfide ($Na_2S{\cdot}9H_2O$) and magnetite NPs (Fe_3O_4, particle size of <50 nm) were obtained from Fisher-Scientific and Sigma Aldrich, respectively, with 99% purity. The basal medium (pH = 7.6) and trace elements solution (1 mL/L) used in chemical reduction experiments were mixtures of several reagents as described in previous works[43,44,57,61]. All solutions were prepared with deionized (DI) water to 18.1 MΩ·cm. GO aqueous suspensions were prepared and purified by a modified Hummers' method as described previously[194,195]. This material has the following characteristics: low density and viscosity, concentration of 1 g/L in aqueous solution, flake size between 0.5 and 1 µm, C/O ratio 3.1[196]. It is important to mention that the GO employed in the studies reported in this chapter is different than the GO reported in chapters 2 and 3.

4.3.2. Synthesis of magnetic graphene oxide nanosacks

The fabrication of MrGO-N was carried out by ultrasonicated nebulization process using a well-mixed colloidal suspension of GO (0.5 mg/mL) and Fe_3O_4 NPs (1 mg/mL), according to methodology proposed by Chen et al.,[127,191]. The MrGO-N were recovered on a filter membrane and dispersed in DI water. Hybrid rGO nanosacks without magnetite (rGO-N) were similarly synthesized to MrGO-N as mentioned above.

4.3.3. Characterization of graphene nanosacks

Morphological characterization of MrGO-N and rGO-N was performed on a LEO 1530 VP Scanning Electron Microscope (SEM) and JEOL JEM-2010 High Resolution Transmission Electron Microscope (HRTEM). Samples were suspended in ethanol and then sonicated for 30 min. After that, the samples were mounted in a Cu TEM grid. Raman spectroscopy was performed on a WITEC-A300M+ Confocal Raman Microscope. Zeta potential measurements of the samples were measured in DI water using a Malvern Nano-ZS dynamic light scattering equipment. X-ray diffraction (XRD) patterns were obtained in a Bruker D8 Advanced diffractometer using CuKα radiation. Infrared spectra were recorded by Fourier transform-infrared (FT-IR) spectroscopy using a Jasco FTIR-4100 Instrument in ATR mode. Finally, oxygenated groups were quantified by Boehm titrations with an automatic titrator Mettler-Toledo T70. Details of experimental conditions and procedures are described in previous work[43].

4.3.4. Batch experiments for the chemical transformation of iopromide

The abiotic reduction of IOP was assessed in batch incubations using MrGO-N and rGO-N as electron shuttles and sulfide as chemical electron donor (HS^- as the reactive species). These experiments were performed as previously proposed by Toral-Sánchez et al.,[43]: in the

current study, 5 mg/L of MrGO-N or rGO-N as electron shuttle were used in a working volume of 50 mL. Experimental controls to verify stability and adsorption of IOP molecule were conducted simultaneously as previously described[43]. In order to monitor the removal of IOP and the chemical transformation byproducts during chemical reduction experiments, samples were analyzed at specific time intervals as described in section 4.3.5.

4.3.5. Analytical procedures

Measures of IOP concentration and identification of its chemical byproducts were performed by high-performance liquid chromatography (HPLC, Agilent Technology 1200 series chromatograph) and HPLC coupled to mass spectroscopy (HPLC-MS, Varian ® 500-MS ion trap mass spectrometer), respectively, using the experimental conditions indicated by Toral-Sánchez et al.,[43].

4.4. Results and discussion

4.4.1. Characterization of graphene nanosacks

During the synthesis process of GNS, the furnace temperature was 600 °C, converting the GO precursor to rGO-N by thermal reduction[191], which involves chemical and structural changes in the nanomaterials. In order to demonstrate the functionalization of MrGO-N with magnetic NPs, XRD analysis of this material was performed as shown in Figure 4.1A. Their XRD pattern shows typical peaks at 2θ = 18.29, 30.09, 35.44, 37.07, 43.07, 53.44, 56.96, 62.55, 74.00 and 89.65, which confirms the presence of magnetite NPs and suggests that the structure of encapsulated Fe_3O_4 particles were preserved during the aerosol processing. Also, Figure 4.1B shows that MrGO-N can be separated from water solution with a magnet demonstrating the strong assembly of Fe_3O_4 NPs in the GNS and the absence of rGO sheets dispersed in solution as previously reported by Chen et al.,[191].

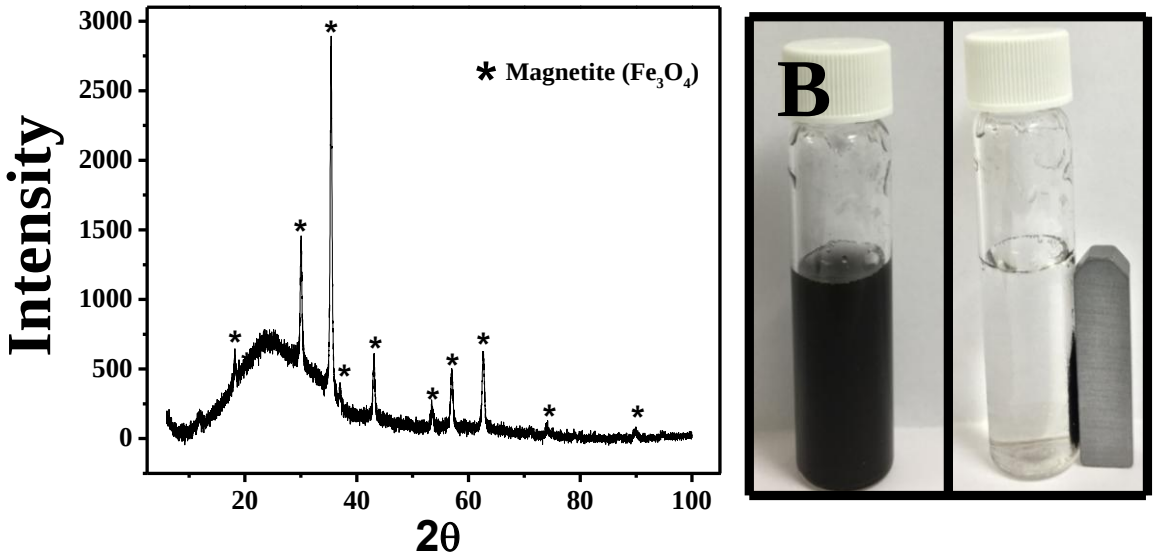

Figure 4.1. XRD pattern of MrGO-N (A) and (B) MrGO-N cleared from DI water solution with hand-held magnet demonstrating stable encapsulation of magnetic NPs.

Micrographs of rGO-N are shown in Figure 4.2A. Wrinkled GNS products with irregular folded nano-structures can be observed. According to Chen et al., the microdroplets drying time is around 0.1 to 100 ms[127], indicating that synthesis of these hybrid GNS was very fast. In addition, the mass ratio of water-GO suspension (2000:1) was estimated previously[127], suggesting that the encapsulation process involves a great size reduction of GO sheets, generating hybrid materials with nanometric size from aerosol suspended droplets[127]. Furthermore, Figure 4.2B and C show the high-resolution micrographs of MrGO-N. It can be seen in Figure 4.2B a successful and almost completely assembly of magnetic NPs inside the sacks, with only few particles appearing on the external surface. Moreover, it can be observed in Figure 4.2C that Fe_3O_4 NPs are covered by partially rGO sheets. On the other hand, it has been reported a high stability (not unfold) of hybrid magnetic GNS into water[124,127]. As mentioned by Chen et al.,[191] the successful

encapsulation and morphology of GNS are related to the electrostatic interactions that occurs in the Fe_3O_4/GO system.

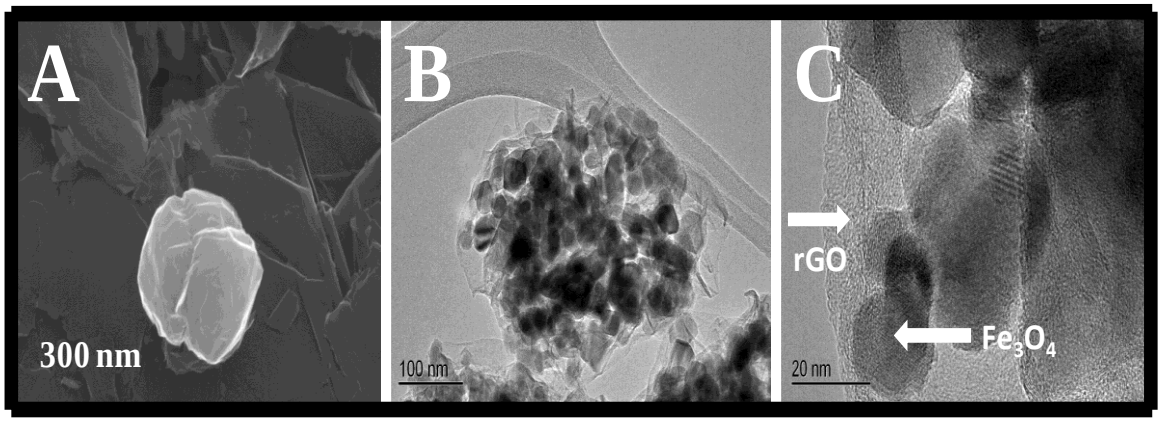

Figure 4.2. SEM images of empty rGO-N (A). HR-TEM images of MrGO-N (B) and multilayer graphene sheets encapsulating magnetic nanoparticles (C).

Previous reports have proposed assembly mechanisms for hybrid GNS formation. Chen et al.,[127] suggested, by molecular simulations, that GO sheets show a preference to adsorb at the air-water interface, forming rGO films that fold during droplet shrinkage external surface in the drying stage. Instead, the magnetic NPs prefer to be transported inside GNS by diffusion. In addition, the simulation analysis predict that the wrinkle locations of GNS are initiated from regions with high concentration of carbonyl and epoxy functionalities or defects in the GO sheets[127]. Moreover, Chen et al.,[191] proposed a theory of NPs encapsulation process in the sacks, which consist in the electrostatic attraction and repulsion behavior of GO/NPs systems as a function of pH-dependent zeta potential. This theory establishes that the charged NPs (with smaller size than GO sheets) have the ability to diffuse from drying droplet external surface toward sack interior and then, charged GNS separation is performed by repulsive electrostatic interactions[191].

In this context, measurements of zeta potential as a function of pH for all nanomaterials were carried out (Figure 4.3). It can be seen that GO has a point of zero charge (pH_{PZC}) of 2.3, in the range of carboxyl group pKa values, suggesting that these oxygenated groups are responsible of negative surface charge. The Fe_3O_4 NPs show a pH_{PZC} of 6.9. The pH value of GO/Fe_3O_4 system was 3.2. At this pH, the magnetic NPs have a positive surface charge, which could interact with the negative charged of GO sheets by electrostatic interactions[191]. These results could explain the successful dispersion and assembly of magnetite in the GNS as observed in Figure 4.2B and C. Moreover, it can be seen in Figure 4.3 that the pH_{PZC} of precursor GO (pH=2.3) is lower with respect to the MrGO-N (pH=3.8), which indicates a partial reduction of GO sheets. Also, the pH_{PZC} of MrGO-N was slightly higher (pH=3.8) in comparison to the rGO-N (pH=3.5), suggesting that a few magnetic NPs are exposed on the outer surface of MrGO-N, as it can be observed in Figure 4.2B.

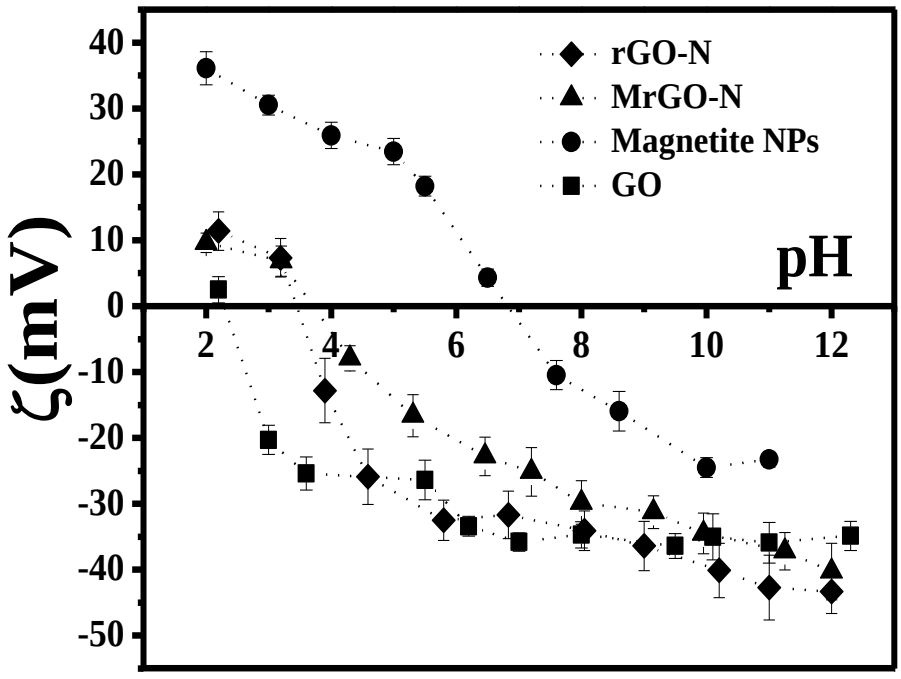

Figure 4.3 Surface charge distribution of GO-based materials and magnetite NPs.

On the other hand, it is possible to observe in Table 4.1 changes in surface chemical properties of hybrid GNS due to the partial thermal reduction of precursor GO sheets during the encapsulation process. The total concentration of acidic oxygenated groups decreased 25 % (from 3.04 to 2.28 milli-equivalents (meq)/g) as thermal reduction process of GO sheets is performed. Also, a slight increase on carbonyl groups was observed, from 1.05 to 1.20 meq/g. According to previous works, quinone groups have been suggested as a main electron shuttle moieties in carbon-based material due to its contribution in the reductive reactions of environmental contaminants[60,153]. Several studies have reported the possible mechanism involved in the thermal reduction of GO sheets. Accordingly, the energy required (binding energy) for bonds break between graphene sheets and different oxygenated groups could be a key factor in the thermal deoxygenation of GO[77], being the epoxy and carboxyl groups the easiest to remove at low temperature because of its chemical nature[95,101,166]. Also, Gao et al.,[101] proposed that hydroxyl and carboxyl groups can be removed from GO sheets at the range of temperature between 100 to 600 °C. In contrast, carbonyl groups are highly stable and removed at critical temperatures above 1730 ° C. Moreover, Huh[99] proposed that during thermal reduction of GO, different stages of deoxygenation exist as the temperature increases. In this sense, the partial removal of carboxyl and hydroxyl groups, vaporization of H_2O, contraction of GO sheets and formation of CO and CO_2 occurs between room temperature and 600 °C. As can be seen in Table 4.1, carbonyl groups were less removed in comparison with hydroxyl and carboxyl groups, which corroborate the aforementioned.

Table 4.1. Surface chemical properties of precursor GO and MrGO-N

Samples	Surface functional groups, (meq/g)					Point of Zero Charge (pH_{PZC})
	Carboxylic	Lactonic	Phenolic	Carbonyl	Total	
GO	1.62	0.20	0.17	1.05	3.04	2.30
MrGO-N	0.87	0.11	0.10	1.20	2.28	3.80

The deoxygenation in the GNS was also confirmed by FT-IR spectroscopy. As shown in Figure 4.4, all nanomaterials present the stretching vibration of O-H groups from 3000 to 3700 cm^{-1}. Also visible are bands corresponding to stretching vibrations of C-OH at 1200 cm^{-1}, C-O (epoxy groups) at 1040 cm^{-1} and C=O can be seen at 1720 cm^{-1} from carboxyl groups, respectively, which decreased after the thermal reduction of GO[43,76,110]. These observations agree with the quantification of oxygenated groups obtained by Boehm titrations (see Table 4.1). Furthermore, the appearance of aromatic C=C stretching vibration at 1620 cm^{-1} and the presence of C=O at 1570 from carbonyl groups[43] was also observed in the spectra of MrGO-N and rGO-N. Finally, the MrGO-N spectrum shows a characteristic band at 585 cm^{-1} corresponding to Fe-O stretching vibration from Fe_3O_4 NPs[197]. These results demonstrate that hybrid GNS are formed with rGO sheets by thermal reduction process of GO precursor.

In order to characterize the evolution of GO precursor and crystallinity of GNS, Raman spectroscopy was employed. Figure 4.5 shows Raman spectra of GO, rGO-N and MrGO-N. The presence of G and D bands at 1597 cm^{-1} and 1350 cm^{-1}, respectively, is evident. The D band is related to defects in the sp2-carbon network, indicating the amorphous character of materials. In contrast, the G band derived from vibrations within the defect-free sp2-carbon network[160]. Structural modifications in GNS can results from thermal reduction of precursor GO due to the reduction of oxygenated functionalities, which was confirmed by

Raman spectra of MrGO-N and rGO-N. It can be seen that the relative intensity of the D band decreased and that of the G band increased as the synthesis of the GNS was conducted. Moreover, it has been reported that the intensity ratio I_D/I_G is usually a measure of structural disorder in carbon materials, where a greater I_D/I_G ratio indicates a pronounced amorphous character (low crystallinity) in the materials[77]. Accordingly, the intensity ratio I_D/I_G decreased as follows: 1.2, 0.94 and 0.93 for GO, MrGO-N and rGO-N, respectively, which suggest that GO precursor undergoes a thermal reduction by heating indicating that synthesized GNS are formed by rGO sheets.

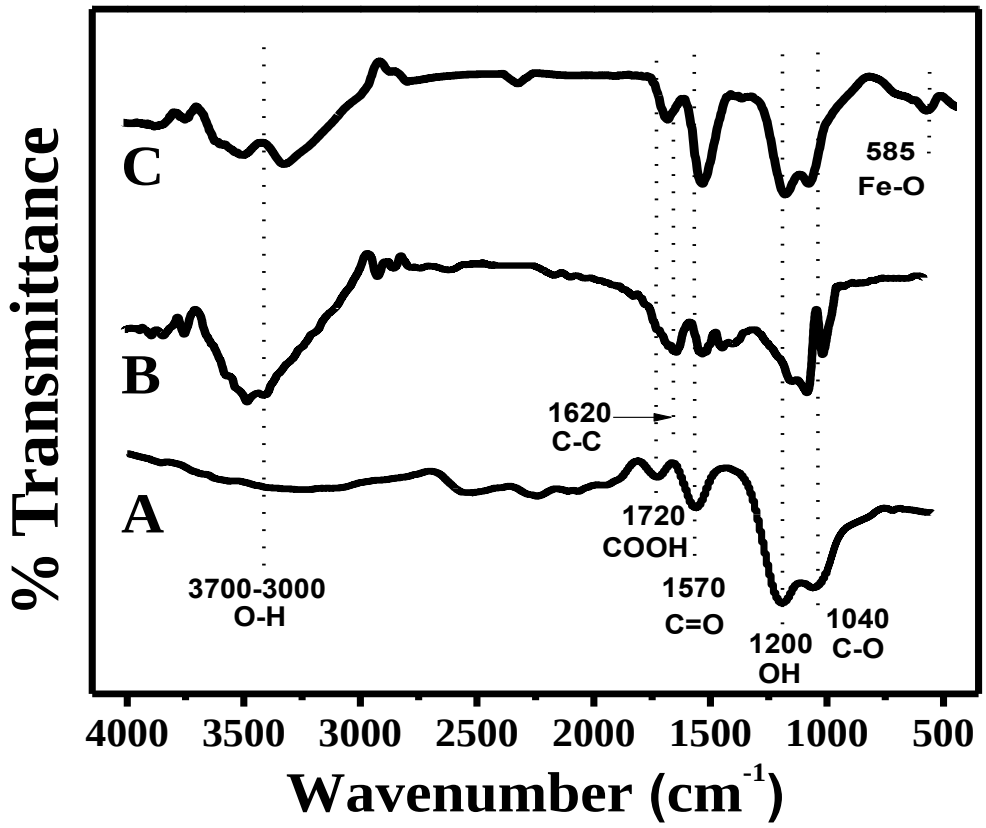

Figure 4.4. FT-IR spectra of GO-based materials: (A) precursor GO, (B) rGO-N and (C) MrGO-N.

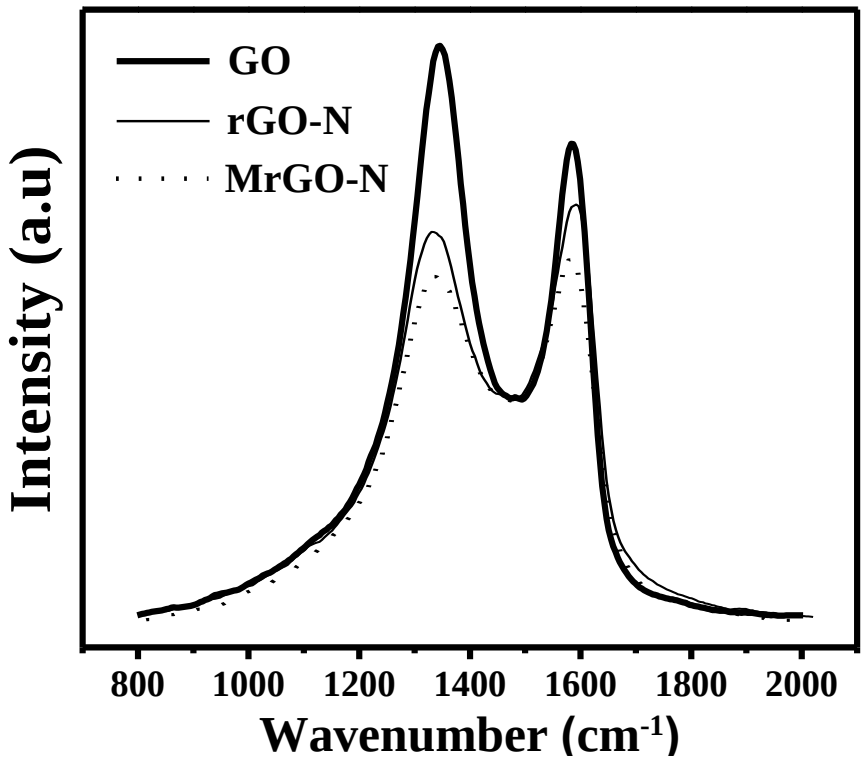

Figure 4.5. Raman spectra of precursor GO, rGO-N and MrGO-N.

4.4.2. Chemical transformation of IOP

The chemical reduction of IOP by reaction with HS^- species along with experimental controls are shown in Figure 4.6. Sulfide cases a decrease in IOP concentration with removal efficiencies of 57 and 72 % after 10 days, experiments involving rGO-N and MrGO-N, respectively. In contrast, low efficiency removal of IOP (25 %) was observed in control experiments without electron shuttle (direct reduction by sulfide). IOP adsorption controls (without sulfide as electron donor) showed a slight decrease on IOP concentration (< 12 % in all cases). Also, good stability of IOP molecule was observed in basal medium, showing a removal lower than 5 %.

Furthermore, the maximum removal rate calculated in chemical incubations conducted with MrGO-N and rGO-N were 57.73 and 38.91 μg/L-d, respectively. Meanwhile, the maximum

removal rate achieved was only 22.58 μg/L-d in the control experiment lacking nanosacks as electron shuttle. These results represent a 2.5 and 1.7-fold increase in the maximum removal rate of IOP in the presence of MrGO-N and rGO-N, respectively, which suggest that the redox activity of MrGO-N as electron shuttle promoted the removal rate and reduction efficiency of IOP[44]. In the following section, it will be explored the molecular pathways involved in the chemical transformation of IOP.

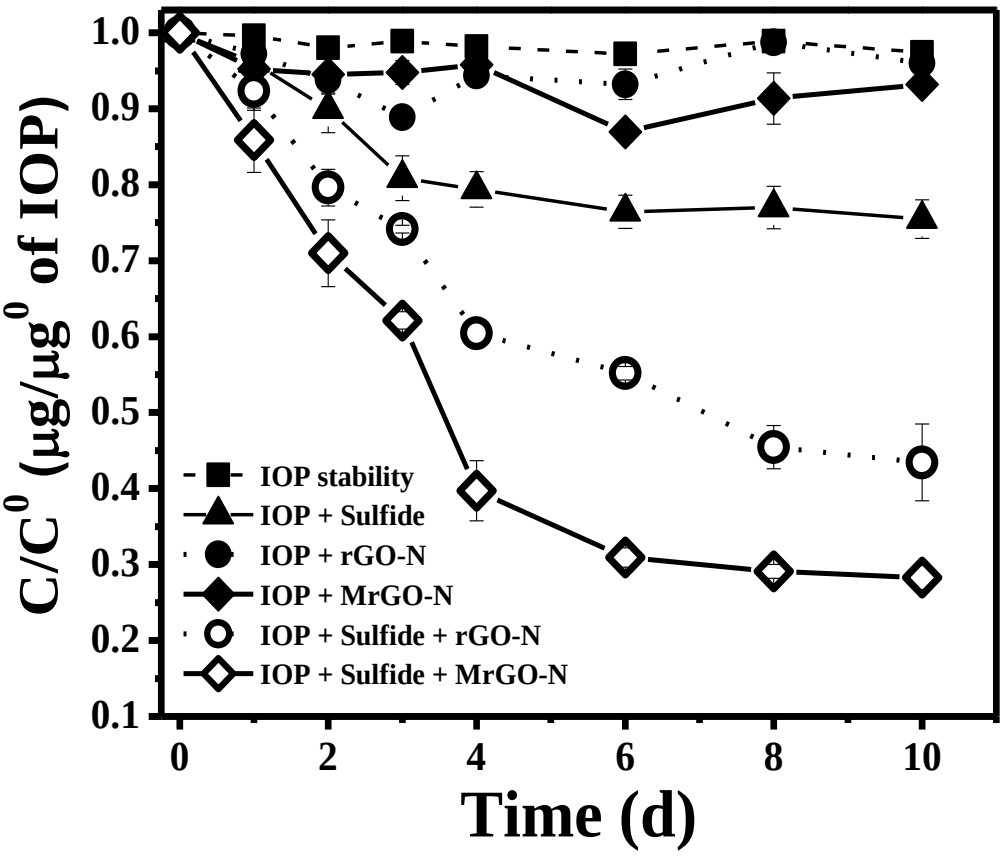

Figure 4.6. GO-based materials catalysis of IOP reduction by sulfide. IOP stability control, direct chemical reduction control (IOP + Sulfide), adsorption controls (IOP + GO-based materials) and reduction experiments (IOP + Sulfide + GO-based materials) of rGO-N and MrGO-N.

4.4.3. Chemical transformation pathway of IOP

Previous studies have elucidated the chemical and biological transformation pathway of IOP using GO and rGO as electron shuttle under non-oxidizing conditions[43,44]. However, the chemical transformation pathways have not been studied for IOP or any other recalcitrant pollutant using hybrid graphene nanosacks as electron shuttle. Samples from incubations using MrGO-N as electron shuttle were analyzed by HPLC-MS in order to identify the chemical byproducts of IOP at specific time intervals during reduction experiments and propose a precise chemical transformation pathway of this pollutant. The molecular weights (*m/z*) of 12 transformation products (TPs) were identified. The elemental composition and suggested chemical structures of the TPs are shown in Figure 4.7, which uses the time-dependent data to sketch the main chemical transformation pathways. Each TP and the reductive reactions that involve their structure modification are briefly described as follows.

The structure of TP 730.85, appearing in the 24 h (day 1) sample, indicates decarboxylation and deacetylation reactions in side chain B. In the day 2 sample, five further transformation products from TP 730.8 were observed. The structure of TP 729.90 and 714.50 implies a slight modification in side chain A, which includes dehydration and demethylation reactions. TP 662.70 indicates an N-demethylation in side chain A, decarboxylation and cleavage of the C-N and amide bonds at the side chain B. The rupture of side chain B, N-demethylation and cleavage of the C-N bond at the side chain A with subsequent removal of two iodine atoms (dehalogenation) of the aromatic ring results in the formation of TP 316.80. TP 248.90 involves the cleavage of C-N bond in side chain B and deiodination of the aromatic ring (HI). After 4 days of incubation, two new chemical byproducts were generated from the original IOP molecule. TP 772.80 and 758.60 involve the loss of a

molecule of H_2O in side chain A and B and sequential demethylation in side chain B. Moreover, TPs identified with *m/z* of 656.50 and 322.70 comes from either TP 729.90 or 714.50 after 6 days of incubation. TP 656.50 involves dehydration and demethylation reactions in side chain A and C-N bond rupture in side chain B. The cleavage of C-N bond and N-demethylation in side chain A, rupture of side chain B, demethylation and dehydration in side chain C and subsequent dehalogenation (removal of two iodine atoms) of the aromatic ring results in the formation of TP 322.70. Finally, the proposed structure of TP 588.70 and 742.70 (generated after 8 days of incubation) represents a modification in side chain A and B of TP 772.80 and 758.60, respectively, which include demethylation, N-demethylation, dehydration and deiodination reactions. After 10 days of incubation, generation of new chemical byproducts was not observed. The mechanisms of the reductive transformation pathway and *m/z* of TPs proposed in this work are consistent with studies using other catalysts, reducing agents and degradation strategies[28,36,43–47,50].

On the other hand, results previously obtained from incubations performed without electron shuttle (direct reduction by sulfide) revealed that the main TPs produced were 646.9, 768.7 and 788.8[43]. In consequence, it can be suggested that the redox catalytic activity of MrGO-N promoted reductive transformation reactions of IOP. This is supported by the generation of chemical byproducts with lower molecular weight as compared with TPs identified in control experiments conducted without MrGO-N (direct reduction of IOP by sulfide). Moreover, it can be observed that the TP with lowest *m/z* (248.90) was generated during the first 48 h. In addition, the complete deiodination of IOP molecule occurred at the same incubation time as can be seen in TP 248.90. These observations suggest that MrGO-N stimulated a greater transformation degree of IOP. The reductive transformation of IOP and

its correlation with the catalytic activity of MrGO-N can be elucidated by physicochemical properties of these hybrid nanomaterials as mentioned below.

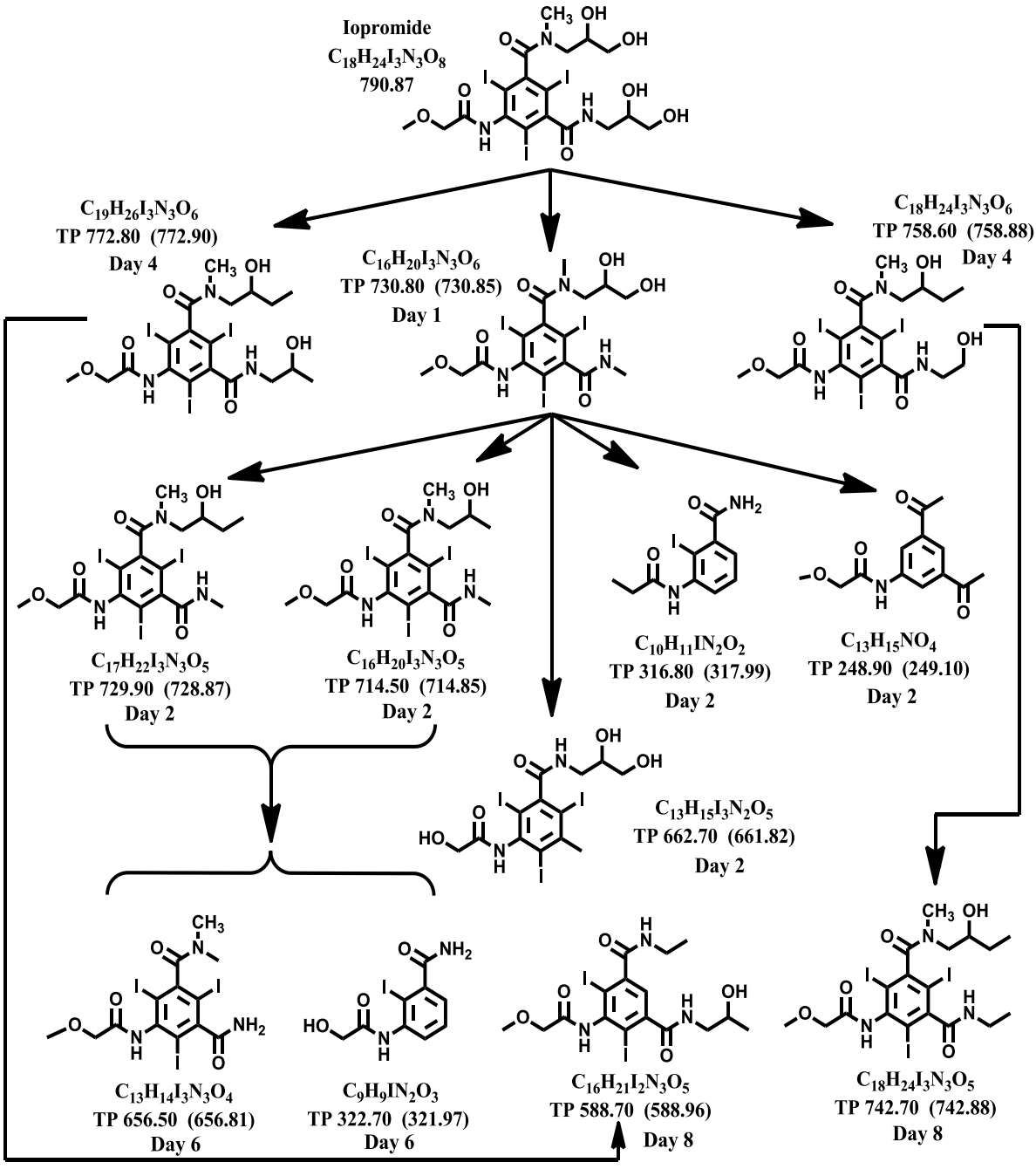

Figure 4.7. Chemical transformation pathway of IOP and generation of byproducts through incubation time by MrGO-N as electron shuttle.

4.4.4. Mechanism of IOP transformation mediated by MrGO-N

Different studies have explored the catalytic properties of carbon-based materials (e.g. activated carbon[56,59,67], carbon nanotubes[73,74] and activated carbon fibers[57,63]) in the reductive transformation of pollutants,[44,56,114] due to the presence of quinone groups in their structure, which serve as electron shuttle[60]. As revealed by titration results (see Table 4.1, section 4.4.1), the MrGO-N have a higher percentage (12.5 % more) of quinone groups, which might satisfactorily explain the transformation degree and removal efficiency of IOP since these functional groups have great redox activity[60,153]. These facts suggest that the redox activity of quinone-hydroquinone couples plays an important role in the reductive transformation mechanisms of IOP due to its contribution in the electron transfer process.

Other potential transformation mechanism of IOP is reported in previous works[43,44], which involves the chemical association of reactive non-bonding π-electrons present at the edges of graphene sheets of MrGO-N with the hydrogen, hydroxyl and halogenated[81] (iodinated) substituents of IOP molecule, promoting reductive reactions of this contaminant. This mechanism is supported by the generation of chemical transformation byproducts (partial rupture) of IOP as observed in the transformation pathway (see Figure 4.7).

Finally, several studies have employed the reducing catalytic power of magnetic NPs in order to improve the reduction of halogenated pollutants, dyes and heavy metals[192,193,198]. Magnetite (Fe_3O_4) is an iron oxide containing ferrous (Fe^{2+}) and ferric (Fe^{3+}) species in its chemical structure[199], which make it a potent reducing agent due to the redox processes than involves the reduction/oxidation of couple Fe^{2+}/ Fe^{3+} [200]. In addition, magnetite has the ability to transfer electrons because of its elevated conductivity by electron hopping between Fe^{2+} and Fe^{3+} ions[199,201]. Accordingly, it is possible to suggest that the presence of magnetic NPs (discussed in section 4.4.1) could be involved in the reductive reactions and

transformation mechanism of IOP due to the rapid electron transfer and redox processes of coupled Fe^{2+}/Fe^{3+} ions. In this context, a mechanism for the reductive transformation of IOP implies that the redox activity of magnetic NPs (oxidation of Fe^{2+}) immobilized on the MrGO-N could transfer electrons to quinone groups of graphene sheets of nanosacks and then to IOP molecule, which is the final electron acceptor in the redox conversion process[192]. Also, a direct electron transfer from couple Fe^{2+}/Fe^{3+} redox activity toward IOP molecule may occur. As discussed in section 4.4.2, the reduction kinetics performed in the presence of MrGO-N showed a higher IOP removal efficiency than rGO-N (72 % compared to 57 %), which demonstrated that the presence of the Fe_3O_4 NPs contribute in the electron transfer process for the reductive transformation of IOP[192]. Based on the above, it can be concluded that the reductive transformation of IOP is complex since several mechanisms in the electron transfer process could be involved.

4.5. Conclusion

The novel and successful application of MrGO-N as electron shuttle is reported for the reductive transformation of IOP. The results obtained from chemical reduction experiments demonstrated that the catalytic activity of MrGO-N enhances the removal and chemical transformation degree of IOP under reducing conditions. The results showed an important contribution of chemical and physical properties of MrGO-N in the electron transfer process for reductive transformation of IOP. Several mechanisms were proposed as key factors in reductive transformation of IOP, which involves high electrical conductivity and chemical reactivity of graphene sheets, redox catalytic activity of quinone-hydroquinone couples presents in MrGO-N, and rapid electron transfer and redox reactions of magnetic NPs immobilized in the nanosacks. The reductive transformation pathway of IOP was proposed. Chemical transformation byproducts with low molecular weight than IOP were

identified, involving complete deiodinated of aromatic ring and partial rupture of ramifications of IOP molecule. Finally, the treatment technique reported in this work visualizes a new approach to potentially apply GO-based materials as redox catalysts in continuous biological wastewater treatment systems in order to promote the reductive conversion of pollutants from contaminated waters.

Chapter 5

Novel application of magnetic nano-carbon composites as redox mediators in the reductive biodegradation of iopromide in anaerobic continuous systems*

*E. Toral-Sánchez, J.R. Rangel-Mendez, Robert H. Hurt, Juan A. Ascacio Valdés, Cristóbal N. Aguilar and F.J. Cervantes. *Submitted.*

5.1. Abstract

The redox-mediating capacity of magnetic reduced graphene oxide nanosacks (MrGO-N) to promote the reductive biodegradation of the halogenated pollutant, iopromide (IOP), was tested. Experiments were performed using glucose as electron donor in an upflow anaerobic sludge blancket (UASB) reactor under methanogenic conditions. High removal efficiency of IOP in the UASB reactor supplied with MrGO-N as redox mediator was observed in comparison with the control reactor lacking MrGO-N. Results showed 82 % of IOP removal efficiency under steady state conditions in the UASB reactor enriched with MrGO-N, while the control reactor showed IOP removal efficiency of 51 %. The precise microbial transformation pathway of IOP was elucidated by high-performance liquid chromatography coupled to mass spectroscopy (HPLC-MS) analysis. Biotransformation byproducts with lower molecular weight than IOP molecule were detected in the reactor supplied with MrGO-N as compared with the control, indicating their contribution in the redox conversion of this halogenated pollutant. Reductive reactions of IOP favored by MrGO-N led to completely dehalogenation of the benzene ring and partial rupture of side chains of this pollutant, which is the first step toward its complete biodegradation. Possible reductive mechanisms that take place in the biodegradation of IOP were stated. Finally, the novel and successful application of magnetic graphene composites in a continuous bioreactor to enhance the microbial transformation of IOP was demonstrated.

5.2. Introduction

Removal of persistent pollutants from contaminated water is challenging due to the potential risk generated in environmental compartments. The employment of carbonaceous materials in the degradation of contaminants by redox processes has been widely reported. Especially, activated carbon[56,59,67,68], activated carbon fibers[57,63] and carbon nanotubes[73,74]

have been studied as electron shuttles in the abiotic/biotic degradation of pollutants. The contribution of these carbon materials lies in the presence of quinone groups in their chemical surface, which are able to accept and donate electrons through oxidation-reduction reactions, serving as redox mediators (RM)[55,60,65]. Quinones are composed of two carbonyl groups in resonant form[60].

Graphene oxide (GO) and its partially reduced materials (rGO) have also been used as electron shuttles to promote the transformation of contaminants due to the redox activity of quinone groups presents in its chemical surface, and their superior catalytic activity in the zigzag edges of graphene sheets[81], which favor the reductive transformation of these compounds[59,61]. For example, the redox properties of GO and rGO have been explored in the degradation of environmental pollutants like azo dyes[118,119], nitro-compounds[120,122,123,132,202] and polyhalogenated organics[73]. These studies indicate a feasible opportunity to apply graphene-based materials as redox catalysts in the reductive degradation of contaminants. However, their implementation at full scale in biological wastewater treatment (WWT) systems is challenging due to the lack of mechanisms to maintain these catalysts inside the treatment systems, which could promote a toxicological effect on microorganisms due to their extended release into environmental compartments[203]. Accordingly, it is necessary the development of novel hybrid nano-carbon composites, with particular features that allow them to be applied in WWT systems by retaining and recovering strategies.

Lately, it has been documented the synthesis of hybrid nano-carbon composites with magnetic properties by aerosol-phase process. In this sense, the fabrication of these composites is performed by the encapsulation of magnetic nanoparticles (NPs) in folded

graphene sheets nanostructures with form of wrinkled rGO nanosacks[126,204,204]. The application of magnetic rGO nanosacks (MrGO-N) has been focused on radiological technologies[191] and on the removal of Cr(VI) from water[126]. However, their use in reductive biotransformation processes of environmental contaminants has not been documented yet. Just a few research works have documented the synthesis and application of carbonaceous materials with magnetic properties in the redox conversion of pollutants. As an example, Pereira et al.,[192] reported the use of carbon composites with magnetic properties as redox catalysts in the reductive degradation of azo dyes in batch assays. The excellent performance of these carbon composites can be explained by the combination of redox properties of both materials (magnetic NPs and carbon materials).

Iopromide (IOP) is a halogenated pharmaceutical compound with three iodine atoms in its aromatic ring. This compound is an X-ray contrast medium widely applied in radiological areas[28]. IOP is considered a priority contaminant because their physicochemical properties and chemical structure[25] confer it persistency in environmental compartments[26,30,31]. During conventional WWT processes, IOP is resistant to microbial degradation and hence released into aquatic environments at relative high concentration (μg/L)[30,31,33]. Consequently, it is demanded to propose novel strategies of IOP removal with the aim to be apply in the biological WWT systems. In this context, it has been studied the reductive biodegradation of IOP in an upflow anaerobic sludge blanket (UASB) reactor using anaerobic sludge enrichment with biogenic Pd^0 [46] and metal-humic substances[47]. Also, our previous works have employed the redox properties of GO and rGO in chemical (Toral-Sánchez et al. 2016) and biological[43,44] reductive transformation of IOP in batch assays. Nevertheless, the application of GO-based materials in a continuous biological system for biotransformation

of IOP has not been reported yet. Accordingly, this study focused on evaluating a novel strategy for reductive biodegradation of IOP by the use of MrGO-N as RM in an anaerobic continuous system. The redox-mediator capacity of these nano-carbon composites was studied in a UASB reactor under methanogenic conditions. Finally, the biodegradation pathway of IOP and reductive reactions mechanisms occurring are also explained.

5.3. Material and methods

5.3.1. Materials and chemicals

IOP (Ultravist ® 370) and Glucose (used as electron donor) were purchased from Bayer Schering Pharma and Aldrich, respectively. Basal medium solution was composed of several mineral salts (K_2HPO_4, $NaHCO_3$, $MgSO_4$, NH_4Cl and $CaCl_2$) and trace elements dissolved in distilled water as described in previous works[43,57,61].

The fabrication of MrGO-N was performed using an aerosol-phase methodology proposed previously[126,191,204] using a colloidal suspension of GO (0.5 mg/mL) and magnetite NPs (1mg/mL). In order to demonstrate the assembly of magnetic NPs in the MrGO-N, micrographs of these nano-carbon composites were performed using a JEOL JEM-2010 High Resolution Transmission Electron Microscope (HRTEM).

5.3.2. Source of anaerobic sludge and activation

Methanogenic granular sludge from a full-scale UASB reactor treating brewery wastewater (Sonora, Mexico) was used as inoculum to evaluate the reductive biotransformation of IOP. Volatile suspended solids (VSS) of methanogenic sludge were previously estimated at 6.15 % based on wet weight[46]. The methanogenic sludge was acclimated for one month in a lab-scale UASB reactor with volume of 1.5 L at room temperature (25 ± 2°C). The hydraulic residence time (HRT) was 24 h. During this operational period, the bioreactor

was constantly fed with 1 g of chemical oxygen demand (COD)/L-d of glucose and mineral medium reached a constant COD removal > 90 % under steady conditions.

5.3.3. Microbial degradation of iopromide in UASB reactors

Two lab-scale UASB reactors (330 mL of working volume) were simultaneously operated and inoculated with 10 g VSS/L of previously acclimated methanogenic granular sludge. The working reactor (R-MN) was enriched with MrGO-N and tailored with a magnetic trap made with 30 H neodymium magnets and in stainless steel to the upper part of the reactor in order to retain and recover the MrGO-N dispersed in the reactor. The control reactor (R-ctrl) was inoculated without MrGO-N. Reactors were operated for 28 days with a constant HRT of 12 h at room temperature (25 ± 2 °C) and sheltered from light to inhibit the photodegradation of IOP and biotransformation byproducts. The reactors were fed during operational period with the mineral medium mentioned above.

Before reactors operation, 150 mL of MrGO-N solution with a concentration of 85 mg/L was mixed with the stabilized sludge in the R-MN and then pre-incubated for 48 h. After this period, R-MN and R-ctrl was continually provided with 1 g COD/L-d of glucose and an initial concentration of 200 μg/L of IOP. During the operation period of R-MN, three pulses of 100 mL of the aforementioned MrGO-N solution were applied on days 7, 15 and 22. The performance of both bioreactors was evaluated by monitoring the effluent pH, ORP of the system and COD removal efficiency. Samples were taken from effluent of anaerobic bioreactors at selected time to determine the IOP removal and generation of its biodegradation byproducts as described below.

5.3.4. Analytical procedures

The IOP concentration in the influent and effluent of both bioreactors was determined by high-performance liquid chromatography (HPLC) using an Agilent Technology 1260 series chromatograph as previously described[43,44]. Identification of biotransformation byproducts of IOP was carried out by HPLC coupled to mass spectroscopy (HPLC-MS) in a Varian ® 500-MS ion trap mass spectrometer as reported in previous work[44]. VSS and COD was estimated according to standard methods[205]. The ORP and pH of the biological system was monitored using a Thermo Scientific STARA2110 Orion Star A211 benchtop pH meter with electrode stand.

5.4. Results

5.4.1. Microbial transformation of IOP in anaerobic continuous systems

The reductive biodegradation of IOP was assessed in continuous UASB reactors (R-ctrl and R-MN). COD removal efficiency, as well as ORP and pH monitored during the operational period of the bioreactors are shown in Figure 5.1. COD removal efficiency (Figure 5.1A) of R-MN remained constant with an average of 93.7 ± 2.22 %. Similarly, ORP of the system (Figure 5.1B) and effluent pH values (Figure 5.1C) of R-MN remained constant during the same operational period with values of -190.1 ± 19.36 mV and 7.27 ± 0.17, respectively. No significant variations of these parameters were detected in R-ctrl (see Figure 5.1) with respect to R-MN, which indicates that there was no negative impact in the performance of the reactor supplemented with MrGO-N. In addition, Table 5.1 shows the performance of R-MN and R-ctrl during the operational period. The average ORP for R-MN and R-ctrl was -190.1 ± 19.36 mV and -179.97 ± 10.76 mV, respectively. Also, the effluent pH for R-MN and R-ctrl was 7.27 ± 0.17 and 7.26 ± 0.06, respectively. Under methanogenic conditions, the optimal ORP of the system is around to -200 mV and the range of pH is between 6.5

and 7.5[206]. These results suggest that the methanogenic conditions remained optimal during the operational period in both reactors. Also, it can be observed that COD removal efficiency, ORP and pH values of R-MN remained constant when the pulses of MrGO-N were applied (see stages of Table 5.1), which confirms the absence of negative impact on this bioreactor when enriched with this carbon composites as electron shuttles.

On the other hand, biodegradation of IOP was also assessed in both UASB reactors at a constant concentration of 200 μg/L for 28 days, with glucose provided as an electron donor and carbon source. The removal efficiency of IOP during the operational period for both reactors is shown in Figure 5.2 and Table 5.1. It can be observed in R-MN and R-ctrl a low and similar IOP removal (~ 40 to 55 %) in the first six days of operation, suggesting an acclimation period of both inocula to the experimental conditions. However, when the first pulse of MrGO-N was applied in R-MN (day 7), an abrupt increase in the IOP removal was observed from 54.4 ± 1.6 to 81.05 ± 1.1 %, which indicates a clear contribution of MrGO-N in the biotic reduction of this pollutant. Subsequently, R-MN achieved an average IOP removal of 82.01 ± 3.83 %. In contrast, R-ctrl achieved only 51.18 ± 6.7 % in average of IOP removal after the sixth day of operation. These results indicate a better performance of IOP removal in R-MN as compared to that observed in R-ctrl, which suggest that catalytic activity of MrGO-N plays a fundamental role during the reductive biodegradation of IOP under methanogenic conditions.

Table 5.1. Performance of R-MN and R-ctrl after application of MrGO-N pulses along the operational period.

	Start-up Day 0-6		**Stage 1 1st. Pulse Day 7-15**		**Stage 2 2nd. Pulse Day 16-22**		**Stage 3 3rd. Pulse Day 23-31**	
	R-ctrl	**R-MN**	**R-ctrl**	**R-MN**	**R-ctrl**	**R-MN**	**R-ctrl**	**R-MN**
% IOP removal	41.89 ± 0.85	51.20 ± 1.31	51.55 ± 1.63	78.32 ± 1.36	51.39 ± 4.19	83.92 ± 1.33	56.35 ± 1.71	81.41 ± 1.73
% COD removal	94.06 ± 1.47	93.30 ± 1.25	95.10 ± 0.67	93.07 ± 1.22	94.16 ± 1.48	95.50 ± 0.61	93.72 ± 0.71	93.32 ± 0.91
ORP (mV)	-166.56 ± 3.59	-180.78 ± 7.83	-174.82 ± 8.37	-191.72 ± 12.45	-195.77 ± 5.24	-188.13 ± 4.14	-182.76 ± 4.82	-189.55 ± 3.99
pH	7.29 ± 0.06	7.41 ± 0.08	7.44 ± 0.04	7.29 ± 0.06	7.08 ± 0.01	7.12 ± 0.07	7.29 ± 0.09	7.27 ± 0.07

The morphology of MrGO-N was observed by high resolution micrographs as reported in Chapter 4, section 4.1.1. It can be seen that magnetic NPs are immobilized inside of nanosacks with a few NPs appearing on the outside of this nano-carbon composite[191]. The presence of magnetic NPs in MrGO-N could contribute in IOP removal as it was observed in R-MN (see Figure5.2). These observations can be explained by the excellent reducing power of magnetic NPs[198,199,207].

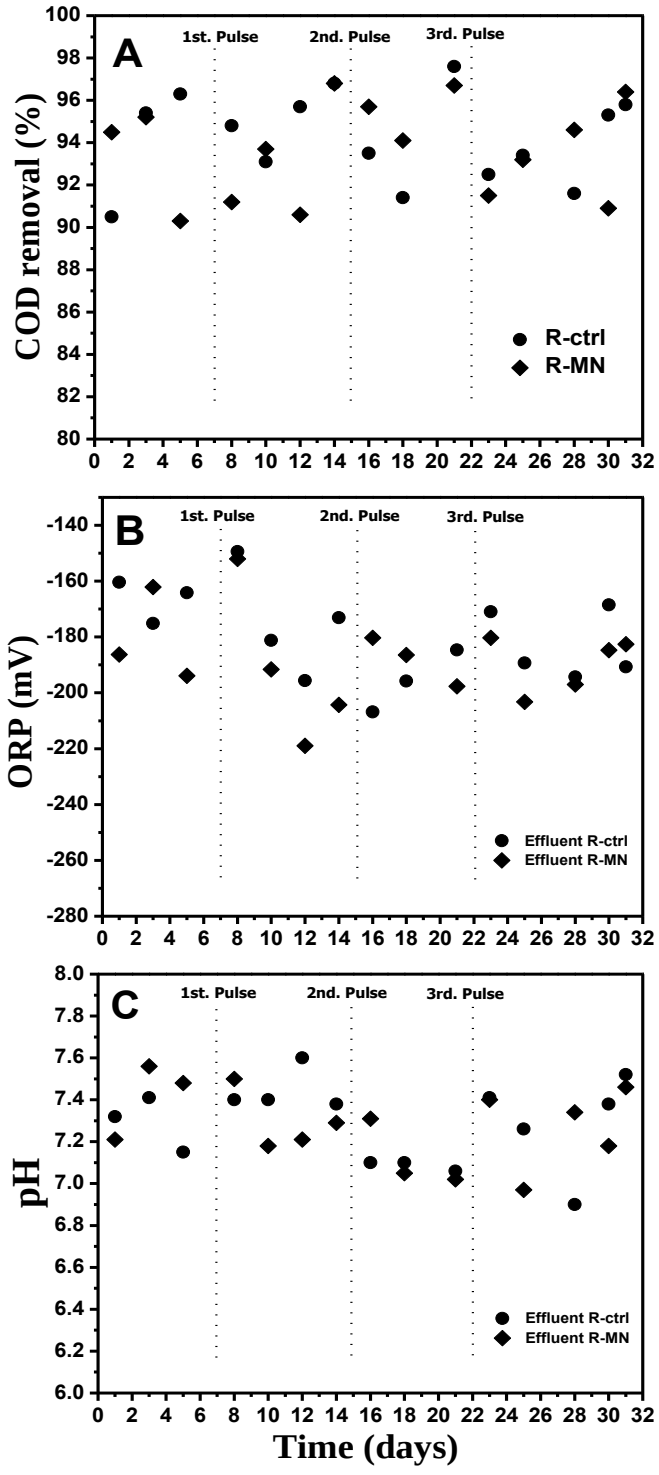

Figure 5.1. Performance of both reactors (R-MN and R-ctrl) regarding to (A) COD removal efficiency, (B) ORP of the system and (C) effluents pH values, as function of operational period.

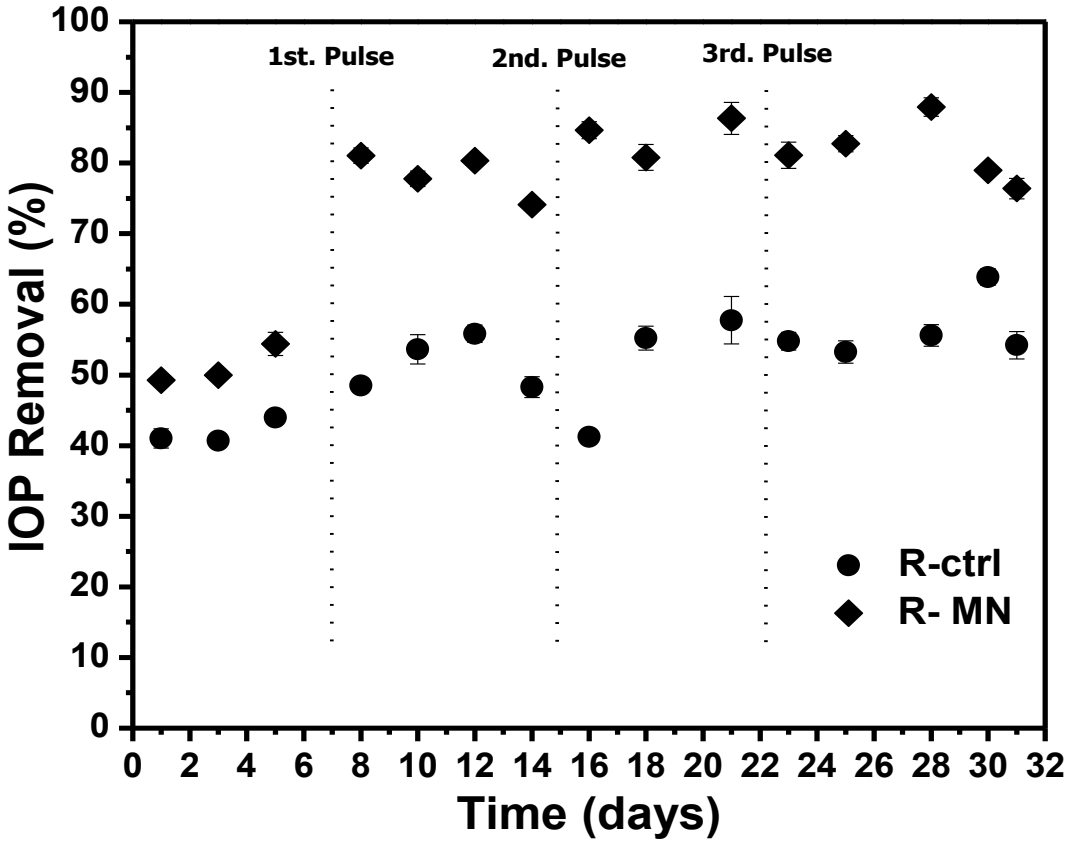

Figure 5.2. Performance of R-MN and R-ctrl regarding IOP removal efficiency during the whole operational period.

5.4.2. Biotransformation pathway of IOP in UASB reactor

With the aim to propose a precise microbial transformation pathway of IOP, byproducts generated from its biodegradation from both reactors (R-MN and R-ctrl) were assessed by HPLC-MS at specific time intervals during the operational period. The molecular weights (m/z) of 28 biotransformation products (TP) were recognized in R-MN. Proposed chemical structure and elemental composition of the TPs are shown in Figure 5.3. The chemical structure modification of IOP along the operational period of R-MN will be concisely explained below.

TP with *m/z* of 788.89, appearing in the first sampling day, indicates a dehydration reaction in side chain B. In sampling day 5 sample, six additional byproducts from TP 788.89 were observed. TPs 714.5, 774.4, 758.5, 744.5, 662.5 and 634.7 imply partial rupture of side chain A and B, including dehydration, demethylation and decarboxylation reactions, and cleavage of the C-N bond. Specially, TP 634.7 implies the elimination of one iodine atom (dehalogenation) from the aromatic ring, and TP 662.5 involves the rupture of side chain B. After 10 days of operational period, six new biological byproducts were generated from different chemical structures. TPs identified with *m/z* of 742.6, 690.6, 674.6 and 728.3 come from either TP 774.4, 758.5 or 744.5. Structures of TP 742.6 and 728.3 involve demethylation and dehydration reactions in side chain A and B. TPs 690.6 and 674.6 involve demethylation and decarboxylation reactions, cleavage of amide bond and subsequent rupture of side chain B ramification. The proposed structure of TP 322.8 exhibits several reductive reactions in side chain A, B and C of either TP 662.5 or 634.7, which included the rupture of C-N bond, demethylation reactions and the double dehalogenation of the benzene ring. TP 390.8 results from dehydration, demethylation and amide bond rupture in side chain A, cleavage of C-N bond in side chain B with a subsequent removal of two iodine molecules of the benzene ring.

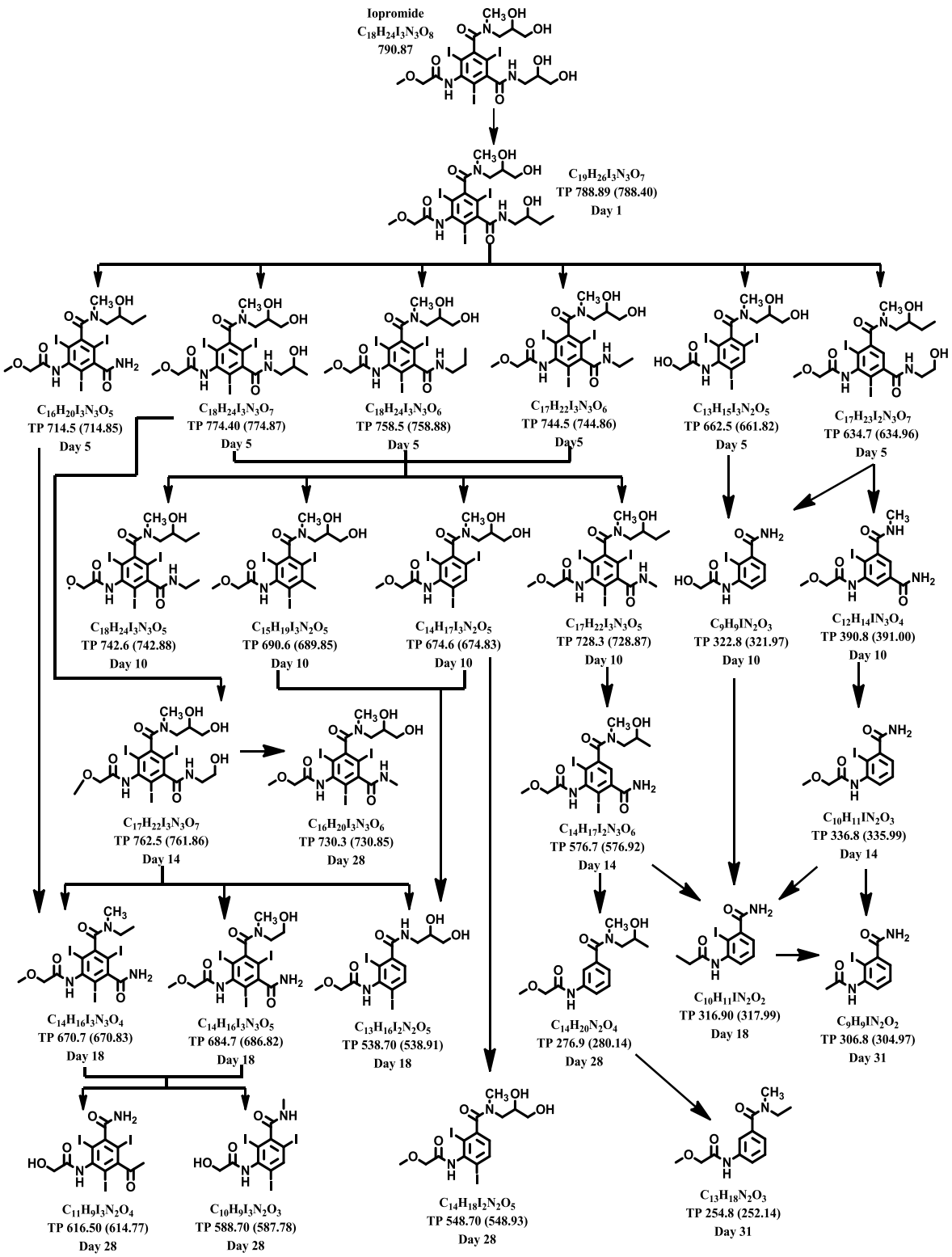

Figure 5.3. Reductive biotransformation pathway of IOP in the UASB reactor supplied with MrGO-N as RM.

Samples collected after 14 days of operational period contained three additional byproducts derived from IOP degradation. TPs 762.5, 576.7 and 336.8 come from TP 774.4, 728.3 and 390.8, respectively. The chemical modification of TP 762.5 involves demethylation of side chain A. TP 576.7 suggest demethylation in side chain A, cleavage of C-N bond in side chain B and deiodination of the aromatic ring. The structure of TP 336.8 implies the rupture of C-N bond in side chain A, rupture of side chain B ramification and dehalogenation of two iodine atoms (HI) of the aromatic ring. Furthermore, after 18 days of operation, generation of four new byproducts was observed. The rupture of C-N bond in side chain B, the loss of H_2O molecules (dehydration) and demethylation reactions in side chain A of TP 762.5 or 714.5 resulted in the evolution of TPs 670.7 and 684.7. The structure proposed for TP 538.7 comes from either TP 762.5, 690.6 or 674.7, which implies the rupture of side chain B ramification and elimination of one iodine atom. Also, dehydration, demethylation and decarboxylation reactions of side chain C of TPs 336.8 and 322.8, as well as the rupture of C-N bond of side chain A, rupture of side chain B ramification and subsequent deionidation of the aromatic ring of TP 576.7 result in the generation of TP 316.9.

Structures of TPs with *m/z* of 730.3, 616.5, 588.7, 548.7 and 276.9 appeared in the day 28 of the operational period. TPs 616.5 and 588.7 result from several reactions, such as demethylation and dehydration of side chain A and B, rupture of C-N and amide bonds in side chain A and rupture of side chain B ramification of either TPs 670.7 or 684.7. TP 548.7 suggests the deionidation of the aromatic ring (HI) of TP 674.6. The rupture of side chain B ramification and the completely dehalogenation of the aromatic ring (removal of three iodine atoms) of TP 576.7 results in the generation of TP 276.9. Finally, two new byproducts were detected on day 31 (end of the operational period). Structure of TP 306.8

shows a partial rupture in side chain C of TP 336.8 and 316.9, including demethylation and removal of one molecule of H_2O. TP 254.8 involves demethylation and dehydration of side chain A of TP 276.9. Similar fragmentation pathway of IOP and *m/z* of biodegradation byproducts identified in this research are suggested in our previous works[43,44] as well as in others studies using different chemical or biological degradation strategies[28,36,43–47,50].

Moreover, TPs with lower m/z (648.6 and 588.7) in R-ctrl were also identified. Therefore, it can be suggested that the enrichment of MrGO-N as electron shuttles in the R-MN promoted a greater degree of IOP biotransformation, which was manifested by the generation of biological byproducts with lower *m/z* in comparison with the byproducts formed in R-ctrl. Furthermore, it can be observed the complete dehalogenation of the aromatic ring of IOP molecule (TPs 276.9 and 254.8) during the operational period of R-MN.

5.5. Discussion

The present study reports the novel application of hybrid graphene materials, in the form of MrGO-N, as RM in the biotransformation of a halogenated pharmaceutical pollutant (IOP) in an UASB reactor. The use of GO and rGO has previously been demonstrated as effective electron shuttles to improve the degradation of this pharmaceutical in chemical and biological batch incubations[43,44]. However, a mechanism to retain and recover these catalysts in a biological continuous system is necessary in order to employ GO-based materials for the reductive transformation of organics presents in WWT facilities. In this sense, the present work reports a strategy for retain novel nano-carbon composites in an UASB bioreactor by magnetic field.

Results from biological experiments conducted in the R-MN showed high removal efficiency of IOP. Also, it was demonstrated that the redox catalytic activity of MrGO-N promoted a further biotransformation degree of this pollutant. This pharmaceutical is a halogenated compound with three iodine atoms bonded to the benzene ring, and hydroxyl and carboxyl groups in their side chains, which makes it a persistent environmental contaminant[25,46]. It has been reported that the degradation of halogenated organics is performed by reductive dehalogenation reactions that take place under reducing environments (≤ -400 mV) and generally requires an external electron donor[46,208]. As discussed in the results section, the average value of ORP during the operational period of R-MN was -190.1 ± 19.36 mV, which suggest that the system conditions drive the reductive dehalogenation (deionidation) of IOP as observed in the biotransformation pathway of this pollutant (see Figure 5.3). On the other hand, it has been reported that the resistance to microbial degradation of halogenated compounds is related to the bond strength between carbon atoms and halogenated groups. Accordingly, it is expected that iodinated organics are more susceptible to biodegradation than other halogenated compounds since C-I bonds are weaker (209 kJ/mol) than others halogen-carbon bonds (C-Br (280 kJ/mol), C-Cl (397 kJ/mol) and C-F (536 kJ/mol))[209].

As documented by several authors [27,28,30], microbial degradation of IOP is challenging due to its high biochemical stability and resistant to reductive transformation. Also, IOP molecule presents a low removal during the application of biological conventional treatments (activated sludge) due to their high polarity (log K_{OW}= −2.33) and high water solubility (0.97 mol/L), thus sorption onto sludge or sediments is negligible[13,26]. Accordingly, several chemical or biological strategies have been studied in order to

facilitate the removal of this halogenated contaminant. As examples, it has been explored the removal of IOP by electron bean irradiation technology[33], advanced oxidation[210,211], reductive hydrodehalogenation with porous palladium-nickel catalyst[27], oxidation by electrochemical treatment[45], ozone oxidation[212], as well as aerobic degradation strategies by activated sludge[48], *Pseudomonas*[51] and fungus *Trametes versicolor*[36]. Anaerobic strategies using methanogenic consortia in UASB reactors have also been employed in order to evaluate their potential application in the reductive transformation of IOP. Pat-Espadas et al., reported an IOP removal efficiency of 81 % using immobilized biogenic Pd(0) as catalyst[46]. Also, Cruz-Zavala et al., achieved a IOP removal efficiency of 80 % applying iron-humic complexes as RM[47]. In addition, these works proposed the biotransformation pathway of IOP, where reductive reactions of IOP molecule generate byproducts with simpler chemical structure. Accordingly, this research work also proposed the biotransformation pathway of IOP using carbon-based composites (MrGO-N) as RM in UASB reactor. Proposed biotransformation pathway (see Figure 5.3) implies that MrGO-N promoted deiodination of aromatic ring and rupture of hydroxyl, carboxyl and methyl bonds from side chains of IOP molecule. The reductive reactions that took place in R-MN could be explained by complex mechanisms that are related to the redox properties and catalytic activity of MrGO-N as electron shuttle.

It has been documented that quinone groups present as of oxygenated functionalities of GO sheets improve the redox conversion of environmental contaminants[56,114], including IOP[43,44], due to their superior redox-mediating capacity[153]. In addition, it has been stated that the redox activity of quinone groups is fundamental in the electron transfer process towards electron acceptor pollutants, improving their reductive transformation reactions[43,55,132]. In this sense, previous works have documented a great stability of

carbonyl groups of GO sheets after thermal reduction processes[77,99,101]. As reported by Chen et al., hybrid MrGO-N are conformed of rGO sheets produced by thermal reduction process during synthesis of filled nanosacks[191]. Also, our previous work showed a high distribution and stability of carbonyl groups in rGO sheets after the reduction process[43]. As a consequence, it can be proposed that the redox-mediating capacity of quinone groups present in rGO sheets of MrGO-N contributed to the reductive reactions of IOP performed in R-MN as observed in previous section (see Figure 5.1 and 5.3). Accordingly, it is expected that the catalytic activity of quinone moieties is involved in the biotransformation mechanisms of this halogenated pollutant.

Moreover, it has been documented that the catalytic activity of graphene sheets improves the conversion rate of chemical compounds by reductive reactions[120,131]. The π-electrons from zigzag edges of rGO have the ability to react with the functionalities bonded of aromatic ring of IOP molecule because of their great chemical reactivity[81]. As aforementioned, the MrGO-N are conformed by rGO sheets, which could interact with iodine atoms and functional groups of side chains of IOP due to the π-electrons reactivity, promoting its molecular activation[43]. These facts suggest another reductive biotransformation mechanism of IOP, which is well founded by the formation of biological TPs as a result of reductive reactions that underwent this halogenated contaminant (see transformation pathway, Figure 5.3).

Until now, chemical mechanisms involved in the microbial transformation of IOP have been proposed. However, the biological processes involved in the reductive reactions of IOP are key drivers in its biotransformation as reported in our previous work[44]. It has been reported that GO-based materials improve the transport of electrons by extracellular electron transfer mechanism, favoring the reductive biological reactions of organic

contaminants[188,189,213]. In this sense, it has been documented that extracellular polymeric substances from microorganisms exhibit redox activity due to the presence of proteins and humic substances, suggesting an important contribution in the redox conversion of environmental pollutants[214,215]. Finally, another biological mechanism implies the biological oxidation of substrate (glucose) by methanogenic consortium, which generates electrons that can be donated directly to the final electron acceptor (IOP). Also, the electron transfer process may take place from the oxidation of glucose to quinone groups of rGO sheets of MrGO-N, which can accept electrons. After that, the electrons can be donates by quinones groups (forming hydroquinones groups) and then, transfer through graphene sheets[60]. Finally, the electrons can be accepted by IOP molecule. Similar mechanisms are proposed in previous works[192].

According to these mechanisms, it can be concluded that the redox behavior of MrGO-N contributed in the redox conversion of IOP since R-MN showed an average IOP removal of 82 % while R-ctrl only achieved 51 % of IOP removal.

The biotransformation mechanisms proposed above may be significant drivers on the reductive reactions of IOP. The anaerobic continuous experiments conducted with MrGO-N as RM showed the generation of biological byproducts with simpler structure than IOP molecule, which are more susceptible to complete biodegradation, mainly due to the reductive deiodination of aromatic ring of this pollutant. The present study exhibits, for the first time, the reductive biodegradation of IOP using MrGO-N as electron shuttle. The novel application of MrGO-N as RM in UASB reactor was demonstrated for the removal of IOP. The great catalytic activity of MrGO-N was evident due to the high removal efficiency and further biotransformation degree of IOP. The main advantage of this reductive transformation strategy lies on the simultaneous use of the redox activity of

MrGO-N and their magnetic properties to be captured inside the biological continuous process. Finally, the removal strategy proposed in this study shows a feasible option to apply hybrid graphene-based materials in biological WWT systems.

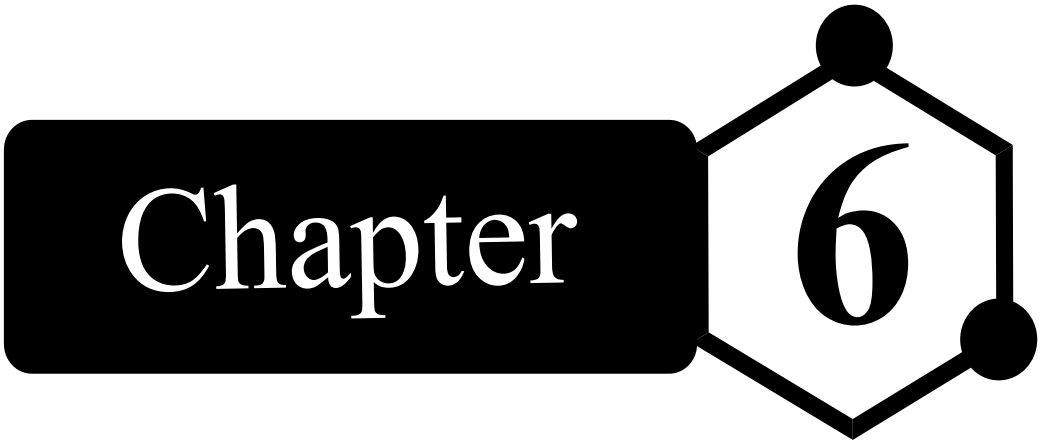

General discussion

6.1. Introduction

Iopromide is a contaminant, which may have important eco-toxicological effects in the environment. Reductive transformation of IOP by the application of GO-based as redox catalysts is a feasible option for pollution control. However, the main challenge of this technology is the tailoring of GO-based materials as RM in continuous biological systems. Hence, this dissertation was mainly focused on exploring the redox-mediating capacity of GO, rGO and MrGO-N in the degradation of the halogenated pollutant, IOP, in batch assays and in a continuous biological system. This study demonstrated that GO-based materials can promote reductive reactions of IOP under abiotic and biotic conditions. These results constitute the first reports on the application of GO-based materials regarding pharmaceuticals degradation, which contribute to the knowledge of these nanomaterials about their ability to act as electron shuttles.

On the other hand, magnetic graphene composites were tested as RM for reductive biodegradation of IOP in a continuous bioreactor under methanogenic conditions. Methanogenesis is complex biological process, which yields methane as a final product and is mediated by anaerobic microorganisms from the archaea domain. Methanogenic consortia consist of three main groups: acidogens, acetogens and methanogens[216,217]. Methanogenesis is the final step in the biological decomposition of biomass in the absence of oxygen[218]. Granular methanogenic sludge offers excellent settling properties, which is ideal for use in UASB reactor[46].

In the present dissertation, key aspects related to the reductive transformation of IOP by the application of GO-based materials as RM were studied, and the discussion focuses on the importance of physicochemical properties of GO-based materials in the reductive reactions of IOP. Likewise, the contribution of metabolic activity of microorganisms in the redox

conversion of the model pollutant, IOP, and the electron transfer mechanisms involved in the microbial degradation processes were discussed. The good knowledge of these factors leads to future employment of GO-based materials as electron shuttles for the degradation of several priority pollutants present in contaminated waters by redox processes.

6.2. Importance of intrinsic properties of GO-based material in the reductive transformation of IOP

In this study, it was demonstrated that one of the most important aspects to consider in the redox conversion of IOP is related to the intrinsic properties of GO-based materials. The results shown in **Chapters 2, 3 and 4** revealed that the chemical surface and physical properties of GO, rGO and MrGO-N play a fundamental role in their redox-mediating activity, and in the reductive transformation of IOP by electrons transfer mechanisms that take place during the redox conversion process. In order to discuss this issue, Table 6.1 summarizes the removal efficiency and maximum removal rate of IOP obtained in the different treatments evaluated in this thesis. Accordingly, it was observed that rGO-4 as electron shuttle achieved the highest removal and maximum removal rate of IOP in both chemical and biological systems. Regarding the chemical assays explored in **Chapter 2**, the removal and maximum removal rate of IOP were 66 % and 64.74 μg/L-d, respectively, when rGO-4 was applied as RM. In contrast, only 54% of IOP removal efficiency and 35.84 μg/L-d as maximum removal rate was observed in the presence of GO as electron shuttle. These results suggested a 1.8-fold increase in the maximum removal rate of IOP in the presence of rGO-4 compared with the experiments amended with GO as electron shuttle.

Moreover, the results shown in **Chapter 4** demonstrated that the use of MrGO-N as RM enhanced the removal efficiency and maximum removal rate of IOP in batch incubations, indicating an IOP removal efficiency of 77 % and a removal rate of 57.73 μg/L-d. In comparison with rGO-4 material, the MrGO-N showed a best performance regarding the removal efficiency of IOP under abiotic conditions.

In addition, the transformation pathways of IOP proposed in **Chapter 2 and 4** (see Figure 2.7 and 4.7, respectively) revealed important differences in the chemical structure of generated byproducts. In this sense, the simpler chemical byproduct identified in experiments conducted with rGO-4 as RM was TP 314.18, indicating the removal of two iodine atoms (dehalogenation) and rupture of side chain A of IOP molecule. Meanwhile, the simpler structure identified in the experiments conducted with MrGO-N as RM was TP 248.90, suggesting the completely reductive dehalogenation (removal of three iodine atoms) and partial rupture of side chain A and B of the aromatic ring of IOP. These results exhibit that the presence of MrGO-N promoted a greater transformation degree of IOP, which was evident by the formation of TP with simpler chemical structure than that observed in experiments amended with rGO-4 as RM.

Table 6.1. Removal efficiency and maximum removal rate of IOP estimated for all experimental treatments explored in this thesis.

	Removal efficiency and maximum removal rate of IOP						
	Chemical system		**Biological systems**				**UASB reactor**
			Methanogenic		**Sulfate-reducing**		
	*(%)	**(μg/L-d)	*(%)	**(μg/L-d)	*(%)	**(μg/L-d)	
IOP stability	5	-----	8	-----	10	-----	-----
Adsorption controls[a]	< 12	-----	< 10	-----	< 13	-----	-----
Na_2S[b]	25	22.58	-----	-----	-----	------	-----
Sterile biomass[c]	-----	-----	9	-----	11	------	-----
Active biomass[d]	-----	-----	20	12.48	38	31.20	52 % during 31 days of operation
GO	54	35.84	64	34.02	61	61.38	-----
rGO-2	58	59.79	75	59.12	80	73.34	-----
rGO-4	66	64.74	77	68.76	85	90.39	-----
MrGO-N	72	57.73	-----	-----	-----	-----	81.01 % during 31 days of operation

[a]Adsorption control experiments without electron donor.
[b]Direct chemical reduction by sulfide (without GO-based materials).
[c]Adsorption control experiments without GO-based materials and electron donor.
[d]Direct biological reduction by active biomass (without GO-based materials).
*These columns indicate the removal efficiency of IOP.
** These columns indicate the maximum removal rate of IOP.

These facts (removal efficiency and transformation degree of IOP) can be explained by the presence of magnetic NPs in MrGO-N immobilized on the external surface of these materials. As discussed in **Chapter 4**, magnetic NPs have an excellent reducing power due to their ability to transfer electrons toward reactants and to their great catalytic activity[198,199,207]. These unique properties are due to magnetite, which contains both iron species (Fe^{2+} and Fe^{3+}) in its chemical structure[199]. Also, the presence of iron species confers redox properties to magnetic NPs because the couple Fe(II)/Fe(III) exhibits reduction-oxidation reactions[200]. In this sense, the redox behavior of magnetite NPs has been explored in the reduction of pollutants like nitrocompounds[198,219], Hg (II)[220], Cr (VI)[221] and U (VI)[199,222]. Accordingly, it is probably that the redox activity of magnetic NPs is involved in the reductive transformation of IOP, which is supported by the results obtained in **Chapter 4**.

Besides what was reported in **Chapters 2 and 4**, IOP removal efficiency using rGO-4 and MrGO-N as RM can be compared with the results of other studies reported in the literature, which explored different removal strategies. Table 6.2 contains the IOP removal of selected studies that were conducted in batch incubations and chemical systems as those reported in this thesis.

In comparison to this research, the advanced oxidation processes (AOP) showed a similar performance regarding IOP removal (see Table 6.2). However, the time with which the removal of IOP is carried out in the AOP is much slower than the reported in this thesis (min vs days). Although it is a good option to use AOP in the removal of recalcitrant pollutants, the main disadvantage of using this technique is the generation of highly reactive OH radicals, which reacts non-selectively with water constituents, including natural organic matter and bicarbonate[27]. On the other hand, the use of Pd-Ni catalysts

considerably improved the IOP removal (95 %) in a short time (see Table 6.2). Nevertheless, the application of Pd-Ni catalysts in the presence of hydrogen as removal technique implies high operational and investment costs. Therefore, development of degradation strategies of IOP, like redox conversion processes, is desirable, which was the motivation of this dissertation. In addition, the strategy proposed in this study was devised to be a complementary treatment technique for complete degradation (mineralization) of IOP by biological conventional systems. Hence, the redox conversion processes by the use of GO-based materials as electron shuttles could be a competitive strategy for reduction of IOP.

Table 6.2. IOP removal efficiency reported by several chemical strategies

Strategy	IOP removal efficiency (%)	Reference
Ozonation/ultrasound.	65 % in 30 min	[52]
Advanced oxidation process.	70 % in 45 min	[53]
Metal-catalyzed (Pd-Ni) hydro-dehalogenation.	95 % in 70 min	27
Redox conversion process using rGO materials as catalysts.	66 % in 12 days	**This work, Chapter 2**
Redox conversion process using MrGO-N as catalysts	72 % in 8 days	**This work, Chapter 4**

On the other hand, the removal efficiency and maximum removal rate of IOP in biological systems discussed in **Chapter 3** showed a similar behavior than chemical systems (Chapter 2). With respect to microbial reduction of IOP under methanogenic conditions, it is possible to observe that rGO-4 material promoted the highest removal efficiency (77 %) and maximum removal rate (68.76 μg/L-d) of IOP, which indicated a 2.0-fold increase in the removal rate of IOP with respect to experiments conducted with GO as RM. Similarly, the reduction experiments of IOP under sulfate-reducing conditions achieved an IOP removal efficiency of 85 % and a maximum removal rate of 90.39 μg/L-d in the presence of rGO-4 as electron shuttle. These results indicated a 1.47-fold increase in the removal rate of IOP as compared to microbial reduction performed with GO as RM. Table 6.3 shows a comparative summary of IOP removal efficiency by selected biological treatment techniques at similar conditions (batch assays) as those explored in this study.

As can be observe in Table 6.3, the removal efficiency of IOP under methanogenic and sulfate-reducing conditions was 77 % and 85 %, respectively. Meanwhile, the IOP removal efficiency by the use of fungus *Trametes versicolor* and groundwater/soil system was 60 % and 80 %, respectively. Accordingly, the highest removal efficiency of IOP in biological systems was achieved by the application of rGO-4 as catalyst, which suggests a potential application of rGO materials as RM in biological wastewater treatment systems.

Table 6.3. IOP removal efficiency reported by several biological strategies

Strategy	IOP removal efficiency (%)	Reference
Aerobic treatment by the use of fungus *Trametes versicolor*.	60 % in 12 days	36
Aerobic treatment in groundwater/solid systems.	80 % in 20 days	28
Anaerobic treatment using rGO-4 as RM under methanogenic conditions.	77 % in 11 days	**This work, Chapter 3**
Anaerobic treatment using rGO-4 as RM under sulfate-reducing conditions.	85 % in 8 days	**This work, Chapter 3**

Moreover, the transformation pathways elucidated in **Chapters 2, 3 and 4** revealed that the presence of rGO-4 as RM stimulated reductive reactions in IOP molecule. Analysis performed with HPLC-MS demonstrated the generation of transformation byproducts with simple chemical structure than IOP in presence of rGO-4 as electron shuttle. In this context, the simpler TPs with *m/z* reported in chemical systems (Figure 2.7), methanogenic (Figure 3.3) and sulfate-reducing (Figure 3.4) conditions were 314.80, 306.80 and 254.70, respectively. Instead, the batch assays performed in absence of RM revealed that the simpler TPs produced were 646.90, 646.60 and 578.9 under chemical, methanogenic and sulfate-reducing conditions, respectively. According to these results, it was demonstrated that the presence of rGO-based materials as RM promoted a higher extent of IOP transformation in both chemical and biological systems, which involves reductive reactions

such as dehalogenation, dehydration, demethylation and decarboxylation, as compared with those incubations carried out without RM.

This behavior can be explained by the intrinsic properties of rGO-4 material. The physicochemical characterization performed in **Chapter 2** reported a great stability of carbonyl groups after the chemical reduction process of GO because of the high energy that is needed to break C=O bonds [95,109,166]. Especial interest in these oxygenated groups lies in the redox activity of quinone/hydroquinone couples, which can promote reductive reactions of organic compounds[58]. Also, it was demonstrated an increase on catalytic activity of rGO-based because of partial removal of oxygenated groups, which enhanced the electronic conductivity in the basal plane, favoring the removal of IOP as observed in Table 6.1. With respect to pH_{PZC}, rGO-4 showed a more basic character than GO, indicating a better performance to transfer electrons toward quinone groups[68] and then to electron-accepting pollutants[192]. Accordingly, it can be concluded that the redox catalytic activity of GO-based materials is related to their chemical surface and physical properties, which was reflected in the removal efficiency and reductive transformation degree of IOP.

6.3. Contribution of biological activity of microorganisms in the redox conversion of IOP

Another fundamental aspect studied in this thesis was the contribution of biological activity in the reductive transformation of IOP. Few studies have reported the application and importance of GO-based materials as redox catalysts in the biodegradation processes of contaminants[118,119,121,122]. However, the relevance of biological activity, especially in anaerobic conditions, for reductive biotransformation of contaminants in the presence of graphene materials as electron shuttles has been poorly studied.

Chapter 3 reports the microbial transformation of IOP under methanogenic and sulfate-reducing conditions with the application of GO and rGO-based materials as electron shuttles and ethanol/lactate as primary electron donors. The results showed that the biological activity improved the removal efficiency and maximum removal rate of IOP in the presence of rGO-4 as RM, as observed in Table 6.1. Also, the generation of simpler biological byproducts of IOP molecule (see Figure 3.3 and 3.4) in comparison with abiotic system (see Figure 2.7) can be attributed to the electron transfer mechanisms by microorganisms as will be discussed later.

Table 6.1 shows that the biological reduction of IOP using rGO-4 as RM was higher under sulfate-reducing conditions than under methanogenic conditions (77 % *vs* 86 %). This behavior can be explain by the redox potential in sulfate-reducing systems[118], which is more negative than methanogenic conditions (-400 mV *vs* -200 mV)[209], indicating a more reduced environment, which favored the biodegradation of IOP.

Sulfate-reducing bacteria are anaerobic microorganisms, which perform its cellular respiration utilizing sulfate (SO_4^{2-}) as terminal electron acceptor, reducing it to hydrogen sulfide (H_2S)[223,224]. Also, sulfate-reducing bacteria have been reported in the degradation of organic compounds[217]. They are ubiquitous in anoxic habitats, where they have a fundamental role in both the sulfur and carbon cycles[225].

For the sulfate-reducing process, the presence of ethanol as substrate promotes better performance and growth of sulfate-reducing microorganisms[226]. The oxidation of ethanol by sulfate-reducing bacteria consists of two steps: i) initial oxidation of ethanol to acetate (reaction 1), and ii) oxidation of acetate to bicarbonate (reaction 2). Likewise, the oxidation of lactate to acetate under sulfate-reducing conditions (reaction 3) is an important step for sulfate reduction as seen below:

Reaction 1: $2CH_3CH_2OH + SO_4^{2-} \longrightarrow 2CH_3COO^- + H^+ + \mathbf{HS^-} + 2H_2O$

Reaction 2: $2CH_3COO^- + 2SO_4^{2-} \longrightarrow 4HCO_3^- + \mathbf{2HS^-}$

Reaction 3: $2CH_3CHOHCOO^- + SO_4^{2-} \longrightarrow 2CH_3COO^- + 2HCO_3^- + \mathbf{HS^-}$

As can be observed in these reactions, biogenic sulfide is generated as HS^- species during the oxidation of substrates in the sulfate-reducing process. It has been reported that biogenic sulfide plays an important role in the reductive transformation of pollutants[181,182]. The HS^- species can serve as electron donor in the chemical transformation of IOP as explained in **Chapter 2**. This fact indicates that the sulfate-reducing conditions involve chemical and biological mechanisms that favor the reduction and higher extent biotransformation of IOP as reviewed in **Chapter 3**.

On the other hand, it has been reported that the biological activity of microorganisms by extracellular electron transfer (EET) process is a key factor for achieving the reductive biodegradation of environmental contaminants[121,190]. The bacteria exploit EET to exchange information and energy with other microorganisms or with their external environments[227,228]. Two pathways have been proposed for EET: i) direct electron conductivity, in which the electrons are transferred via conductive pili/nanowires or redox proteins located in the microbial outer membrane; and ii) indirect EET, where the electron transport is mediated by mobile or spatially fixed molecular redox shuttles[189,229,230]. Figure 6.1 shows schematically the mechanism of EET.

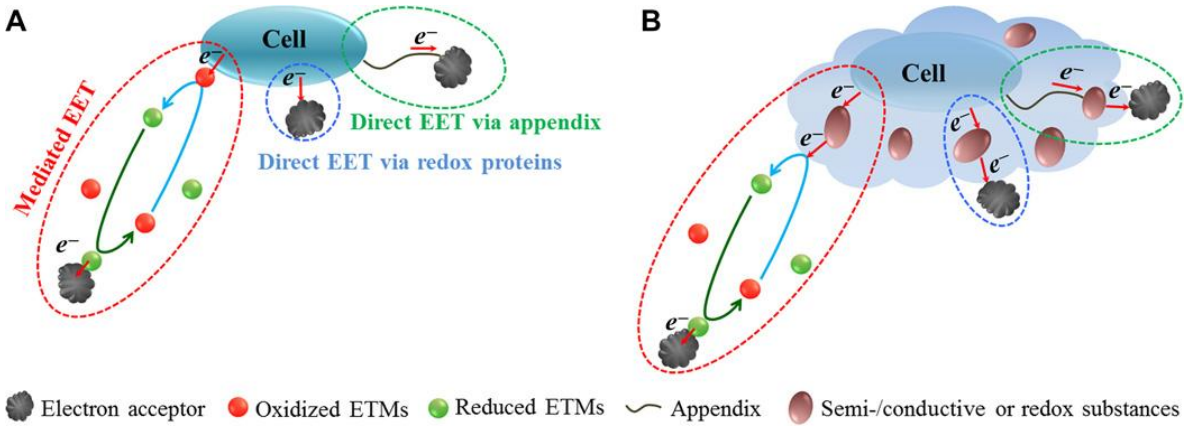

Figure 6.1. Representation of microbial EET mechanisms. A) Direct EET mechanisms and B) Indirect EET mechanisms mediated by electron transfer mediators (ETMs). Taken from reference[231].

Indirect EET is a relevant microbial EET pathway, which benefits from the presence of extracellular polymeric substance (EPS) due to a high concentration of electron shuttles in the gap between cells and electron acceptors/donors[229,231]. In this sense, EPS constitute a complex high-molecular-weight polymer mixture composed mainly of proteins, polysaccharides and humic substances that are secreted by microorganisms in pure and mixed cultures[215,232]. EPS in EET are essential in microbiology and microbial exploitation for biomineralization, biosorption, bioenergy production and corrosion processes. Also, EPS contribute to biogeochemical cycles of organic matter and nutrient elements[231]. It has been suggested that the redox properties of EPS may arise from bacterial refractory polymer, such as redox proteins and humic substances, which could serve as electron donors or acceptor in bacterial biofilms[214]. In addition, other electrochemically active substances, such as flavins and c-type cytochromes, can act as electron transit media in

EPS[181,229,231]. The redox properties of EPS in microorganisms is important due to their ability to biochemically modify metals and transform redox-sensitive pollutants[215].

Several studies have documented the role of EPS in reductive processes of environmental pollutants. For example, it has been reported that EPS extracted from electroactive bacterium, *Shewanella*, are involved in the reduction of U(VI)[232,233] and biotransformation of nitrobenzene[234]. Also, the relevance of EPS in the anaerobic reduction of azo dyes by *Sphingomonas sp.* Strain BN6 was studied[235]. In addition, Li et al.,[215] reported that heme-binding proteins are important redox components in EPS of *S.oneidensis* and *P. putida* strains for electroactive bacterial EET. Heme-binding proteins in EPS of microorganisms are usually able to transfer electrons from membrane-bound reduction systems to terminal electron acceptors by the participation of enzymes (cytochrome c) that are involved in the respiratory chain[215]. According to these reports, studying the redox properties of EPS could provide understanding of the interactions between bacteria and external electron acceptors, like organic contaminants, which is important for understanding microbial EET[215].

As discussed in **Chapters 3 and 5**, microbial EET could be a possible mechanism involved in the reductive biotransformation of IOP due to EPS secreted by anaerobic consortia[236,237], which is favored by the presence of GO-based materials[188,189]. In addition, the removal efficiency (see Table 6.1) and higher extent of IOP biotransformation (see Figure 3.3 and 3.4) using GO-based materials as RM were more favorable in biological assays (methanogenic and sulfate-reducing conditions) than in chemical systems. For example, the removal efficiency of IOP in the presence of rGO-4 as electron shuttle under methanogenic and sulfate-reducing conditions was 77 % and 85 %, respectively. Instead, the removal efficiency of IOP in chemical incubation with sulfide as electron donor was only 66 %. In addition, chemically simpler TPs with *m/z* identified in methanogenic and sulfate-reducing

conditions were 306.80 and 254.70, respectively. Meanwhile, simpler TP identified in chemical incubations using rGO-4 as RM was 314.80. These results suggest that the redox properties of EPS play an important role in the electron transfer toward terminal electron acceptor by EET process, which was evident by the higher reduction and transformation degree of IOP in biological incubations by microorganisms presents in anaerobic sludge.

6.4. Application of GO-based materials as RM in an UASB reactor to enhances the reductive biotransformation of IOP

In **Chapters 2 and 3**, it was demonstrated the feasible application of GO and rGO-based materials as RM for chemical and biological transformation of IOP in batch assays. However, the implementation of these carbon nanomaterials as redox catalysts in continuous biological systems is limited due to their eventual loss from the treatment process. Hence, it is demanded to generate hybrid graphene composites with specific properties that allow them to be retained into the biological process, which was a fundamental objective raised in this thesis. Therefore, MrGO-N were synthesized and proved as RM for chemical transformation of IOP in batch incubations (discussed in **Chapter 4)** for its subsequent application in a continuous biological system. **Chapter 5** reported the successful application of MrGO-N as RM for the biotransformation of IOP in an UASB reactor under methanogenic conditions. According to what was reviewed in the literature, this is the first study that has evaluated the redox activity of GO-based materials for the microbial degradation of any recalcitrant pollutant in a bioreactor.

Table 6.1 shows the IOP removal efficiency in the UASB reactor in the presence of MrGO-N as RM, which was 81.01 % during 31 days of operation. Also, the simpler biological byproduct identified from the transformation pathway of IOP had a *m/z* of 254.80, which involves the complete dehalogenation (removal of three iodine atoms) of

aromatic ring, rupture of side chain B and dehydration with subsequent demethylation in side chain A (see Figure 5.3). In contrast, control reactor (without MrGO-N) showed only 51.18 % of IOP removal efficiency and produced a TP with m/z of 588.70 as reviewed in **Chapter 5**. These results indicated that the presence of MrGO-N as electron shuttle enhanced the reductive biotransformation of IOP, which was explained by the importance of intrinsic properties of GO-based materials and microbial EET mechanisms as argued in sections 6.2 and 6.3. In addition, it was exhibited that the engineered of MrGO-N combined with biological activity of methanogenic microorganisms efficiently promoted the biodegradation of IOP. Figure 6.2 shows schematically the proposed mechanisms involved in the reductive biotransformation of IOP under methanogenic conditions in the UASB reactor.

Otherwise, Table 6.1 reported the IOP reduction in biological assays using GO-based materials as redox catalysts. The IOP removal efficiency in the presence of rGO-4 as electron shuttle was estimated in 77 % and 85 % for methanogenic and sulfate-reducing conditions, respectively. Meanwhile, the IOP removal in the R-MN achieved 81 %. According to these results, it can be concluded that the best performances regarding IOP reduction were observed in the experiments conducted under sulfate-reducing conditions and using rGO-4 as RM (85 % *vs* 81.01 %).

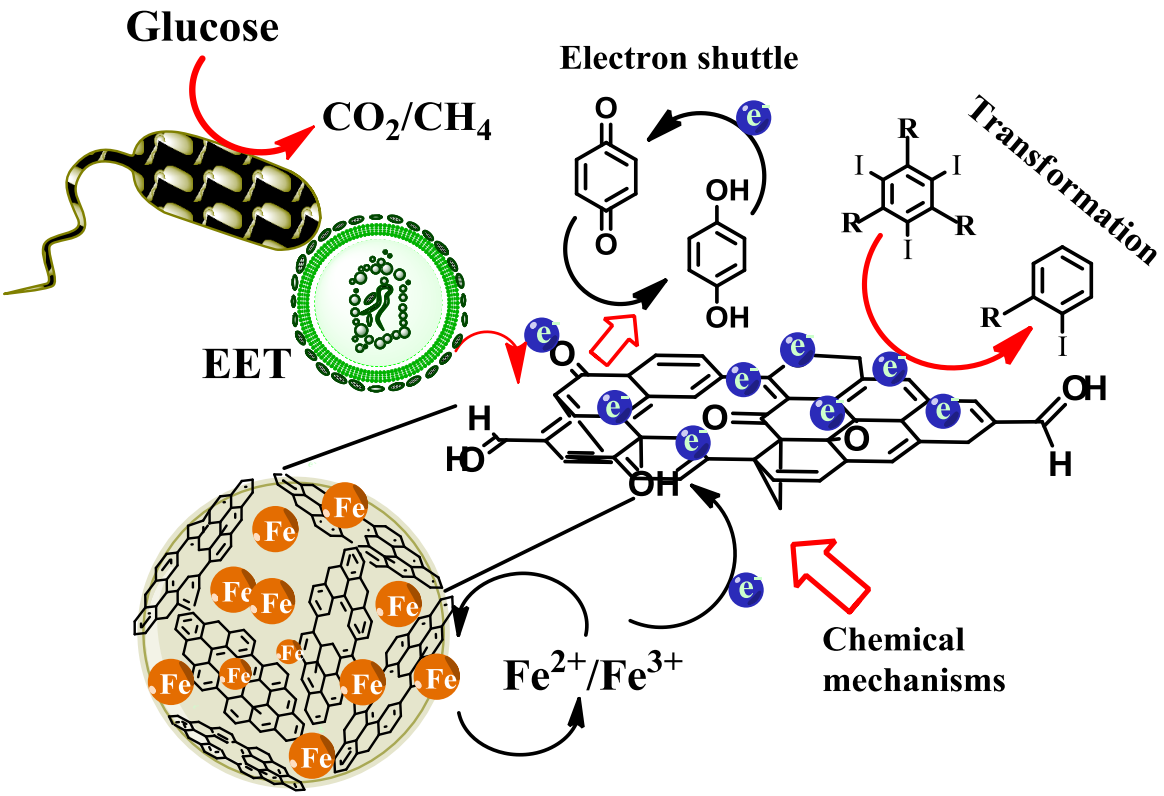

Figure 6.2. Proposed mechanisms involved in reductive biotransformation of IOP.

Although the application of rGO-4 as a catalyst in an UASB reactor could be a good strategy to enhance the reductive biotransformation of IOP, their practical application in a biological WWT system would not be convenient for two main reasons: i) the continuous supplementation of rGO-based materials in biological systems makes operational costs more expensive because of the loss of these nanomaterials during the process, and ii) the continuous loss of rGO-based materials leads to their release into environmental compartments, eventually causing eco-toxicological impacts on living systems. Among toxicological effects generated by GO-based materials at cellular level are cell-cycle alterations, apoptosis, oxidative stress, cytotoxicity and cell membrane accumulation[183]. Therefore, the removal strategy proposed in **Chapter 5** is the most feasible option for

enhancing the biodegradation of IOP since these hybrid-composites can be retained and possibly recirculated in the continuous biological system through a magnetic field.

Derived from this doctoral thesis, some works to enhance the reductive transformation of IOP must be carried out in order to evaluate the feasibility of tailoring of GO-based materials as RM in biological WWT systems as will be reviewed below.

Chapter 7

Final conclusions, perspectives and scientific products

7.1. Final conclusions

In recent years, several investigations have focused on the degradation of priority water pollutants due to the adverse effects generated by their presence in environmental compartments. As a consequence, the development of degradation technologies are demanded to mitigate this problem.

This study demonstrated, for the first time, that GO-based materials like GO, rGO and MrGO-N can serve as RM in the abiotic/biotic reduction of the halogenated pharmaceutical, IOP, under anaerobic conditions.

In the present work, it was demonstrated the fundamental role and correlation of chemical surface and physical properties of GO-based materials and their redox-mediating capacity in the reductive transformation of IOP.

Also, the biological and chemical transformation pathways of IOP were elucidated using GO-based materials as redox catalysts. In this sense, transformation byproducts with simpler chemical structure than IOP molecule were identified, which is important to propose complementary degradation techniques for the mineralization of IOP.

Potential reductive transformation mechanisms that carried out during the redox conversion of IOP were proposed, in which the chemical surface and physical properties of GO-based materials, as well as the EET mechanisms by microorganisms are key drivers for the degradation of this pharmaceutical.

Furthermore, the application of MrGO- N as RM in a continuous biological system (UASB reactor) was evaluated and constitutes the first report demonstrating the successful and effective retention of these catalysts, improving the reductive biotransformation of IOP.

The proposed degradation technology for the reductive transformation of IOP by using GO-based materials as RM is the first step toward a feasible and practical option to tailoring these nanomaterials in a biological WWT system.

Finally, the good understanding of transformation mechanisms that take place in the redox conversion process of IOP by deep characterization of GO-based materials and the study of biological activity of anaerobic microorganisms contributes to scientific knowledge of graphene-based catalysts and removal of water pollutants areas.

7.2. Perspectives and future opportunities

The results presented in this doctoral thesis demonstrated the potential application of GO-based materials as electron shuttles on the chemical and biological transformation of IOP in batch assays and in continuous biological system. Nevertheless, there are several works that can be conducted for a better understanding of redox conversion process and to enhance the reduction of IOP. Also, the application of GO-based materials as RM in a bioreactor has important challenges, which should be considered before their tailoring in a WWT plant. In the next paragraphs, the most important perspectives and future opportunities are discussed.

i) *Modification of GO-based materials.* Carbon materials have the great versatility of being chemically or physically modified with the aim of optimizing or conferring new properties for specific applications. Previously, rGO-based materials have been modified with anthraquinone-2-sulfonic acid (AQS) for enhancing the decolorization of azo dye Acid Yellow 36[119]. The model quinones AQS or anthraquinone-2,6-disulfonate (AQDS) have been widely studied as catalysts due to their great redox catalytic activity in the reductive transformation of priority contaminants, serving as redox moieties[55,61,72].

Therefore, it can be proposed the modification of GO-based materials employed in this work with model quinones AQS or AQDS to enhance their catalytic activity performance for the reductive transformation of IOP or other environmental pollutants. The experiments could be done in batch assays and biological continuous systems.

ii) *Interference of other pharmaceuticals.* The presence of several pharmaceuticals such as, analgesic and anti-inflammatories, antibiotic, hormones and steroids, lipids regulators and ICM in effluents of WWT systems[2,8,10] could cause interference and lead to a decrease in the removal efficiency and transformation degree of IOP. For these reason, it is fundamental to perform reduction experiments of IOP using GO-based materials as redox catalysts in the presence of other pharmaceuticals in order to evaluated competitive effects in the redox conversion process of IOP.

iii) *Experimental works*. As proposed in **Chapters 4 and 5**, the presence of magnetic NPs immobilized in graphene nanosacks could promote reductive reaction of IOP in chemical and biological systems. However, this hypothesis it was not demonstrated convincingly. Accordingly, it is important to perform control experiments in which the direct reduction of IOP in the presence of magnetic NPs is evaluated with the aim to demonstrate their contribution in degradation mechanisms that take place in the redox conversion IOP, which contributes to a better understanding of electron transfer processes in the degradation of IOP.

Moreover, the experiments performed in this thesis were carried out in ideal environments (deionized or distilled water, mineral medium and IOP).

Nevertheless, for practical application, it is important to evaluate IOP removal in conditions that resemble reality. In this sense, it would be convenient to evaluate the reductive transformation of IOP in batch and continuous systems using GO-based materials as RM in hospital synthetic water and synthetic wastewater, which could indicate the true potential of these nanomaterials to be applied in a biological WWT plant.

iv) *Experiments regarding UASB reactor.* As discussed in section 6.4, the best performance regarding the reductive transformation of IOP was observed in experiments performed with rGO-4 as RM under sulfate-reducing conditions in batch incubations. Also, this doctoral thesis studied the applications of MrGO-N as electron shuttles under methanogenic conditions in an UASB reactor. However, the same system for reductive biodegradation of IOP under sulfate-reducing conditions was not explored. The application of MrGO-N as RM under sulfate-reducing conditions in UASB reactor is fundamental since it would be expected a greater removal efficiency and transformation degree of IOP due to the contribution of redox activity of magnetic NPs and biogenic HS^- species generated during the sulfate-reducing process.

Another major aspect to consider for the application of MrGO-N in continuous biological systems is to evaluate their catalytic performance regarding IOP removal and magnetic character after its use in the bioreactor. According to that, MrGO-N could be recovered from anaerobic sludge by magnetic field and vigorous stirring for a subsequent application in successive cycles. Likewise, the deep characterization of MrGO-N after its use as RM in the bioreactor could

document if there was a chemical or physical modification of these catalysts due to the interaction with microorganisms.

v) *UASB reactor design*. The strategy proposed in **Chapter 5** was focused on the retention of MrGO-N as RM in an UASB reactor by adapting a magnet in the outlet of this bioreactor, preventing the loss of graphene nanoacks. However, it is important to design a system that allows MrGO-N to be recovered and recirculated into the continuous process. Accordingly, the design of a UASB reactor with recirculation is demanded for a future application in the microbial degradation of IOP. The implementation of this recirculation system would contribute to a better performance in IOP reduction, as well as to lower operational costs because a lower concentration of catalysts would be required in the process.

vi) *Future opportunities*. The information derived from the present study suggests that the GO-based materials could significantly promote dehalogenation and further reductive transformation reactions of IOP, which is relevant for similar emerging pollutants. In this context, the future opportunities of the present degradation technology are focused on its application to enhance the reduction of several contaminants from water. The proposed redox conversion strategy could be applied for the reduction of diatrizoate, the most recalcitrant ICM, as well as nitrocompounds, polyhalogenated organics and other pharmaceuticals. Finally, the novel treatment technique proposed in this thesis is an opportunity area for future researches to apply GO-based materials in continuous biological systems for the biodegradation of environmental contaminants.

List of scientific publications derived from this research work

1. Toral-Sánchez E, Ascacio-Valdés JA, Aguilar CN, Cervantes FJ, Rangel-Mendez JR. Role of the intrinsic properties of partially reduced graphene oxides on the chemical transformation of iopromide. ***Carbon*** **(**2016), 99:456-465

2. Toral-Sánchez E, Ascacio-Valdés JA, Aguilar CN, Cervantes FJ, Rangel-Mendez JR. Tailoring partially reduced graphene oxide as redox mediator for enhanced biotransformation of iopromide under methanogenic and sulfate-reducing conditions. ***Bioresource Technology*** (2017), 223:269–276

3. Toral-Sánchez E, Hurt RH, Ascacio-Valdés JA, Aguilar CN, Cervantes FJ, Rangel-Mendez JR. Improved reductive transformation of iopromide by hybrid magnetic graphene nanosacks as electron shuttles. ***Submitted***

4. Toral-Sánchez E, Hurt RH, Ascacio-Valdés JA, Aguilar CN, Cervantes FJ, Rangel-Mendez JR. Novel application of magnetic nano-carbon composite as redox mediators in the microbial transformation of iopromide in UASB reactors. ***Submitted***

Contributions to conferences and symposia

Toral-Sánchez E, Cervantes FJ, Rangel-Mendez JR. **Reducción química de iopromida utilizando óxido de grafeno como mediador redox**. 4th. IWA Young Water Professional Conference, April 27-29, 2015. Guanajuato, Mexico.

Toral-Sánchez E, Cervantes FJ, Rangel-Mendez JR. **Efecto del grado de reducción del óxido de grafeno en la transformación química de iopromida**. 1st Mexican Carbon Association Conference, November 10-13, 2015. San Luis Potosí, Mexico.

Toral-Sánchez E, Cervantes FJ, Rangel-Mendez JR. **Tailoring graphene oxide as a redox mediator to promote the chemical transformation of iopromide**. Carbon Conference, July 10-15, 2016. Penn State, USA.

Toral-Sánchez E, Cervantes FJ, Rangel-Mendez JR. **Evaluación de las propiedades intrínsecas del óxido de grafeno en la transformación química y biológica de iopromida**. II Latin American Workshop on Carbon Materials, November 16-18, 2016. Termas de Chillan, Chile.

Toral-Sánchez E, Hurt RH, Cervantes FJ, Rangel-Mendez JR. **Aplicación novedosa de nanomateriales a base de óxido de grafeno en la transformación química y biológica de iopromida.** 8th Environmental Sciences Symposium IPICyT, April 20, 2017. San Luis Potosí, Mexico. *Third place better oral presentation*

Toral-Sánchez E, Hurt RH, Cervantes FJ, Rangel-Mendez JR. **Síntesis de nanosacos magnéticos de óxido de grafeno y su aplicación en la transformación química de iopromida**. 5th. IWA Young Water Professional Conference, May 24-26, 2017. Michoacán, Mexico.

Toral-Sánchez E, Hurt RH, Cervantes FJ, Rangel-Mendez JR. **Aplicación de nanosacos magnéticos de óxido de grafeno en la transformación reductiva de iopromida**. 2nd Mexican Carbon Association Conference, November 14-17, 2017. San Luis Potosí, Mexico. *Second place better oral presentation*

References

(1) Laws, E. A. *Aquatic Pollution: An Introductory Text*; John Wiley & Sons, 2017.

(2) Heberer, T. Occurrence, Fate, and Removal of Pharmaceutical Residues in the Aquatic Environment: A Review of Recent Research Data. *Toxicol. Lett.* **2002**, *131* (1–2), 5–17.

(3) Löffler, D.; Römbke, J.; Meller, M.; Ternes, T. A. Environmental Fate of Pharmaceuticals in Water/Sediment Systems. *Environ. Sci. Technol.* **2005**, *39* (14), 5209–5218.

(4) Jeong, J.; Jung, J.; Cooper, W. J.; Song, W. Degradation Mechanisms and Kinetic Studies for the Treatment of X-Ray Contrast Media Compounds by Advanced Oxidation/Reduction Processes. *Water Res.* **2010**, *44* (15), 4391–4398.

(5) Sacher, F.; Lange, F. T.; Brauch, H.J.; Blankenhorn, I. Pharmaceuticals in Groundwaters: Analytical Methods and Results of a Monitoring Program in Baden-Württemberg, Germany. *J. Chromatogr. A* **2001**, *938* (1), 199–210.

(6) Daughton, C. G.; Ternes, T. A. Pharmaceuticals and Personal Care Products in the Environment: Agents of Subtle Change? *Environ. Health Perspect.* **1999**, *107* (Suppl 6), 907–938.

(7) Deblonde, T.; Cossu-Leguille, C.; Hartemann, P. Emerging Pollutants in Wastewater: A Review of the Literature. *Int. J. Hyg. Environ. Health* **2011**, *214* (6), 442–448.

(8) Sui, Q.; Cao, X.; Lu, S.; Zhao, W.; Qiu, Z.; Yu, G. Occurrence, Sources and Fate of Pharmaceuticals and Personal Care Products in the Groundwater: A Review. *Emerg. Contam.* **2015**, *1* (1), 14–24.

(9) Li, W. C. Occurrence, Sources, and Fate of Pharmaceuticals in Aquatic Environment and Soil. *Environ. Pollut.* **2014**, *187*, 193–201.

(10) Díaz-Cruz, S.; Barceló, D. Occurrence and Analysis of Selected Pharmaceuticals and Metabolites as Contaminants Present in Waste Waters, Sludge and Sediments. In *Series Anthropogenic Compounds*; The Handbook of Environmental Chemistry; Springer, Berlin, Heidelberg, 2004; pp 227–260.

(11) Segura, P. A.; François, M.; Gagnon, C.; Sauvé, S. Review of the Occurrence of Anti-Infectives in Contaminated Wastewaters and Natural and Drinking Waters. *Environ. Health Perspect.* **2009**, *117* (5), 675–684.

(12) Leung, H. W.; Jin, L.; Wei, S.; Tsui, M. M. P.; Zhou, B.; Jiao, L.; Cheung, P. C.; Chun, Y. K.; Murphy, M. B.; Lam, P. K. S. Pharmaceuticals in Tap Water: Human Health Risk Assessment and Proposed Monitoring Framework in China. *Environ. Health Perspect.* **2013**, *121* (7), 839–846.

(13) Petrovic, M.; Barceló, D. *Analysis, Removal, Effects and Risk of Pharmaceuticals in the Water Cycle: Occurrence and Transformation in the Environment*; Elsevier: The Netherlands, 2007; Vol. 50.

(14) Pérez, S.; Barceló, D. Fate and Occurrence of X-Ray Contrast Media in the Environment. *Anal. Bioanal. Chem.* **2007**, *387* (4), 1235–1246.

(15) Drewes, J. E.; Heberer, T.; Rauch, T.; Reddersen, K. Fate of Pharmaceuticals During Ground Water Recharge. *Ground Water Monit. Remediat.* **2003**, *23* (3), 64–72.

(16) Andreozzi, R.; Raffaele, M.; Nicklas, P. Pharmaceuticals in STP Effluents and Their Solar Photodegradation in Aquatic Environment. *Chemosphere* **2003**, *50* (10), 1319–1330.

(17) Ferrer, I.; Heine, C. E.; Thurman, E. M. Combination of LC/TOF-MS and LC/Ion Trap MS/MS for the Identification of Diphenhydramine in Sediment Samples. *Anal. Chem.* **2004**, *76* (5), 1437–1444.

(18) *Pharmaceuticals in the Environment: Sources, Fate, Effects and Risks*, 3rd ed.; Kümmerer, K., Ed.; Springer-Verlag: Berlin Heidelberg, 2008.

(19) Escher, B. I.; Baumgartner, R.; Koller, M.; Treyer, K.; Lienert, J.; McArdell, C. S. Environmental Toxicology and Risk Assessment of Pharmaceuticals from Hospital Wastewater. *Water Res.* **2011**, *45* (1), 75–92.

(20) Bruce, G. M.; Pleus, R. C.; Snyder, S. A. Toxicological Relevance of Pharmaceuticals in Drinking Water. *Environ. Sci. Technol.* **2010**, *44* (14), 5619–5626.

(21) Lahti, M.; Brozinski, J.-M.; Segner, H.; Kronberg, L.; Oikari, A. Bioavailability of Pharmaceuticals in Waters Close to Wastewater Treatment Plants: Use of Fish Bile for Exposure Assessment. *Environ. Toxicol. Chem.* **2012**, *31* (8), 1831–1837.

(22) Muir, D.; Simmons, D.; Wang, X.; Peart, T.; Villella, M.; Miller, J.; Sherry, J. Bioaccumulation of Pharmaceuticals and Personal Care Product Chemicals in Fish Exposed to Wastewater Effluent in an Urban Wetland. *Sci. Rep.* **2017**, *7*.

(23) Christiansen, C. X-Ray Contrast Media--an Overview. *Toxicology* **2005**, *209* (2), 185–187.

(24) Busetti, F.; Linge, K. L.; Rodriguez, C.; Heitz, A. Occurrence of Iodinated X-Ray Contrast Media in Indirect Potable Reuse Systems. *J. Environ. Sci. Health Part A Tox. Hazard. Subst. Environ. Eng.* **2010**, *45* (5), 542–548.

(25) Putschew, A.; Wischnack, S.; Jekel, M. Occurrence of Triiodinated X-Ray Contrast Agents in the Aquatic Environment. *Sci. Total Environ.* **2000**, *255* (1–3), 129–134.

(26) Steger-Hartmann, T.; Länge, R.; Schweinfurth, H. Environmental Risk Assessment for the Widely Used Iodinated X-Ray Contrast Agent Iopromide (Ultravist). *Ecotoxicol. Environ. Saf.* **1999**, *42* (3), 274–281.

(27) Knitt, L. E.; Shapley, J. R.; Strathmann, T. J. Rapid Metal-Catalyzed Hydrodehalogenation of Iodinated X-Ray Contrast Media. *Environ. Sci. Technol.* **2008**, *42* (2), 577–583.

(28) Schulz, M.; Löffler, D.; Wagner, M.; Ternes, T. A. Transformation of the X-Ray Contrast Medium Iopromide In Soil and Biological Wastewater Treatment. *Environ. Sci. Technol.* **2008**, *42* (19), 7207–7217.

(29) Bottinor, W.; Polkampally, P.; Jovin, I. Adverse Reactions to Iodinated Contrast Media. *Int. J. Angiol. Off. Publ. Int. Coll. Angiol. Inc* **2013**, *22* (3), 149–154.

(30) Onesios, K. M.; Yu, J. T.; Bouwer, E. J. Biodegradation and Removal of Pharmaceuticals and Personal Care Products in Treatment Systems: A Review. *Biodegradation* **2009**, *20* (4), 441–466.

(31) Ternes, T. A.; Hirsch, R. Occurrence and Behavior of X-Ray Contrast Media in Sewage Facilities and the Aquatic Environment. *Environ. Sci. Technol.* **2000**, *34* (13), 2741–2748.

(32) Carballa, M.; Omil, F.; Lema, J. M.; Llompart, M.; García-Jares, C.; Rodríguez, I.; Gómez, M.; Ternes, T. Behavior of Pharmaceuticals, Cosmetics and Hormones in a Sewage Treatment Plant. *Water Res.* **2004**, *38* (12), 2918–2926.

(33) Kwon, M.; Yoon, Y.; Cho, E.; Jung, Y.; Lee, B.-C.; Paeng, K.-J.; Kang, J.-W. Removal of Iopromide and Degradation Characteristics in Electron Beam Irradiation Process. *J. Hazard. Mater.* **2012**, *227–228*, 126–134.

(34) Santos, L. H. M. L. M.; Gros, M.; Rodriguez-Mozaz, S.; Delerue-Matos, C.; Pena, A.; Barceló, D.; Montenegro, M. C. B. S. M. Contribution of Hospital Effluents to the Load of Pharmaceuticals in Urban Wastewaters: Identification of Ecologically Relevant Pharmaceuticals. *Sci. Total Environ.* **2013**, *461–462*, 302–316.

(35) Emmanuel, E.; Perrodin, Y.; Keck, G.; Blanchard, J.-M.; Vermande, P. Ecotoxicological Risk Assessment of Hospital Wastewater: A Proposed Framework for Raw Effluents Discharging into Urban Sewer Network. *J. Hazard. Mater.* **2005**, *117* (1), 1–11.

(36) Gros, M.; Cruz-Morato, C.; Marco-Urrea, E.; Longrée, P.; Singer, H.; Sarrà, M.; Hollender, J.; Vicent, T.; Rodriguez-Mozaz, S.; Barceló, D. Biodegradation of the X-Ray Contrast Agent Iopromide and the Fluoroquinolone Antibiotic Ofloxacin by the White Rot Fungus *Trametes Versicolor* in Hospital Wastewaters and Identification of Degradation Products. *Water Res.* **2014**, *60*, 228–241.

(37) Wang, Z.; Huang, Q.; Yu, Y.; Wang, C.; Ou, W.; Peng, X. Stereoisomeric Profiling of Pharmaceuticals Ibuprofen and Iopromide in Wastewater and River Water, China. *Environ. Geochem. Health* **2013**, *35* (5), 683–691.

(38) Kreuzinger, N.; Clara, M.; Strenn, B.; Vogel, B. Investigation on the Behaviour of Selected Pharmaceuticals in the Groundwater after Infiltration of Treated Wastewater. *Water Sci. Technol.* **2004**, *50* (2), 221–228.

(39) Ternes, J. S. T. A. Ozonation: A Tool for Removal of Pharmaceuticals, Contrast Media and Musk Fragrances from Wastewater? *Water Res.* **2003**, *37* (8), 1976–1982.

(40) Peer, A.; Averbukh, Z.; Berman, S.; Modai, D.; Averbukh, M.; Weissgarten, J. Contrast Media Augmented Apoptosis of Cultured Renal Mesangial, Tubular, Epithelial, Endothelial, and Hepatic Cells. *Invest. Radiol.* **2003**, *38* (3), 177–182.

(41) Zhao, Y.; Tao, Z.; Xu, Z.; Tao, Z.; Chen, B.; Wang, L.; Li, C.; Chen, L.; Jia, Q.; Jia, E.; et al. Toxic Effects of a High Dose of Non-Ionic Iodinated Contrast Media on Renal Glomerular and Aortic Endothelial Cells in Aged Rats in Vivo. *Toxicol. Lett.* **2011**, *202* (3), 253–260.

(42) Jeong, C. H.; Machek, E. J.; Shakeri, M.; Duirk, S. E.; Ternes, T. A.; Richardson, S. D.; Wagner, E. D.; Plewa, M. J. The Impact of Iodinated X-Ray Contrast Agents on Formation and Toxicity of Disinfection by-Products in Drinking Water. *J. Environ. Sci.* **2017**, *58*, 173–182.

(43) Toral-Sánchez, E.; Ascacio Valdés, J. A.; Aguilar, C. N.; Cervantes, F. J.; Rangel-Mendez, J. R. Role of the Intrinsic Properties of Partially Reduced Graphene Oxides on the Chemical Transformation of Iopromide. *Carbon* **2016**, *99*, 456–465.

(44) Toral-Sánchez, E.; Rangel-Mendez, J. R.; Ascacio Valdés, J. A.; Aguilar, C. N.; Cervantes, F. J. Tailoring Partially Reduced Graphene Oxide as Redox Mediator for Enhanced Biotransformation of Iopromide under Methanogenic and Sulfate-Reducing Conditions. *Bioresour. Technol.* **2017**, *223*, 269–276.

(45) Lütke Eversloh, C.; Henning, N.; Schulz, M.; Ternes, T. A. Electrochemical Treatment of Iopromide under Conditions of Reverse Osmosis Concentrates – Elucidation of the Degradation Pathway. *Water Res.* **2014**, *48*, 237–246.

(46) Pat-Espadas, A. M.; Razo-Flores, E.; Rangel-Mendez, J. R.; Ascacio-Valdes, J. A.; Aguilar, C. N.; Cervantes, F. J. Immobilization of Biogenic Pd(0) in Anaerobic Granular Sludge for the Biotransformation of Recalcitrant Halogenated Pollutants in UASB Reactors. *Appl. Microbiol. Biotechnol.* **2015**, 1–10.

(47) Cruz-Zavala, A. S.; Pat-Espadas, A. M.; Rangel-Mendez, J. R.; Chazaro-Ruiz, L. F.; Ascacio-Valdes, J. A.; Aguilar, C. N.; Cervantes, F. J. Immobilization of Metal–humic Acid Complexes in Anaerobic Granular Sludge for Their Application as Solid-Phase Redox Mediators in the Biotransformation of Iopromide in UASB Reactors. *Bioresour. Technol.* **2016**, *207*, 39–45.

(48) Kalsch, W. Biodegradation of the Iodinated X-Ray Contrast Media Diatrizoate and Iopromide. *Sci. Total Environ.* **1999**, *225* (1), 143–153.

(49) Batt, A. L.; Kim, S.; Aga, D. S. Enhanced Biodegradation of Iopromide and Trimethoprim in Nitrifying Activated Sludge†. *Environ. Sci. Technol.* **2006**, *40* (23), 7367–7373.

(50) Pérez, S.; Eichhorn, P.; Celiz, M. D.; Aga, D. S. Structural Characterization of Metabolites of the X-Ray Contrast Agent Iopromide in Activated Sludge Using Ion Trap Mass Spectrometry. *Anal. Chem.* **2006**, *78* (6), 1866–1874.

(51) Xu, B.; Gao, P.; Liu, Z.; Xue, G.; Liu, Y.; Wu, F. Influence of Cosubstrates on Iopromide Degradation by *Pseudomonas* Sp. I-24. *Water. Air. Soil Pollut.* **2014**, *225* (2), 1849.

(52) Ning, B.; Graham, N. J. D.; Lickiss, P. D. Degradation of X-Ray Contrast Media Compounds by Combined Ozone and Ultrasound. *Water Environ. Res. Res. Publ. Water Environ. Fed.* **2007**, *79* (12), 2427–2436.

(53) Doll, T. E.; Frimmel, F. H. Kinetic Study of Photocatalytic Degradation of Carbamazepine, Clofibric Acid, Iomeprol and Iopromide Assisted by Different TiO_2 Materials—determination of Intermediates and Reaction Pathways. *Water Res.* **2004**, *38* (4), 955–964.

(54) Huber, M. M.; GÖbel, A.; Joss, A.; Hermann, N.; LÖffler, D.; McArdell, C. S.; Ried, A.; Siegrist, H.; Ternes, T. A.; von Gunten, U. Oxidation of Pharmaceuticals during Ozonation of Municipal Wastewater Effluents: A Pilot Study. *Environ. Sci. Technol.* **2005**, *39* (11), 4290–4299.

(55) van der Zee, F. P.; Cervantes, F. J. Impact and Application of Electron Shuttles on the Redox (Bio)Transformation of Contaminants: A Review. *Biotechnol. Adv.* **2009**, *27* (3), 256–277.

(56) van der Zee, F. P.; Bisschops, I. A. E.; Lettinga, G.; Field, J. A. Activated Carbon as an Electron Acceptor and Redox Mediator during the Anaerobic Biotransformation of Azo Dyes. *Environ. Sci. Technol.* **2003**, *37* (2), 402–408.

(57) Amezquita-Garcia, H. J.; Razo-Flores, E.; Cervantes, F. J.; Rangel-Mendez, J. R. Activated Carbon Fibers as Redox Mediators for the Increased Reduction of Nitroaromatics. *Carbon* **2013**, *55*, 276–284.

(58) Cervantes, F. J.; van der Velde, S.; Lettinga, G.; Field, J. A. Quinones as Terminal Electron Acceptors for Anaerobic Microbial Oxidation of Phenolic Compounds. *Biodegradation* **2000**, *11* (5), 313–321.

(59) Pereira, R. A.; Pereira, M. F. R.; Alves, M. M.; Pereira, L. Carbon Based Materials as Novel Redox Mediators for Dye Wastewater Biodegradation. *Appl. Catal. B Environ.* **2014**, *144*, 713–720.

(60) Leon y Leon, C. A.; Radovic, L. R. Interfacial Chemistry and Electrochemistry of Carbon Surfaces. In *Chemistry and Physics of Carbon*; Peter A. Thrower Marcel Delcker: New York, 1994; Vol. 2, pp 213–311.

(61) Cervantes, F. J.; van der Velde, S.; Lettinga, G.; Field, J. A. Quinones as Terminal Electron Acceptors for Anaerobic Microbial Oxidation of Phenolic Compounds. *Biodegradation* **2000**, *11* (5), 313–321.

(62) Lovley, D. R.; Fraga, J. L.; Coates, J. D.; Blunt-Harris, E. L. Humics as an Electron Donor for Anaerobic Respiration. *Environ. Microbiol.* **1999**, *1* (1), 89–98.

(63) Emilia Rios-Del Toro, E.; Celis, L. B.; Cervantes, F. J.; Rangel-Mendez, J. R. Enhanced Microbial Decolorization of Methyl Red with Oxidized Carbon Fiber as Redox Mediator. *J. Hazard. Mater.* **2013**, *260*, 967–974.

(64) Fu, H.; Zhu, D. Graphene Oxide-Facilitated Reduction of Nitrobenzene in Sulfide-Containing Aqueous Solutions. *Environ. Sci. Technol.* **2013**, *47* (9), 4204–4210.

(65) Guin, P. S.; Das, S.; Mandal, P. C. Electrochemical Reduction of Quinones in Different Media: A Review. *Int. J. Electrochem.* **2011**, *2011*, 1–22.

(66) Stein, S. E.; Golden, D. M. Resonance Stabilization Energies in Polycyclic Aromatic Hydrocarbon Radicals. *J. Org. Chem.* **1977**, *42* (5), 839–841.

(67) Mezohegyi, G.; Gonçalves, F.; Órfão, J. J. M.; Fabregat, A.; Fortuny, A.; Font, J.; Bengoa, C.; Stuber, F. Tailored Activated Carbons as Catalysts in Biodecolourisation of Textile Azo Dyes. *Appl. Catal. B Environ.* **2010**, *94* (1–2), 179–185.

(68) Pereira, L.; Pereira, R.; Pereira, M. F. R.; van der Zee, F. P.; Cervantes, F. J.; Alves, M. M. Thermal Modification of Activated Carbon Surface Chemistry Improves Its Capacity as Redox Mediator for Azo Dye Reduction. *J. Hazard. Mater.* **2010**, *183* (1–3), 931–939.

(69) Baeta, B. E. L.; Luna, H. J.; Sanson, A. L.; Silva, S. Q.; Aquino, S. F. Degradation of a Model Azo Dye in Submerged Anaerobic Membrane Bioreactor (SAMBR) Operated with Powdered Activated Carbon (PAC). *J. Environ. Manage.* **2013**, *128*, 462–470.

(70) Li, L.; Zhou, J.; Wang, J.; Yang, F.; Jin, C.; Zhang, G. Anaerobic Biotransformation of Azo Dye Using Polypyrrole/Anthraquinonedisulphonate Modified Active Carbon Felt as a Novel Immobilized Redox Mediator. *Sep. Purif. Technol.* **2009**, *66* (2), 375–382.

(71) Nguyen, L. N.; Hai, F. I.; Price, W. E.; Leusch, F. D. L.; Roddick, F.; Ngo, H. H.; Guo, W.; Magram, S. F.; Nghiem, L. D. The Effects of Mediator and Granular Activated Carbon Addition on Degradation of Trace Organic Contaminants by an Enzymatic Membrane Reactor. *Bioresour. Technol.* **2014**, *167*, 169–177.

(72) Amezquita-Garcia, H. J.; Rangel-Mendez, J. R.; Cervantes, F. J.; Razo-Flores, E. Activated Carbon Fibers with Redox-Active Functionalities Improves the Continuous Anaerobic Biotransformation of 4-Nitrophenol. *Chem. Eng. J.* **2016**, *286*, 208–215.

(73) Fu, H.; Guo, Y.; Chen, W.; Gu, C.; Zhu, D. Reductive Dechlorination of Hexachloroethane by Sulfide in Aqueous Solutions Mediated by Graphene Oxide and Carbon Nanotubes. *Carbon* **2014**, *72*, 74–81.

(74) Chen, W.; Zhu, D.; Zheng, S.; Chen, W. Catalytic Effects of Functionalized Carbon Nanotubes on Dehydrochlorination of 1,1,2,2-Tetrachloroethane. *Environ. Sci. Technol.* **2014**, *48* (7), 3856–3863.

(75) Geim, A. K.; Novoselov, K. S. The Rise of Graphene. *Nat. Mater.* **2007**, *6* (3), 183–191.

(76) Geim, A. K. Graphene: Status and Prospects. *Science* **2009**, *324* (5934), 1530–1534.

(77) Pei, S.; Cheng, H.-M. The Reduction of Graphene Oxide. *Carbon* **2012**, *50* (9), 3210–3228.

(78) Novoselov, K. S.; Jiang, Z.; Zhang, Y.; Morozov, S. V.; Stormer, H. L.; Zeitler, U.; Maan, J. C.; Boebinger, G. S.; Kim, P.; Geim, A. K. Room-Temperature Quantum Hall Effect in Graphene. *Science* **2007**, *315* (5817), 1379.

(79) Novoselov, K. S.; Geim, A. K.; Morozov, S. V.; Jiang, D.; Zhang, Y.; Dubonos, S. V.; Grigorieva, I. V.; Firsov, A. A. Electric Field Effect in Atomically Thin Carbon Films. *Science* **2004**, *306* (5696), 666–669.

(80) Stankovich, S.; Dikin, D. A.; Dommett, G. H. B.; Kohlhaas, K. M.; Zimney, E. J.; Stach, E. A.; Piner, R. D.; Nguyen, S. T.; Ruoff, R. S. Graphene-Based Composite Materials. *Nature* **2006**, *442* (7100), 282–286.

(81) Jiang, D.; Sumpter, B. G.; Dai, S. The Unique Chemical Reactivity of a Graphene Nanoribbon's Zigzag Edge. *J. Chem. Phys.* **2007**, *126* (13), 134701.

(82) Papageorgiou, D. G.; Kinloch, I. A.; Young, R. J. Mechanical Properties of Graphene and Graphene-Based Nanocomposites. *Prog. Mater. Sci.* **2017**, *90*, 75–127.

(83) Castro Neto, A. H.; Guinea, F.; Peres, N. M. R.; Novoselov, K. S.; Geim, A. K. The Electronic Properties of Graphene. *Rev. Mod. Phys.* **2009**, *81* (1), 109–162.

(84) Stankovich, S.; Dikin, D. A.; Piner, R. D.; Kohlhaas, K. A.; Kleinhammes, A.; Jia, Y.; Wu, Y.; Nguyen, S. T.; Ruoff, R. S. Synthesis of Graphene-Based Nanosheets via Chemical Reduction of Exfoliated Graphite Oxide. *Carbon* **2007**, *45* (7), 1558–1565.

(85) Zhang, Y.; Zhang, L.; Zhou, C. Review of Chemical Vapor Deposition of Graphene and Related Applications. *Acc. Chem. Res.* **2013**, *46* (10), 2329–2339.

(86) Hernandez, Y.; Nicolosi, V.; Lotya, M.; Blighe, F. M.; Sun, Z.; De, S.; McGovern, I. T.; Holland, B.; Byrne, M.; Gun'Ko, Y. K.; et al. High-Yield Production of Graphene by Liquid-Phase Exfoliation of Graphite. *Nat. Nanotechnol.* **2008**, *3* (9), 563–568.

(87) Park, S.; Ruoff, R. S. Chemical Methods for the Production of Graphenes. *Nat. Nanotechnol.* **2009**, *4* (4), 217–224.

(88) Yi, M.; Shen, Z. A Review on Mechanical Exfoliation for the Scalable Production of Graphene. *J. Mater. Chem. A* **2015**, *3* (22), 11700–11715.

(89) Hammond, J. L.; Formisano, N.; Estrela, P.; Carrara, S.; Tkac, J. Electrochemical Biosensors and Nanobiosensors. *Essays Biochem.* **2016**, *60* (1), 69–80.

(90) Dreyer, D. R.; Park, S.; Bielawski, C. W.; Ruoff, R. S. The Chemistry of Graphene Oxide. *Chem. Soc. Rev.* **2009**, *39* (1), 228–240.

(91) Compton, O. C.; Nguyen, S. T. Graphene Oxide, Highly Reduced Graphene Oxide, and Graphene: Versatile Building Blocks for Carbon-Based Materials. *Small* **2010**, *6* (6), 711–723.

(92) Zaaba, N. I.; Foo, K. L.; Hashim, U.; Tan, S. J.; Liu, W.-W.; Voon, C. H. Synthesis of Graphene Oxide Using Modified Hummers Method: Solvent Influence. *Procedia Eng.* **2017**, *184*, 469–477.

(93) Szabó, T.; Berkesi, O.; Forgó, P.; Josepovits, K.; Sanakis, Y.; Petridis, D.; Dékány, I. Evolution of Surface Functional Groups in a Series of Progressively Oxidized Graphite Oxides. *Chem. Mater.* **2006**, *18* (11), 2740–2749.

(94) Lerf, A.; He, H.; Forster, M.; Klinowski, J. Structure of Graphite Oxide Revisited. *J. Phys. Chem. B* **1998**, *102* (23), 4477–4482.

(95) Bagri, A.; Mattevi, C.; Acik, M.; Chabal, Y. J.; Chhowalla, M.; Shenoy, V. B. Structural Evolution during the Reduction of Chemically Derived Graphene Oxide. *Nat. Chem.* **2010**, *2* (7), 581–587.

(96) Gao, W.; Alemany, L. B.; Ci, L.; Ajayan, P. M. New Insights into the Structure and Reduction of Graphite Oxide. *Nat. Chem.* **2009**, *1* (5), 403–408.

(97) Fuente, E.; Menéndez, J. A.; Díez, M. A.; Suárez, D.; Montes-Morán, M. A. Infrared Spectroscopy of Carbon Materials: A Quantum Chemical Study of Model Compounds. *J. Phys. Chem. B* **2003**, *107* (26), 6350–6359.

(98) Chen, W.; Yan, L.; Bangal, P. R. Preparation of Graphene by the Rapid and Mild Thermal Reduction of Graphene Oxide Induced by Microwaves. *Carbon* **2010**, *48* (4), 1146–1152.

(99) Huh, S. H. Thermal Reduction of Graphene Oxide. *Phys. Appl. Graphene InTechOpen* **2011**, 73–90.

(100) Chen, W.; Yan, L. Preparation of Graphene by a Low-Temperature Thermal Reduction at Atmosphere Pressure. *Nanoscale* **2010**, *2* (4), 559–563.

(101) Gao, X.; Jang, J.; Nagase, S. Hydrazine and Thermal Reduction of Graphene Oxide: Reaction Mechanisms, Product Structures, and Reaction Design. *J. Phys. Chem. C* **2010**, *114* (2), 832–842.

(102) Solís-Fernández, P.; Rozada, R.; Paredes, J. I.; Villar-Rodil, S.; Fernández-Merino, M. J.; Guardia, L.; Martínez-Alonso, A.; Tascón, J. M. D. Chemical and Microscopic Analysis of Graphene Prepared by Different Reduction Degrees of Graphene Oxide. *J. Alloys Compd.* **2012**, *536*, *Supplement 1*, S532–S537.

(103) Paredes, J. I.; Villar-Rodil, S.; Solís-Fernández, P.; Martínez-Alonso, A.; Tascón, J. M. D. Atomic Force and Scanning Tunneling Microscopy Imaging of Graphene Nanosheets Derived from Graphite Oxide. *Langmuir* **2009**, *25* (10), 5957–5968.

(104) Chua, C. K.; Pumera, M. Chemical Reduction of Graphene Oxide: A Synthetic Chemistry Viewpoint. *Chem. Soc. Rev.* **2013**, *43* (1), 291–312.

(105) Stankovich, S.; Piner, R. D.; Chen, X.; Wu, N.; Nguyen, S. T.; Ruoff, R. S. Stable Aqueous Dispersions of Graphitic Nanoplatelets via the Reduction of Exfoliated Graphite Oxide in the Presence of Poly(Sodium 4-Styrenesulfonate). *J. Mater. Chem.* **2006**, *16* (2), 155–158.

(106) Chua, C. K.; Pumera, M. The Reduction of Graphene Oxide with Hydrazine: Elucidating Its Reductive Capability Based on a Reaction-Model Approach. *Chem. Commun. Camb. Engl.* **2016**, *52* (1), 72–75.

(107) Park, S.; An, J.; Potts, J. R.; Velamakanni, A.; Murali, S.; Ruoff, R. S. Hydrazine-Reduction of Graphite- and Graphene Oxide. *Carbon* **2011**, *49* (9), 3019–3023.

(108) Guo, H.L.; Wang, X.F.; Qian, Q.Y.; Wang, F.B.; Xia, X.H. A Green Approach to the Synthesis of Graphene Nanosheets. *ACS Nano* **2009**, *3* (9), 2653–2659.

(109) Gao, J.; Liu, F.; Liu, Y.; Ma, N.; Wang, Z.; Zhang, X. Environment-Friendly Method To Produce Graphene That Employs Vitamin C and Amino Acid. *Chem. Mater.* **2010**, *22* (7), 2213–2218.

(110) Fernández-Merino, M. J.; Guardia, L.; Paredes, J. I.; Villar-Rodil, S.; Solís-Fernández, P.; Martínez-Alonso, A.; Tascón, J. M. D. Vitamin C Is an Ideal Substitute for Hydrazine in the Reduction of Graphene Oxide Suspensions. *J. Phys. Chem. C* **2010**, *114* (14), 6426–6432.

(111) Zhang, J.; Yang, H.; Shen, G.; Cheng, P.; Zhang, J.; Guo, S. Reduction of Graphene Oxide Via L-Ascorbic Acid. *Chem. Commun.* **2010**, *46* (7), 1112–1114.

(112) Zhu, Y.; Murali, S.; Cai, W.; Li, X.; Suk, J. W.; Potts, J. R.; Ruoff, R. S. Graphene and Graphene Oxide: Synthesis, Properties, and Applications. *Adv. Mater.* **2010**, *22* (35), 3906–3924.

(113) Chen, D.; Feng, H.; Li, J. Graphene Oxide: Preparation, Functionalization, and Electrochemical Applications. *Chem. Rev.* **2012**, *112* (11), 6027–6053.

(114) Larsen, J. W.; Freund, M.; Kim, K. Y.; Sidovar, M.; Stuart, J. L. Mechanism of the Carbon Catalyzed Reduction of Nitrobenzene by Hydrazine. *Carbon* **2000**, *38* (5), 655–661.

(115) Chen, Y.; Guo, F.; Qiu, Y.; Hu, H.; Kulaots, I.; Walsh, E.; Hurt, R. H. Encapsulation of Particle Ensembles in Graphene Nanosacks as a New Route to Multifunctional Materials. *ACS Nano* **2013**, *7* (5), 3744–3753.

(116) Kirui, D. K.; Rey, D. A.; Batt, C. A. Gold Hybrid Nanoparticles for Targeted Phototherapy and Cancer Imaging. *Nanotechnology* **2010**, *21* (10), 105105.

(117) Cho, N.H.; Cheong, T.C.; Min, J. H.; Wu, J. H.; Lee, S. J.; Kim, D.; Yang, J.S.; Kim, S.; Kim, Y. K.; Seong, S.Y. A Multifunctional Core–shell Nanoparticle for Dendritic Cell-Based Cancer Immunotherapy. *Nat. Nanotechnol.* **2011**, *6* (10), 675–682.

(118) Colunga, A.; Rangel-Mendez, J. R.; Celis, L. B.; Cervantes, F. J. Graphene Oxide as Electron Shuttle for Increased Redox Conversion of Contaminants under Methanogenic and Sulfate-Reducing Conditions. *Bioresour. Technol.* **2015**, *175*, 309–314.

(119) Lu, H.; Zhang, H.; Wang, J.; Zhou, J.; Zhou, Y. A Novel Quinone/Reduced Graphene Oxide Composite as a Solid-Phase Redox Mediator for Chemical and Biological Acid Yellow 36 Reduction. *RSC Adv.* **2014**, *4* (88), 47297–47303.

(120) Gao, Y.; Ma, D.; Wang, C.; Guan, J.; Bao, X. Reduced Graphene Oxide as a Catalyst for Hydrogenation of Nitrobenzene at Room Temperature. *Chem. Commun.* **2011**, *47* (8), 2432–2434.

(121) Wang, J.; Wang, D.; Liu, G.; Jin, R.; Lu, H. Enhanced Nitrobenzene Biotransformation by Graphene-Anaerobic Sludge Composite. *J. Chem. Technol. Biotechnol.* **2014**, *89* (5), 750–755.

(122) Li, L.; Liu, Q.; Wang, Y.X.; Zhao, H.Q.; He, C.S.; Yang, H.Y.; Gong, L.; Mu, Y.; Yu, H.Q. Facilitated Biological Reduction of Nitroaromatic Compounds by Reduced Graphene Oxide and the Role of Its Surface Characteristics. *Sci. Rep.* **2016**, *6*, 30082.

(123) Oh, S.Y.; Son, J.G.; Chiu, P. C. Black Carbon-Mediated Reductive Transformation of Nitro Compounds by Hydrogen Sulfide. *Environ. Earth Sci.* **2014**, *73* (4), 1813–1822.

(124) Luo, J.; Jang, H. D.; Sun, T.; Xiao, L.; He, Z.; Katsoulidis, A. P.; Kanatzidis, M. G.; Gibson, J. M.; Huang, J. Compression and Aggregation-Resistant Particles of Crumpled Soft Sheets. *ACS Nano* **2011**, *5* (11), 8943–8949.

(125) Luo, J.; Zhao, X.; Wu, J.; Jang, H. D.; Kung, H. H.; Huang, J. Crumpled Graphene-Encapsulated Si Nanoparticles for Lithium Ion Battery Anodes. *J. Phys. Chem. Lett.* **2012**, *3* (13), 1824–1829.

(126) Lv, X. S.; Qiu, Y.; Wang, Z. Y.; Jiang, G. M.; Chen, Y. T.; Xu, X. H.; Hurt, R. H. Aerosol Synthesis of Phase-Controlled Iron–graphene Nanohybrids through FeOOH Nanorod Intermediates. *Environ. Sci. Nano* **2016**, *3* (5), 1215–1221.

(127) Chen, Y.; Guo, F.; Jachak, A.; Kim, S.P.; Datta, D.; Liu, J.; Kulaots, I.; Vaslet, C.; Jang, H. D.; Huang, J.; et al. Aerosol Synthesis of Cargo-Filled Graphene Nanosacks. *Nano Lett.* **2012**, *12* (4), 1996–2002.

(128) Zhou, S.; Zhang, H.; Zhao, Q.; Wang, X.; Li, J.; Wang, F. Graphene-Wrapped Polyaniline Nanofibers as Electrode Materials for Organic Supercapacitors. *Carbon* **2013**, *52*, 440–450.

(129) Evers, S.; Nazar, L. F. Graphene-Enveloped Sulfur in a One Pot Reaction: A Cathode with Good Coulombic Efficiency and High Practical Sulfur Content. *Chem. Commun.* **2012**, *48* (9), 1233–1235.

(130) Mao, S.; Wen, Z.; Kim, H.; Lu, G.; Hurley, P.; Chen, J. A General Approach to One-Pot Fabrication of Crumpled Graphene-Based Nanohybrids for Energy Applications. *ACS Nano* **2012**, *6* (8), 7505–7513.

(131) Enoki, T.; Kobayashi, Y.; Fukui, K. Electronic Structures of Graphene Edges and Nanographene. *Int. Rev. Phys. Chem.* **2007**, *26* (4), 609–645.

(132) Fu, H.; Zhu, D. Graphene Oxide-Facilitated Reduction of Nitrobenzene in Sulfide-Containing Aqueous Solutions. *Environ. Sci. Technol.* **2013**, *47* (9), 4204–4210.

(133) Agnoli, S.; Granozzi, G. Second Generation Graphene: Opportunities and Challenges for Surface Science. *Surf. Sci.* **2013**, *609*, 1–5.

(134) Oh, S.Y.; Chiu, P. C. Graphite- and Soot-Mediated Reduction of 2,4-Dinitrotoluene and Hexahydro-1,3,5-Trinitro-1,3,5-Triazine. *Environ. Sci. Technol.* **2009**, *43* (18), 6983–6988.

(135) Gong, W.; Liu, X.; Tao, L.; Xue, W.; Fu, W.; Cheng, D. Reduction of Nitrobenzene with Sulfides Catalyzed by the Black Carbons from Crop-Residue Ashes. *Environ. Sci. Pollut. Res.* **2014**, *21* (9), 6162–6169.

(136) Xu, W.; Pignatello, J. J.; Mitch, W. A. Reduction of Nitroaromatics Sorbed to Black Carbon by Direct Reaction with Sorbed Sulfides. *Environ. Sci. Technol.* **2015**, *49* (6), 3419–3426.

(137) Yu, X.; Gong, W.; Liu, X.; Shi, L.; Han, X.; Bao, H. The Use of Carbon Black to Catalyze the Reduction of Nitrobenzenes by Sulfides. *J. Hazard. Mater.* **2011**, *198*, 340–346.

(138) Millerick, K.; Drew, S. R.; Finneran, K. T. Electron Shuttle-Mediated Biotransformation of Hexahydro-1,3,5-Trinitro-1,3,5-Triazine Adsorbed to Granular Activated Carbon. *Environ. Sci. Technol.* **2013**, *47* (15), 8743–8750.

(139) Kemper, J. M.; Ammar, E.; Mitch, W. A. Abiotic Degradation of Hexahydro-1,3,5-Trinitro-1,3,5-Triazine in the Presence of Hydrogen Sulfide and Black Carbon. *Environ. Sci. Technol.* **2008**, *42* (6), 2118–2123.

(140) Xu, W.; Pignatello, J. J.; Mitch, W. A. Role of Black Carbon Electrical Conductivity in Mediating Hexahydro-1,3,5-Trinitro-1,3,5-Triazine (RDX) Transformation on Carbon Surfaces by Sulfides. *Environ. Sci. Technol.* **2013**, *47* (13), 7129–7136.

(141) Xu, W.; Dana, K. E.; Mitch, W. A. Black Carbon-Mediated Destruction of Nitroglycerin and RDX By Hydrogen Sulfide. *Environ. Sci. Technol.* **2010**, *44* (16), 6409–6415.

(142) Oh, S.Y.; Son, J.G.; Chiu, P. C. Biochar-Mediated Reductive Transformation of Nitro Herbicides and Explosives. *Environ. Toxicol. Chem.* **2013**, *32* (3), 501–508.

(143) Oh, S.Y.; Son, J.G.; Lim, O.T.; Chiu, P. C. The Role of Black Carbon as a Catalyst for Environmental Redox Transformation. *Environ. Geochem. Health* **2011**, *34* (1), 105–113.

(144) Hennebel, T.; De Corte, S.; Vanhaecke, L.; Vanherck, K.; Forrez, I.; De Gusseme, B.; Verhagen, P.; Verbeken, K.; Van der Bruggen, B.; Vankelecom, I.; et al. Removal of Diatrizoate with Catalytically Active Membranes Incorporating Microbially Produced Palladium Nanoparticles. *Water Res.* **2010**, *44* (5), 1498–1506.

(145) Haiß, A.; Kümmerer, K. Biodegradability of the X-Ray Contrast Compound Diatrizoic Acid, Identification of Aerobic Degradation Products and Effects against Sewage Sludge Micro-Organisms. *Chemosphere* **2006**, *62* (2), 294–302.

(146) Boehm, H. P. Some Aspects of the Surface Chemistry of Carbon Blacks and Other Carbons. *Carbon* **1994**, *32* (5), 759–769.

(147) Bandosz, T. J.; Jagiello, J.; Contescu, C.; Schwarz, J. A. Characterization of the Surfaces of Activated Carbons in Terms of Their Acidity Constant Distributions. *Carbon* **1993**, *31* (7), 1193–1202.

(148) Jagiello, J. Stable Numerical Solution of the Adsorption Integral Equation Using Splines. *Langmuir* **1994**, *10* (8), 2778–2785.

(149) Li, Y.; Du, Q.; Liu, T.; Peng, X.; Wang, J.; Sun, J.; Wang, Y.; Wu, S.; Wang, Z.; Xia, Y.; et al. Comparative Study of Methylene Blue Dye Adsorption onto Activated Carbon, Graphene Oxide, and Carbon Nanotubes. *Chem. Eng. Res. Des.* **2013**, *91* (2), 361–368.

(150) Krishnamoorthy, K.; Veerapandian, M.; Yun, K.; Kim, S.-J. The Chemical and Structural Analysis of Graphene Oxide with Different Degrees of Oxidation. *Carbon* **2013**, *53*, 38–49.

(151) Jung, I.; Dikin, D. A.; Piner, R. D.; Ruoff, R. S. Tunable Electrical Conductivity of Individual Graphene Oxide Sheets Reduced at "Low" Temperatures. *Nano Lett.* **2008**, *8* (12), 4283–4287.

(152) Koch, F. A.; Oldham, W. K. Oxidation-Reduction Potential — A Tool for Monitoring, Control and Optimization of Biological Nutrient Removal Systems http://www.iwaponline.com/wst/01711/wst017110259.htm (accessed Nov 29, 2014).

(153) Montes-Morán, M. A.; Suárez, D.; Menéndez, J. A.; Fuente, E. On the Nature of Basic Sites on Carbon Surfaces: An Overview. *Carbon* **2004**, *42* (7), 1219–1225.

(154) Menéndez, J. A.; Phillips, J.; Xia, B.; Radovic, L. R. On the Modification and Characterization of Chemical Surface Properties of Activated Carbon: In the Search of Carbons with Stable Basic Properties. *Langmuir* **1996**, *12* (18), 4404–4410.

(155) Moreno-Castilla, C.; Rivera-Utrilla, J.; Joly, J. P.; López-Ramón, M. V.; Ferro-García, M. A.; Carrasco-Marín, F. Thermal Regeneration of an Activated Carbon Exhausted with Different Substituted Phenols. *Carbon* **1995**, *33* (10), 1417–1423.

(156) Noh, C. H.; Jung, J. E.; Kim, J. Y.; Sakong, D. S.; Choi, K. S. A Study on the Morphology and Electro-Optic Properties of Liquid Crystal-Polymer Composite Films. *Mol. Cryst. Liq. Cryst. Sci. Technol. Sect. Mol. Cryst. Liq. Cryst.* **1993**, *237* (1), 299–309.

(157) Deng, Y.; Gu, A.; Fang, Z. The Effect of Morphology on the Optical Properties of Transparent Epoxy/Montmorillonite Composites. *Polym. Int.* **2004**, *53* (1), 85–91.

(158) Nair, R. R.; Blake, P.; Grigorenko, A. N.; Novoselov, K. S.; Booth, T. J.; Stauber, T.; Peres, N. M. R.; Geim, A. K. Fine Structure Constant Defines Visual Transparency of Graphene. *Science* **2008**, *320* (5881), 1308–1308.

(159) Niyogi, S.; Bekyarova, E.; Itkis, M. E.; McWilliams, J. L.; Hamon, M. A.; Haddon, R. C. Solution Properties of Graphite and Graphene. *J. Am. Chem. Soc.* **2006**, *128* (24), 7720–7721.

(160) Wang, G.; Yang, J.; Park, J.; Gou, X.; Wang, B.; Liu, H.; Yao, J. Facile Synthesis and Characterization of Graphene Nanosheets. *J. Phys. Chem. C* **2008**, *112* (22), 8192–8195.

(161) Venugopal, G.; Jung, M.-H.; Suemitsu M; Kim S-J. Fabrication of Nanoscale Three-Dimensional Graphite Stacked Junctions by Focused-Ion-Beam and Observation of Anomalous Transport Characteristics. *Carbon* **2011**, *49* (8), 2766–2772.

(162) Ferrari, A. C.; Robertson, J. Interpretation of Raman Spectra of Disordered and Amorphous Carbon. *Phys. Rev. B* **2000**, *61* (20), 14095–14107.

(163) Tuinstra, F.; Koenig, J. L. Raman Spectrum of Graphite. *J. Chem. Phys.* **1970**, *53* (3), 1126–1130.

(164) Knight, D. S.; White, W. B. Characterization of Diamond Films by Raman Spectroscopy. *J. Mater. Res.* **1989**, *4* (02), 385–393.

(165) Cançado, L. G.; Takai, K.; Enoki, T.; Endo, M.; Kim, Y. A.; Mizusaki, H.; Jorio, A.; Coelho, L. N.; Magalhães-Paniago, R.; Pimenta, M. A. General Equation for the Determination of the Crystallite Size La of Nanographite by Raman Spectroscopy. *Appl. Phys. Lett.* **2006**, *88* (16), 163106.

(166) Kim, M. C.; Hwang, G. S.; Ruoff, R. S. Epoxide Reduction with Hydrazine on Graphene: A First Principles Study. *J. Chem. Phys.* **2009**, *131* (6), 064704.

(167) Boehm, H. P. Surface Oxides on Carbon and Their Analysis: A Critical Assessment. *Carbon* **2002**, *40* (2), 145–149.

(168) Briceño, N. O.; Guzmán, M. Y.; Díaz, J. de J. Surface Groups on Carbonaceous Materials.Characterization by Different Techniques. *Rev. Colomb. Quím.* **2007**, *36* (1), 121–130.

(169) Taniguchi, T.; Kurihara, S.; Tateishi, H.; Hatakeyama, K.; Koinuma, M.; Yokoi, H.; Hara, M.; Ishikawa, H.; Matsumoto, Y. PH-Driven, Reversible Epoxy Ring Opening/Closing in Graphene Oxide. *Carbon* **2015**, *84*, 560–566.

(170) Konkena, B.; Vasudevan, S. Understanding Aqueous Dispersibility of Graphene Oxide and Reduced Graphene Oxide through PKa Measurements. *J. Phys. Chem. Lett.* **2012**, *3* (7), 867–872.

(171) Castro-Beltrán, A.; Sepúlveda-Guzmán, S.; De a Cruz-Hernandez, W.; Cruz-Silva, R. Obtención de grafeno mediante la reducción química del óxido de grafito. *Ingenierías* **2011**, *14* (52), 34–43.

(172) Chen, W.; Yan, L.; Bangal, P. R. Chemical Reduction of Graphene Oxide to Graphene by Sulfur-Containing Compounds. *J. Phys. Chem. C* **2010**, *114* (47), 19885–19890.

(173) Pumera, M. Electrochemistry of Graphene, Graphene Oxide and Other Graphenoids: Review. *Electrochem. Commun.* **2013**, *36*, 14–18.

(174) Ramesha, G. K.; Sampath, S. Electrochemical Reduction of Oriented Graphene Oxide Films: An in Situ Raman Spectroelectrochemical Study. *J. Phys. Chem. C* **2009**, *113* (19), 7985–7989.

(175) Zhou, M.; Wang, Y.; Zhai, Y.; Zhai, J.; Ren, W.; Wang, F.; Dong, S. Controlled Synthesis of Large-Area and Patterned Electrochemically Reduced Graphene Oxide Films. *Chem. – Eur. J.* **2009**, *15* (25), 6116–6120.

(176) Ambrosi, A.; Chua, C. K.; Khezri, B.; Sofer, Z.; Webster, R. D.; Pumera, M. Chemically Reduced Graphene Contains Inherent Metallic Impurities Present in Parent Natural and Synthetic Graphite. *Proc. Natl. Acad. Sci. U. S. A.* **2012**, *109* (32), 12899–12904.

(177) Kim, H.; Hwang, Y. S.; Sharma, V. K. Adsorption of Antibiotics and Iopromide onto Single-Walled and Multi-Walled Carbon Nanotubes. *Chem. Eng. J.* **2014**, *255*, 23–27.

(178) Gallegos-Garcia, M.; Celis, L. B.; Rangel-Méndez, R.; Razo-Flores, E. Precipitation and Recovery of Metal Sulfides from Metal Containing Acidic Wastewater in a Sulfidogenic Down-Flow Fluidized Bed Reactor. *Biotechnol. Bioeng.* **2009**, *102* (1), 91–99.

(179) Martínez, C. M.; Celis, L. B.; Cervantes, F. J. Immobilized Humic Substances as Redox Mediator for the Simultaneous Removal of Phenol and Reactive Red 2 in a UASB Reactor. *Appl. Microbiol. Biotechnol.* **2013**, *97* (22), 9897–9905.

(180) Cervantes, F. J.; Santos, A. B. D. Reduction of Azo Dyes by Anaerobic Bacteria: Microbiological and Biochemical Aspects. *Rev. Environ. Sci. Biotechnol.* **2011**, *10* (2), 125–137.

(181) Cervantes, F. J.; Enríquez, J. E.; Galindo-Petatán, E.; Arvayo, H.; Razo-Flores, E.; Field, J. A. Biogenic Sulphide Plays a Major Role on the Riboflavin-Mediated Decolourisation of Azo Dyes under Sulphate-Reducing Conditions. *Chemosphere* **2007**, *68* (6), 1082–1089.

(182) Prato-Garcia, D.; Cervantes, F. J.; Buitrón, G. Azo Dye Decolorization Assisted by Chemical and Biogenic Sulfide. *J. Hazard. Mater.* **2013**, *250–251*, 462–468.

(183) Bianco, A. Graphene: Safe or Toxic? The Two Faces of the Medal. *Angew. Chem. Int. Ed Engl.* **2013**, *52* (19), 4986–4997.

(184) Liu, S.; Zeng, T. H.; Hofmann, M.; Burcombe, E.; Wei, J.; Jiang, R.; Kong, J.; Chen, Y. Antibacterial Activity of Graphite, Graphite Oxide, Graphene Oxide, and Reduced Graphene Oxide: Membrane and Oxidative Stress. *ACS Nano* **2011**, *5* (9), 6971–6980.

(185) Ahmed, F.; Rodrigues, D. F. Investigation of Acute Effects of Graphene Oxide on Wastewater Microbial Community: A Case Study. *J. Hazard. Mater.* **2013**, *256–257*, 33–39.

(186) dos Santos, A. B.; de Madrid, M. P.; de Bok, F. A. M.; Stams, A. J. M.; van Lier, J. B.; Cervantes, F. J. The Contribution of Fermentative Bacteria and Methanogenic Archaea to Azo Dye Reduction by a Thermophilic Anaerobic Consortium. *Enzyme Microb. Technol.* **2006**, *39* (1), 38–46.

(187) Nieto-Delgado, C.; Rangel-Mendez, J. R. Anchorage of Iron Hydro(Oxide) Nanoparticles onto Activated Carbon to Remove As(V) from Water. *Water Res.* **2012**, *46* (9), 2973–2982.

(188) Logan, B. E.; Rabaey, K. Conversion of Wastes into Bioelectricity and Chemicals by Using Microbial Electrochemical Technologies. *Science* **2012**, *337* (6095), 686–690.

(189) Reguera, G.; McCarthy, K. D.; Mehta, T.; Nicoll, J. S.; Tuominen, M. T.; Lovley, D. R. Extracellular Electron Transfer via Microbial Nanowires. *Nature* **2005**, *435* (7045), 1098–1101.

(190) Summers, Z. M.; Fogarty, H. E.; Leang, C.; Franks, A. E.; Malvankar, N. S.; Lovley, D. R. Direct Exchange of Electrons within Aggregates of an Evolved Syntrophic Coculture of Anaerobic Bacteria. *Science* **2010**, *330* (6009), 1413–1415.

(191) Chen, Y.; Guo, F.; Qiu, Y.; Hu, H.; Kulaots, I.; Walsh, E.; Hurt, R. H. Encapsulation of Particle Ensembles in Graphene Nanosacks as a New Route to Multifunctional Materials. *ACS Nano* **2013**, *7* (5), 3744–3753.

(192) Pereira, L.; Dias, P.; Soares, O. S. G. P.; Ramalho, P. S. F.; Pereira, M. F. R.; Alves, M. M. Synthesis, Characterization and Application of Magnetic Carbon Materials as Electron Shuttles for the Biological and Chemical Reduction of the Azo Dye Acid Orange 10. *Appl. Catal. B Environ.* **2017**, *212*, 175–184.

(193) Pereira, C.; Pereira, A. M.; Fernandes, C.; Rocha, M.; Mendes, R.; Fernández-García, M. P.; Guedes, A.; Tavares, P. B.; Grenèche, J.-M.; Araújo, J. P.; et al. Superparamagnetic MFe_2O_4 (M = Fe, Co, Mn) Nanoparticles: Tuning the Particle Size and Magnetic Properties through a Novel One-Step Coprecipitation Route. *Chem. Mater.* **2012**, *24* (8), 1496–1504.

(194) Guo, F.; Silverberg, G.; Bowers, S.; Kim, S.-P.; Datta, D.; Shenoy, V.; Hurt, R. H. Graphene-Based Environmental Barriers. *Environ. Sci. Technol.* **2012**, *46* (14), 7717–7724.

(195) Kim, F.; Luo, J.; Cruz-Silva, R.; Cote, L. J.; Sohn, K.; Huang, J. Self-Propagating Domino-like Reactions in Oxidized Graphite. *Adv. Funct. Mater.* **2010**, *20* (17), 2867–2873.

(196) Spitz Steinberg, R.; Cruz, M.; Mahfouz, N. G. A.; Qiu, Y.; Hurt, R. H. Breathable Vapor Toxicant Barriers Based on Multilayer Graphene Oxide. *ACS Nano* **2017**, *11* (6), 5670–5679.

(197) Maity, D.; Kale, S. N.; Kaul-Ghanekar, R.; Xue, J.-M.; Ding, J. Studies of Magnetite Nanoparticles Synthesized by Thermal Decomposition of Iron (III) Acetylacetonate in Tri(Ethylene Glycol). *J. Magn. Magn. Mater.* **2009**, *321* (19), 3093–3098.

(198) Gorski, C. A.; Nurmi, J. T.; Tratnyek, P. G.; Hofstetter, T. B.; Scherer, M. M. Redox Behavior of Magnetite: Implications for Contaminant Reduction. *Environ. Sci. Technol.* **2010**, *44* (1), 55–60.

(199) Scott, T. B.; Allen, G. C.; Heard, P. J.; Randell, M. G. Reduction of U(VI) to U(IV) on the Surface of Magnetite. *Geochim. Cosmochim. Acta* **2005**, *69* (24), 5639–5646.

(200) White, A. F.; Peterson, M. L. Reduction of Aqueous Transition Metal Species on the Surfaces of Fe(II) -Containing Oxides. *Geochim. Cosmochim. Acta* **1996**, *60* (20), 3799–3814.

(201) C. Allen, G.; T. Curtis, M.; J. Hooper, A.; M. Tucker, P. X -Ray Photoelectron Spectroscopy of Iron–oxygen Systems. *J. Chem. Soc. Dalton Trans.* **1974**, *0* (14), 1525–1530.

(202) Wang, J.; Wang, D.; Liu, G.; Jin, R.; Lu, H. Enhanced Nitrobenzene Biotransformation by Graphene-Anaerobic Sludge Composite. *J. Chem. Technol. Biotechnol.* **2014**, *89* (5), 750–755.

(203) Seabra, A. B.; Paula, A. J.; de Lima, R.; Alves, O. L.; Durán, N. Nanotoxicity of Graphene and Graphene Oxide. *Chem. Res. Toxicol.* **2014**, *27* (2), 159–168.

(204) Chen, Y.; Guo, F.; Jachak, A.; Kim, S.-P.; Datta, D.; Liu, J.; Kulaots, I.; Vaslet, C.; Jang, H. D.; Huang, J.; et al. Aerosol Synthesis of Cargo-Filled Graphene Nanosacks. *Nano Lett.* **2012**, *12* (4), 1996–2002.

(205) Eaton, A.; Franson, M. *Standard Methods for the Examination of Water & Wastewater*. *American Public Health Association*; 2005.

(206) Fetzer, S.; Conrad, R. Effect of Redox Potential on Methanogenesis by *Methanosarcina Barkeri*. *Arch. Microbiol.* **1993**, *160* (2), 108–113.

(207) Allen, G. C.; Curtis, M. T.; Hooper, A. J.; Tucker, P. M. X-Ray Photoelectron Spectroscopy of Iron–oxygen Systems. *J. Chem. Soc. Dalton Trans.* **1974**, *0* (14), 1525–1530.

(208) Knackmuss, H.-J. Basic Knowledge and Perspectives of Bioelimination of Xenobiotic Compounds. *J. Biotechnol.* **1996**, *51* (3), 287–295.

(209) Rittmann, B.; McCarty, P. L. Detoxification of Hazardous Chemicals. In *Environmental Biotechnology: Principles and Applications*; McGRAW-HILL INTERNATIONAL EDITIONS: United States of America, 1999; Vol. 1, pp 637–694.

(210) Jeong, J.; Jung, J.; Cooper, W. J.; Song, W. Degradation Mechanisms and Kinetic Studies for the Treatment of X-Ray Contrast Media Compounds by Advanced Oxidation/Reduction Processes. *Water Res.* **2010**, *44* (15), 4391–4398.

(211) Azerrad, S. P.; Gur-Reznik, S.; Heller-Grossman, L.; Dosoretz, C. G. Advanced Oxidation of Iodinated X-Ray Contrast Media in Reverse Osmosis Brines: The Influence of Quenching. *Water Res.* **2014**, *62*, 107–116.

(212) Snyder, S. A.; Wert, E. C.; Rexing, D. J.; Zegers, R. E.; Drury, D. D. Ozone Oxidation of Endocrine Disruptors and Pharmaceuticals in Surface Water and Wastewater. *Ozone Sci. Eng.* **2006**, *28* (6), 445–460.

(213) Patil, S. A.; Hägerhäll, C.; Gorton, L. Electron Transfer Mechanisms between Microorganisms and Electrodes in Bioelectrochemical Systems. *Bioanal. Rev.* **2012**, *4* (2–4), 159–192.

(214) Flemming, H.-C.; Neu, T. R.; Wozniak, D. J. The EPS Matrix: The "House of Biofilm Cells." *J. Bacteriol.* **2007**, *189* (22), 7945–7947.

(215) Li, S.-W.; Sheng, G.-P.; Cheng, Y.-Y.; Yu, H.-Q. Redox Properties of Extracellular Polymeric Substances (EPS) from Electroactive Bacteria. *Sci. Rep.* **2016**, *6*, 39098.

(216) Quarmby Joanne; Forster Christopher F. A Comparative Study of the Internal Architecture of Anaerobic Granular Sludges. *J. Chem. Technol. Biotechnol.* **2004**, *63* (1), 60–68.

(217) Grotenhuis, J. T. C.; Smit, M.; Lammeren, A. A. M. van; Stams, A. J. M.; Zehnder, A. J. B. Localization and Quantification of Extracellular Polymers in Methanogenic Granular Sludge. *Appl. Microbiol. Biotechnol.* **1991**, *36* (1), 115–119.

(218) Yoo, R.; Kim, J.; McCarty, P. L.; Bae, J. Anaerobic Treatment of Municipal Wastewater with a Staged Anaerobic Fluidized Membrane Bioreactor (SAF-MBR) System. *Bioresour. Technol.* **2012**, *120*, 133–139.

(219) Gorski, C. A.; Scherer, M. M. Influence of Magnetite Stoichiometry on FeII Uptake and Nitrobenzene Reduction. *Environ. Sci. Technol.* **2009**, *43* (10), 3675–3680.

(220) Wiatrowski, H. A.; Das, S.; Kukkadapu, R.; Ilton, E. S.; Barkay, T.; Yee, N. Reduction of Hg(II) to Hg(0) by Magnetite. *Environ. Sci. Technol.* **2009**, *43* (14), 5307–5313.

(221) Dos Santos Coelho, F.; Ardisson, J. D.; Moura, F. C. C.; Lago, R. M.; Murad, E.; Fabris, J. D. Potential Application of Highly Reactive Fe(0)/Fe3O4 Composites for the Reduction of Cr(VI) Environmental Contaminants. *Chemosphere* **2008**, *71* (1), 90–96.

(222) Crane, R. A.; Dickinson, M.; Popescu, I. C.; Scott, T. B. Magnetite and Zero-Valent Iron Nanoparticles for the Remediation of Uranium Contaminated Environmental Water. *Water Res.* **2011**, *45* (9), 2931–2942.

(223) Muyzer, G.; Stams, A. J. M. The Ecology and Biotechnology of Sulphate-Reducing Bacteria. *Nat. Rev. Microbiol.* **2008**, *6* (6), 441–454.

(224) Barton, L. L.; Tomei, F. A. Characteristics and Activities of Sulfate-Reducing Bacteria. In *Sulfate-Reducing Bacteria*; Biotechnology Handbooks; Springer, Boston, MA, 1995; pp 1–32.

(225) Hao, O. J.; Chen, J. M.; Huang, L.; Buglass, R. L. Sulfate-reducing Bacteria. *Crit. Rev. Environ. Sci. Technol.* **1996**, *26* (2), 155–187.

(226) Liamleam, W.; Annachhatre, A. P. Electron Donors for Biological Sulfate Reduction. *Biotechnol. Adv.* **2007**, *25* (5), 452–463.

(227) Shi, L.; Dong, H.; Reguera, G.; Beyenal, H.; Lu, A.; Liu, J.; Yu, H.-Q.; Fredrickson, J. K. Extracellular Electron Transfer Mechanisms between Microorganisms and Minerals. *Nat. Rev. Microbiol.* **2016**, *14* (10), 651–662.

(228) Hernandez, M. E.; Newman, D. K. Extracellular Electron Transfer. *Cell. Mol. Life Sci. CMLS* **2001**, *58* (11), 1562–1571.

(229) Marsili, E.; Baron, D. B.; Shikhare, I. D.; Coursolle, D.; Gralnick, J. A.; Bond, D. R. Shewanella Secretes Flavins That Mediate Extracellular Electron Transfer. *Proc. Natl. Acad. Sci.* **2008**, *105* (10), 3968–3973.

(230) Newman, D. K.; Kolter, R. A Role for Excreted Quinones in Extracellular Electron Transfer. *Nature* **2000**, *405* (6782), 94.

(231) Xiao, Y.; Zhang, E.; Zhang, J.; Dai, Y.; Yang, Z.; Christensen, H. E. M.; Ulstrup, J.; Zhao, F. Extracellular Polymeric Substances Are Transient Media for Microbial Extracellular Electron Transfer. *Sci. Adv.* **2017**, *3* (7), e1700623.

(232) Cao, B.; Ahmed, B.; Kennedy, D. W.; Wang, Z.; Shi, L.; Marshall, M. J.; Fredrickson, J. K.; Isern, N. G.; Majors, P. D.; Beyenal, H. Contribution of Extracellular Polymeric Substances from Shewanella Sp. HRCR-1 Biofilms to U(VI) Immobilization. *Environ. Sci. Technol.* **2011**, *45* (13), 5483–5490.

(233) Canstein, H. von; Ogawa, J.; Shimizu, S.; Lloyd, J. R. Secretion of Flavins by Shewanella Species and Their Role in Extracellular Electron Transfer. *Appl. Environ. Microbiol.* **2008**, *74* (3), 615–623.

(234) Wang, J.; Lu, H.; Zhou, Y.; Song, Y.; Liu, G.; Feng, Y. Enhanced Biotransformation of Nitrobenzene by the Synergies of Shewanella Species and Mediator-Functionalized Polyurethane Foam. *J. Hazard. Mater.* **2013**, *252–253*, 227–232.

(235) Kudlich, M.; Keck, A.; Klein, J.; Stolz, A. Localization of the Enzyme System Involved in Anaerobic Reduction of Azo Dyes by Sphingomonas Sp. Strain BN6 and Effect of Artificial Redox Mediators on the Rate of Azo Dye Reduction. *Appl. Environ. Microbiol.* **1997**, *63* (9), 3691–3694.

(236) Ye, J.; Hu, A.; Ren, G.; Chen, M.; Tang, J.; Zhang, P.; Zhou, S.; He, Z. Enhancing Sludge Methanogenesis with Improved Redox Activity of Extracellular Polymeric Substances by Hematite in Red Mud. *Water Res.* **2018**, *134*, 54–62.

(237) Liu, X.M.; Sheng, G.P.; Luo, H.W.; Zhang, F.; Yuan, S.J.; Xu, J.; Zeng, R. J.; Wu, J.G.; Yu, H.Q. Contribution of Extracellular Polymeric Substances (EPS) to the Sludge Aggregation. *Environ. Sci. Technol.* **2010**, *44* (11), 4355–4360.

Appendix section

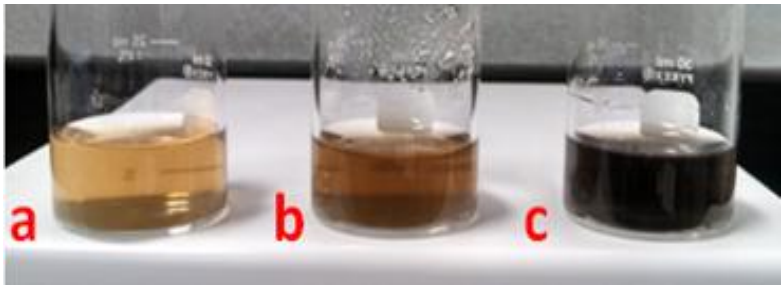

Figure A1. Photographic images of GO-based materials with different reduction degrees: (a) GO, (b) rGO-2 h and (c) rGO-4 h.

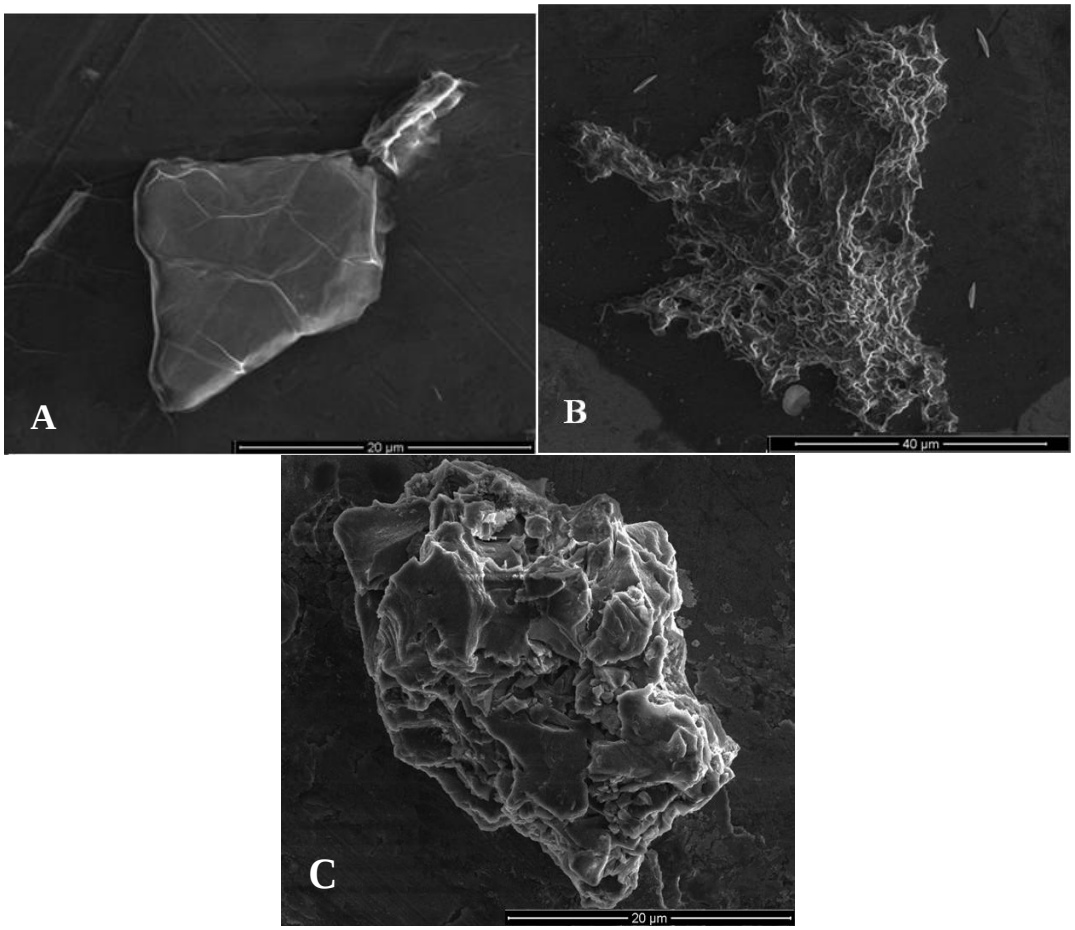

Figure A2. SEM images of GO-based materials: (A) GO, (B) rGO-2 and (C) rGO-4

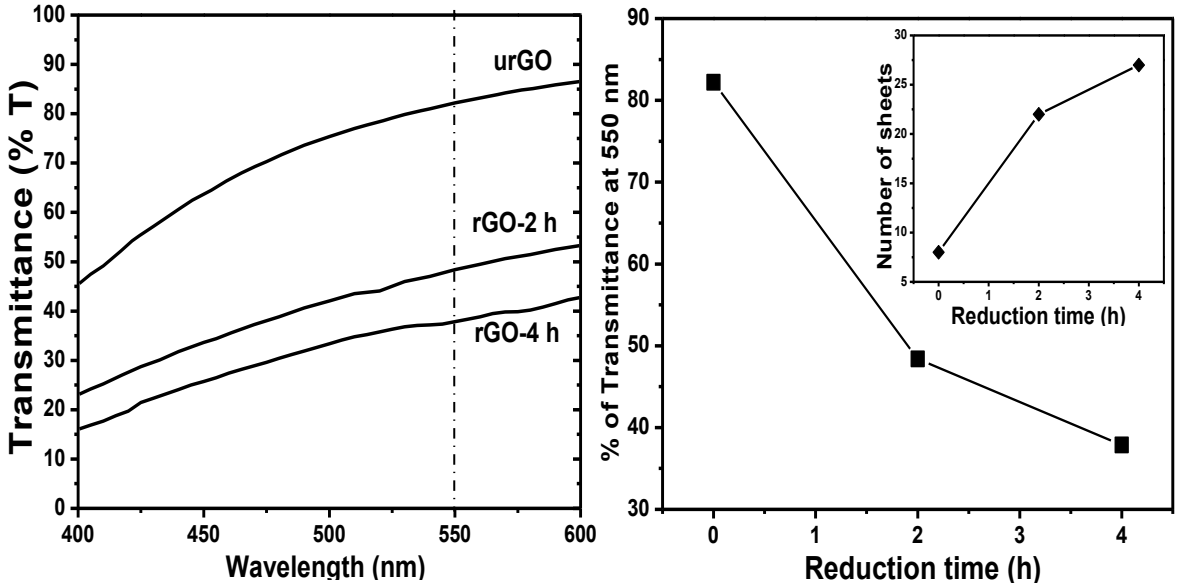

Figure A3. UV-Vis transmission spectra of GO-based materials and transmittance of GO-based materials at 550 nm and estimated number of GO sheets (inset)

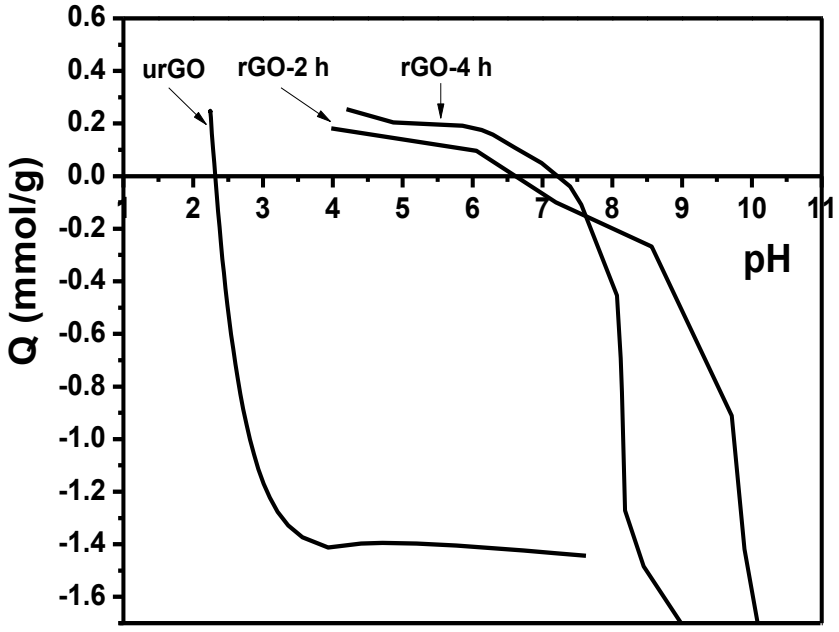

Figure A4. The point of zero charge (pH_{PZC}) and surface charge distribution of GO-based materials at different pH.

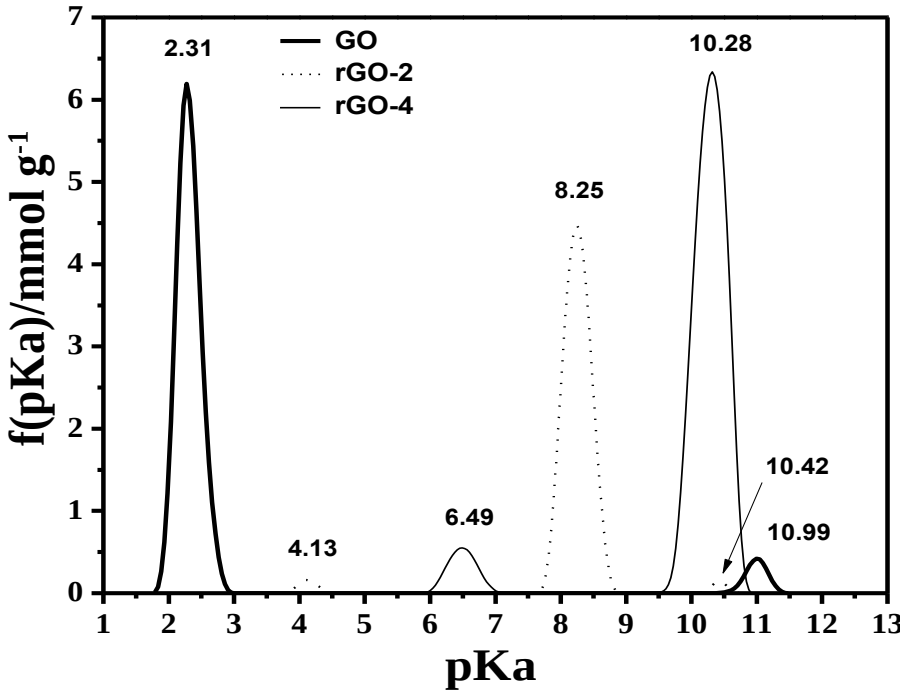

Figure A5. pKa distribution of GO-based materials with different reduction degrees.

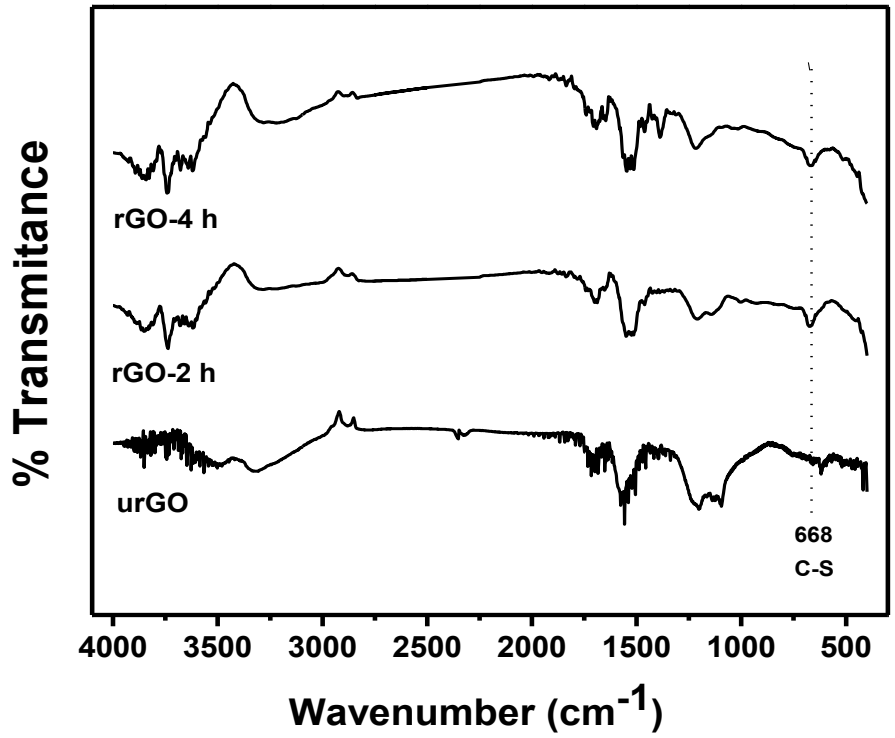

Figure A6. FT-IR spectra of GO-based materials pre-incubated for 1 day with Na_2S 2.6 mol/L.

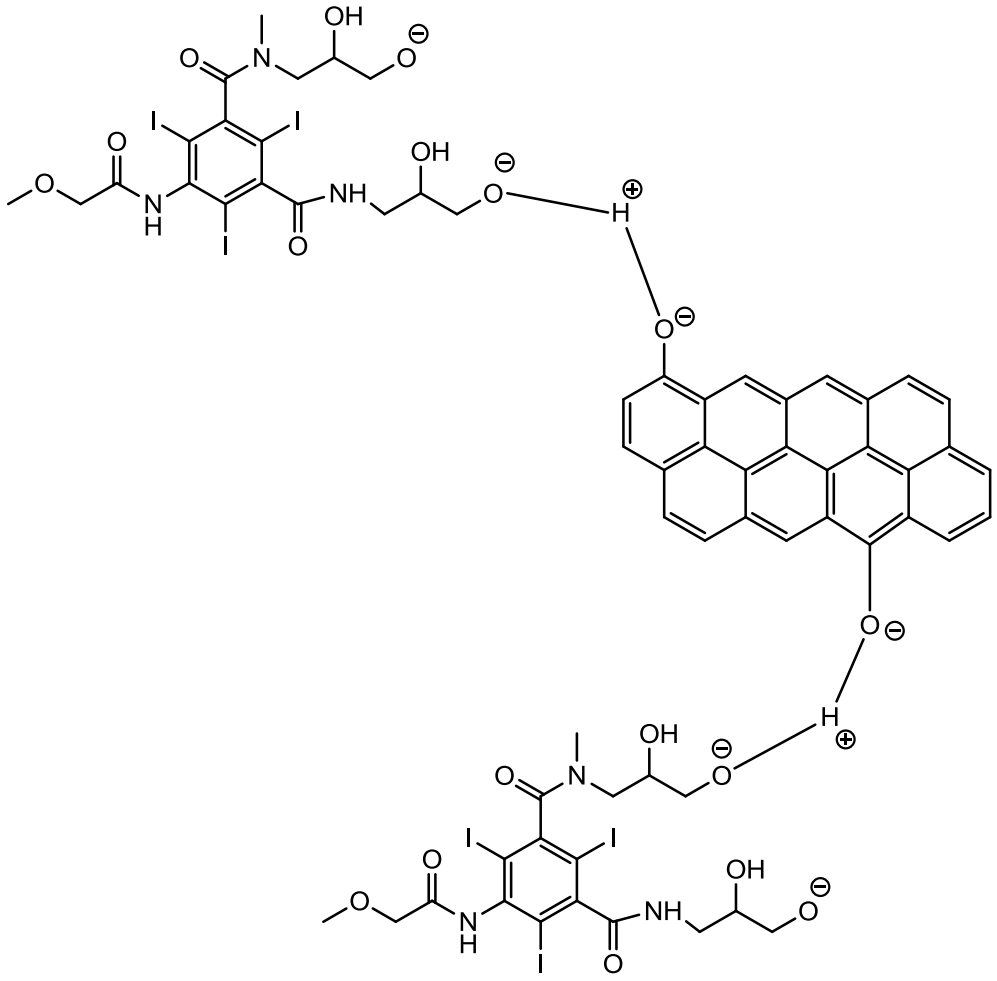

Figure A7. Scheme of IOP adsorption mechanism

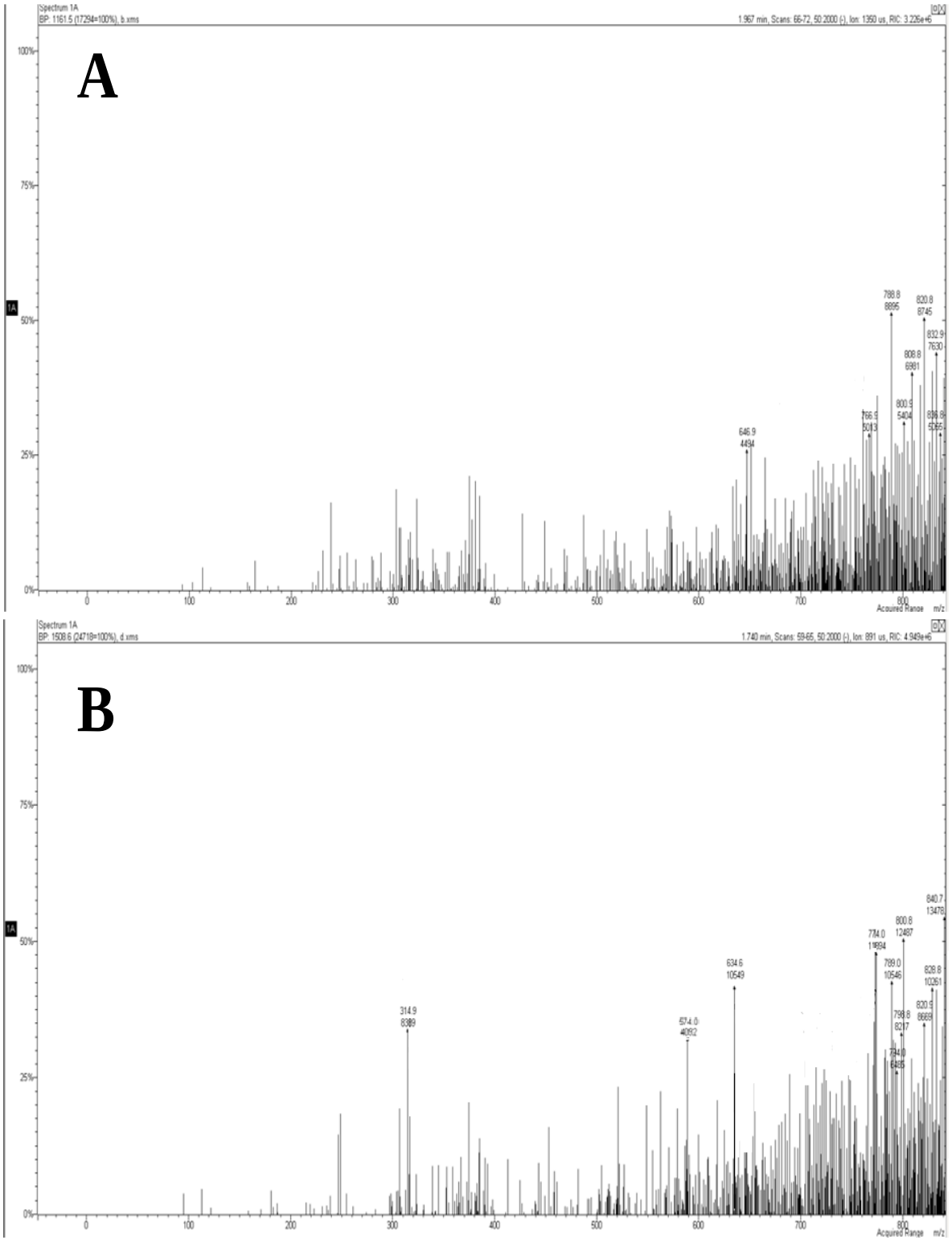

Figure A8. Extracted ion chromatograms of the transformation product of IOP: (A) not-exposed to redox mediator (Na_2S+IOP control) and (B) experiment in presence of rGO-4h as redox mediator.

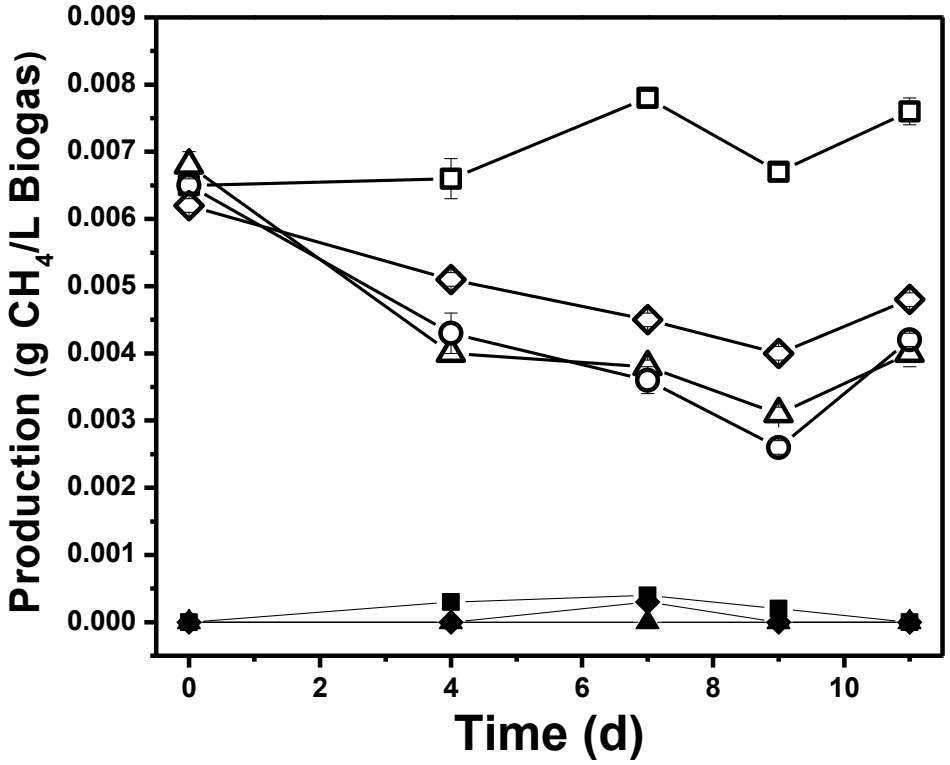

Figure A9. Methane production profile during biological reduction of IOP under methanogenic conditions. Sterilized controls (full symbols). Incubations with and without GO-based materials as RM: without RM and activated biomass (squares), in presence of GO (triangles), rGO-2 (circles) and rGO-4 (diamonds).

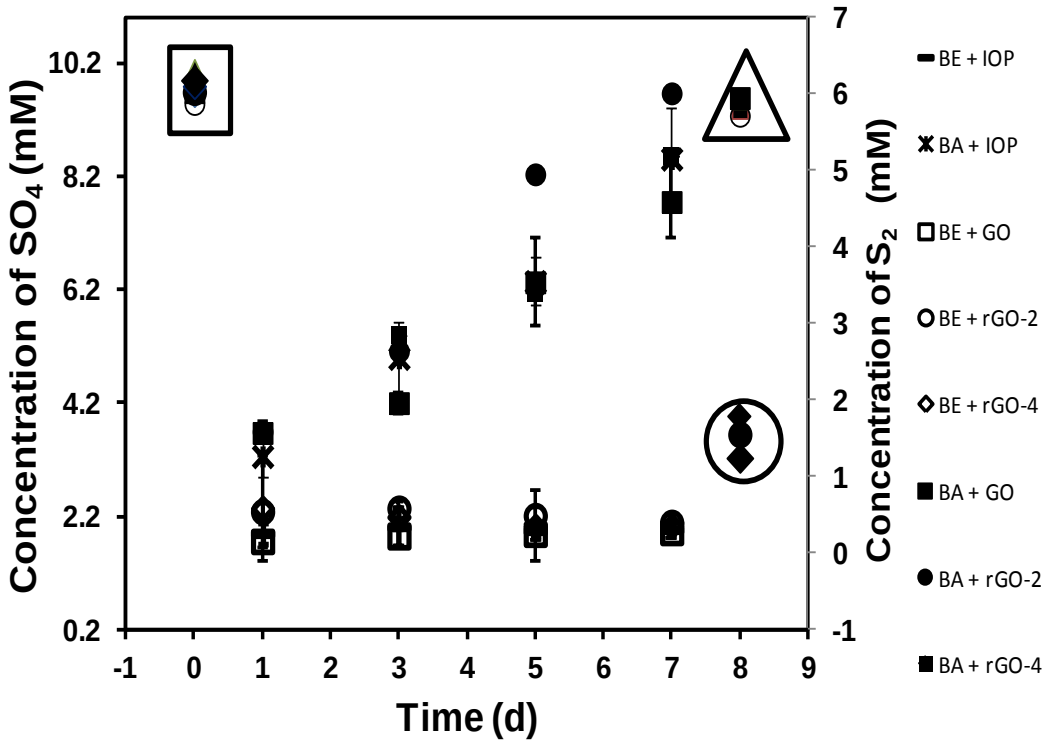

Figure A10. Sulfate Reduction and sulfide production profiles during biological reduction of IOP under sulfate-reducing conditions. Initial concentration of sulfate in all incubations (symbols locked in square) and final concentration of sulfate in the incubations with activated biomass and RM (symbols locked in circle) and sterilized controls (symbols locked in triangle). Symbols without enclosing are profiles of sulfide production BA: activated biomass and BE: sterilized biomass.

The research described in this doctoral thesis was carried out at the
Division of Environmental Sciences of the
Institute for Scientific and Technological Research of San Luis Potosi